PhD Dissertation / Tesis Doctoral

CARBON BALANCE AND DETERMINANT PROCESSES IN SEMIARID ECOSYSTEMS OF SOUTHEAST SPAIN

EL BALANCE DE CARBONO Y PROCESOS DETERMINANTES EN ECOSISTEMAS SEMIÁRIDOS DEL SUDESTE DE ESPAÑA

Memoria presentada por **Ana López Ballesteros** para optar al Grado de Doctor en Ciencias de la Tierra por la Universidad de Granada.

Programa de Doctorado en Ciencias de la Tierra

Universidad de Granada

Abril 2017

La doctoranda / *The doctoral candidate* **Ana López Ballesteros** y los directores de la tesis / *and the thesis supervisors:* **Penélope Serrano Ortiz** y **Francisco Domingo Poveda**,

Garantizamos al firmar esta tesis, que el trabajo ha sido realizado por el doctorando bajo la dirección de los directores de la tesis y hasta donde nuestro conocimiento alcanza, en la realización del trabajo, se han respetado los derechos de los autores citados, cuando se han utilizado sus resultados o publicaciones.

Guarantee, by signing this doctoral thesis, that the work has been done by the candidate under the direction of the thesis supervisors and, as far as our knowledge in the performance of the work, the rights of other authors to be cited (when their results of publications have been used) have been respected.

Lugar y fecha / *Place and date:*

Granada, 17 de abril de 2017

Vº Bº Directora de Tesis   Vº Bº Director de Tesis

Fdo. Penélope Serrano Ortiz   Fdo. Francisco Domingo Poveda
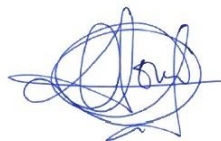
Vº Bº Doctoranda

Fdo. Ana López Ballesteros

CONTENTS

INTRODUCTION

1. GENERAL CONTEXT

Climate change (CC) represents the most important global challenge of the 21st century, as also recognized by international institutions, such as the United Nations Framework Convention on Climate Change (UNFCCC). In this regard, global warming is one of the backbones of the CC paradigm, which is greatly caused by the increase of atmospheric carbon dioxide (CO_2), the most abundant greenhouse gas (GHG) in the Earth's atmosphere (IPCC, 2007). Overall, the global carbon (C) cycle depends on the balance between those processes acting as CO_2 sinks and sources within the several Earth subsystems: atmosphere, biosphere, cryosphere, hydrosphere and lithosphere. These processes occur at different temporal scales and modify the amount of C accumulated in the C reservoirs of every subsystem. Nevertheless, fossil fuel combustion, industrial activities and land use change have provoked the rise of atmospheric CO_2 molar fraction since the pre-Industrial Era to the present, from 275–284 ppm (Etheridge et al., 1996) to 406 ppm (Dlugokencky and Tans, 2014). Accordingly, the main goal of UNCFCC became to stabilize GHG concentrations "at a level that would prevent dangerous anthropogenic interference with the climate system". As a result, Kyoto Protocol arose in 1997 with the aim to limit global GHG emissions but also to protect and enhance GHG sinks and reservoirs as well as to promote sustainable forest management practices. Recently, the Paris Agreement (December 2015) undertook an ambitious effort to bound GHG emissions at an international scale with a primary goal of limiting global warming to well below 2°C and as close to 1.5°C as possible to prevent dangerous tipping points in the climate system. This objective, hence, entails a global and prompt reduction of GHG emissions to achieve climate neutrality in the second half of the century. Unfortunately, 40%

of the participating countries (192 and European Union in total) have not ratified the agreement yet.

Besides this collective institutional effort, during last two decades, anthropogenic CO_2 emissions has been still increasing up to a current estimated rate of ~10 Gt of C yr^{-1} (Le Quéré et al., 2015). However, the CO_2 growth rate within the atmosphere is half than expected owing to the mitigation role of biosphere, where terrestrial and aquatic ecosystems globally act as carbon sinks. In this regard, terrestrial ecosystems absorb a higher amount of atmospheric CO_2 compared to the ocean (Fig. 1) but also present a higher inter-annual variability that greatly drives the atmospheric CO_2 patterns (Le Quéré et al., 2015).
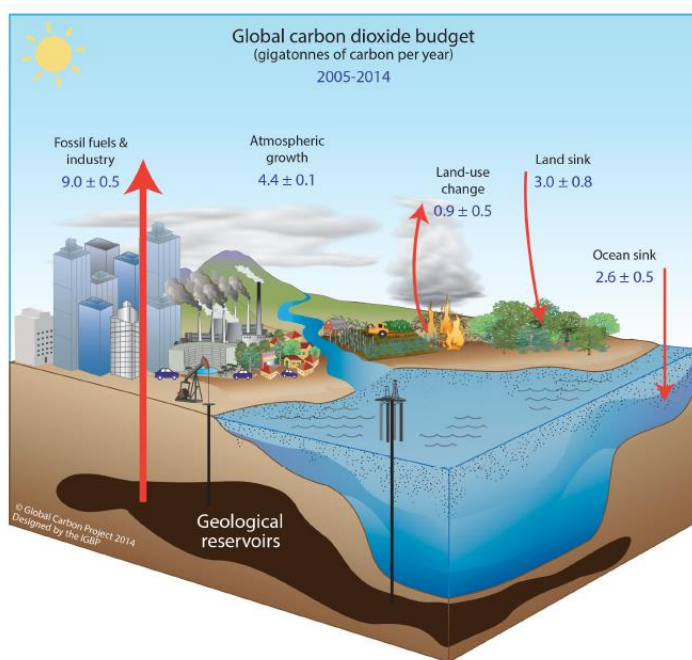
Figure 1. Schematic representation of the overall perturbation of the global carbon cycle caused by anthropogenic activities, averaged globally for the decade 2005–2014. The arrows represent emission and uptake of carbon dioxide in units of Gt C yr^{-1}. Source: Global Carbon Budget 2015 by Le Quére et al. (2015).

Therefore, to understand how terrestrial ecosystems actually behave is a precondition to know how they will respond to temperature and precipitation regimens associated to future CC scenarios. Additionally, the research of the feedback mechanisms that are actually occurring and are expected to continue in the future should be imperative. Overall, the complexity of the scheme is, in turn, the reason why an international and coordinate effort is needed over the long-term in order to design proper prevention, mitigation and adaptation policies based on the scientific evidence.

2. RESERVOIRS AND PROCESSES INVOLVED IN THE TERRESTRIAL CARBON CYCLE

In terrestrial ecosystems, soil corresponds to the major C reservoir, where ~1600 Gt of soil organic C (SOC) together with ~950 Gt of soil inorganic C (SIC) are stored (Safriel and Adeel, 2005), resulting in a total C reservoir of ~2500 Gt in the solid phase (Jobbagy and Jackson, 2000). In addition, the estimated global karst C storage in the gas phase within the vadose zone equates to ~2 Gt (Serrano Ortiz et al., 2011). Given that C atmospheric reservoir equates to approximately 800 Gt and global terrestrial biomass to ~600 Gt of C, soil C reservoir is three and four times the atmospheric and biomass reservoirs, respectively (Schlesinger, 1997). In this regard, the global C cycle is strongly linked to the terrestrial C balance owing to the wide array of involved processes that transfer a certain amount of C from one reservoir to another and also interact at several spatial and temporal scales. Apart from anthropogenic CO_2 emissions, these processes can be divided into biological and non-biological ones depending on their link with living organisms.

On one hand, biological processes are carried out by autotrophs and heterotrophs organisms. The term of Gross Primary Production (GPP)

corresponds to the amount CO_2 absorbed from the atmosphere by autotrophs organisms (i.e. plants) by means of the photosynthesis, through which plants convert solar radiation in chemical energy destined to biomass growth. Some of this fixed C is emitted to the atmosphere through roots, trunk, branches and leaves by means of autotrophic respiration (AR). Accordingly, the Net Primary Productivity (NPP) equates to the subtraction of AR to GPP (Fig. 2). Likewise, Aboveground NPP (ANPP) corresponds to the subtraction of aerial AR to aerial GPP, which includes the whole plant excepting the roots.

$$NEE = - NEP = - GPP + R_{eco}$$
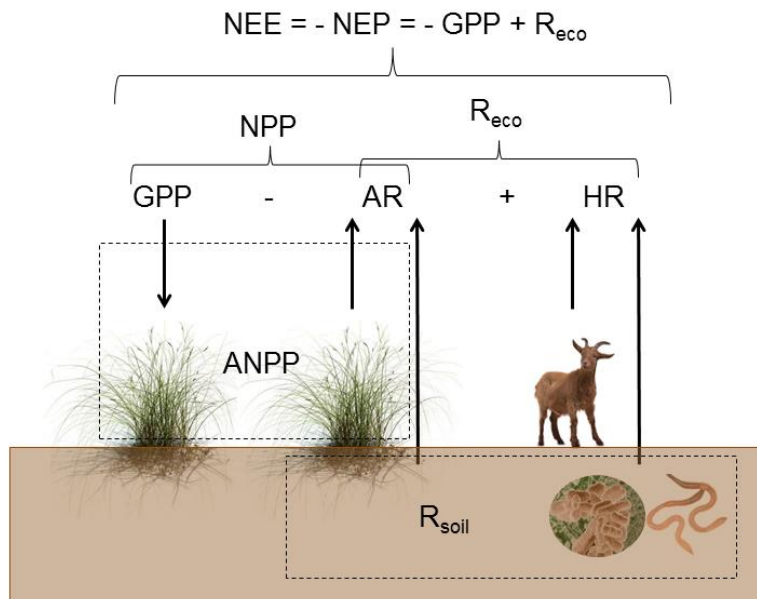
Figure 2. Schematic diagram of the biological processes composing the terrestrial C cycle.

Conversely, soil macro- and micro-organisms (and animals), as heterotrophs, degrade the non-recalcitrant components of senescent biomass by emitting CO_2 to the atmosphere through the heterotrophic respiration (HR). The sum of AR and HR is termed as the ecosystem respiration (R_{eco}; Fig. 2), while soil respiration (R_{soil}) corresponds to the sum of belowground AR (i.e. root respiration) and HR. The recalcitrant components of senescent biomass stabilize

and accumulate in the soils in the long-term, resulting in the greatest reservoir of organic C in terrestrial ecosystems. Overall, by upscaling NPP to the ecosystem level Net Ecosystem Productivity (NEP) is obtained, which roughly corresponds to the subtraction of R_{eco} to GPP. Likewise, Net Ecosystem CO_2 Exchange (NEE; Fig. 2) is the opposite of the NEP in the absence of other processes different to photosynthesis and respiration (Chapin et al., 2006).

On the other hand, the main non-biological processes related to terrestrial C cycle correspond to geochemical weathering processes, photodegradation, erosion and subterranean ventilation (Serrano-Ortiz et al., 2012). In this regard, geochemical weathering includes carbonates precipitation and dissolution, which can provoke net CO_2 uptake and release, respectively, at the short-term. Photodegradation consists on the breakdown of organic matter compounds by the direct incidence of solar radiation (Austin and Vivanco, 2006) provoking CO_2 effluxes (Rutledge et al., 2010). Erosion is a natural process that occurs when a liquid (air or water) moves into and/or across a soil surface with subsequent transport of the detached particles to another location reducing the amount of SOC in the eroded soil. Finally, subterranean ventilation (also termed "atmospheric or pressure pumping") corresponds to the advective transport of CO_2-rich air from the vadose zone to atmosphere (Sanchez-Cañete et al., 2011). All these processes acquire relevance when biological ones are constrained by some limiting factors, such as water, and can greatly contribute to the net C balance, especially in drylands.

3. AVAILABLE METHODOLOGIES TO QUANTIFY CO_2 EXCHANGE

Currently, there are several available techniques that allow the estimation of the biosphere-atmosphere CO_2 exchange. These methodologies can be

differentiated by their operational spatial scales but all of them entail the use of an Infrared Gas Analyzer (IRGA), which measures the amount of gaseous CO_2 within in a given gas volume.

In this regard, soil chambers permit the monitoring of the CO_2 efflux coming from soil patches, usually equated to R_{soil}. Similarly, the net CO_2 exchange between the leaves and atmosphere, namely ANPP, can be measured by using leaf cuvettes. However, when using this technique, the measurement of a high amount of leaves is necessary in order to acquire an accurate estimate of the plant-atmosphere CO_2 exchange. Consequently, canopy chambers can enclose a whole plant, shrub or tree and hence, result in a more suitable method to measure the whole canopy CO_2 flux, which also equates to ANPP. Apart from chamber methods, CO_2 probes has been utilized since last decade and permits the continuous measurement of the amount of CO_2 within the soil and vadose zone as well as the estimation of the soil CO_2 efflux. In general, first measurements of the gaseous CO_2 exchange between terrestrial ecosystems and atmosphere were performed in the 60s by using these manual chambers, allowing punctual measurements of separated components of an ecosystem (i.e., soil, plants or leaves). However, these chamber methods show low temporal and spatial resolutions since, logistically, it is difficult to obtain long-term measurements with a high number of replicates in order to acquire statistically reliable results (Baldocchi et al., 1988) and moreover, its use entails the perturbation of the measured targets. Subsequently, more sophisticated and less invasive methods such as the Eddy Covariance (EC) technique was developed thanks to the technological progress occurred over the 80s (Baldocchi, 2008).

This micrometeorogical technique permits non-invasive, long-term monitoring of turbulent energy, momentum and mass fluxes, including the net CO_2 flux, at ecosystem scale and at a high temporal resolution (from minutes to

hours). Thus, one of the main advantages of the EC methodology is that allows continuous measurements of *in situ* net ecosystem-atmosphere CO_2 exchange (NEE) without its perturbation. Additionally, one time-averaged EC measurement at a point integrates the flux rates generated within a whole influencing area, also termed as footprint, as a result of the turbulent transport. This footprint area must be located within the fetch, a delimited and homogeneous area where the ecosystem of study is well represented. Therefore, the EC spatial resolution corresponds to an intermediate scale between satellite pixels (from hundreds of squared meters to kilometers) and experimental inventories, which commonly focus on ecosystems' plots or plant individuals. Accordingly, EC measurements integrate the ecological systems complexity, which is defined by multi-scale processes that occur simultaneously, interact and ultimately determine the whole ecosystem structure and functioning. However, by using solely the EC technique, we cannot quantify the component processes of the NEE without its combination with other methods, such as flux chambers.

Therefore, the implementation of EC stations has expanded from the 80s, especially, in developed countries. In fact, in 1997, a global network called FLUXNET was created (Baldocchi et al., 2001) encompassing, in turn, two main regional networks set in Europe (EUROFLUX) and North America (AMERIFLUX). Consequently, the majority of EC stations working over longer periods have been concentrating in the Northern hemisphere and at medium latitudes, concretely in Central Europe, Japan or United States (Fig. 3). Consequently, the unevenly distribution of the monitored terrestrial ecosystems has leaded to a deeper knowledge of the mechanisms and processes that drive C cycle in temperate ecosystems in detriment of other ecosystems types, such as

drylands.
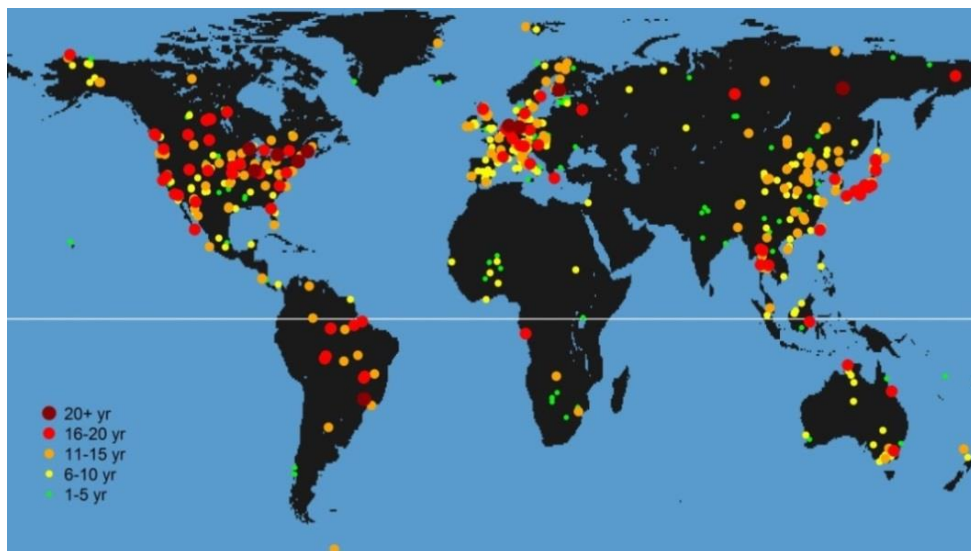
Figure 3. All experimental sites included in the FLUXNET network in 2015.
Source: http://fluxnet.fluxdata.org/community/photo-gallery/

4. DRYLANDS' CARBON CYCLE

Currently, drylands occupy more than one third of the global land surface and are inhabited by 36% of Earth's population (Fig. 4; Safriel and Adeel, 2005). Indeed, drylands have expanded for the last sixty years and, even, are projected to expand under future climate change scenarios (Feng and Fu, 2013). Regarding their C cycle, while only 14% of the global biotic C pool is found in drylands (IPCC, 2011), soil organic and inorganic C pools equate to 431 and 916 Gt of C, respectively, corresponding to 27% and 97% of the global soil organic and inorganic C reservoirs (Allen-Diaz et al., 1995; Eswaran et al. 2000). Drylands subtypes encompass hyper-arid, arid, semiarid and dry subhumid areas with deserts, grasslands, shrublands and forests biomes. The major fraction of drylands corresponds to semiarid ecosystems with 37% of the global dryland area (Safriel and Adeel, 2005), where the dominant biome is

grassland. Overall, drylands are deemed to be dynamic but vulnerable natural systems against climatic changes and degradation processes associated to global change (Lal, 2001).
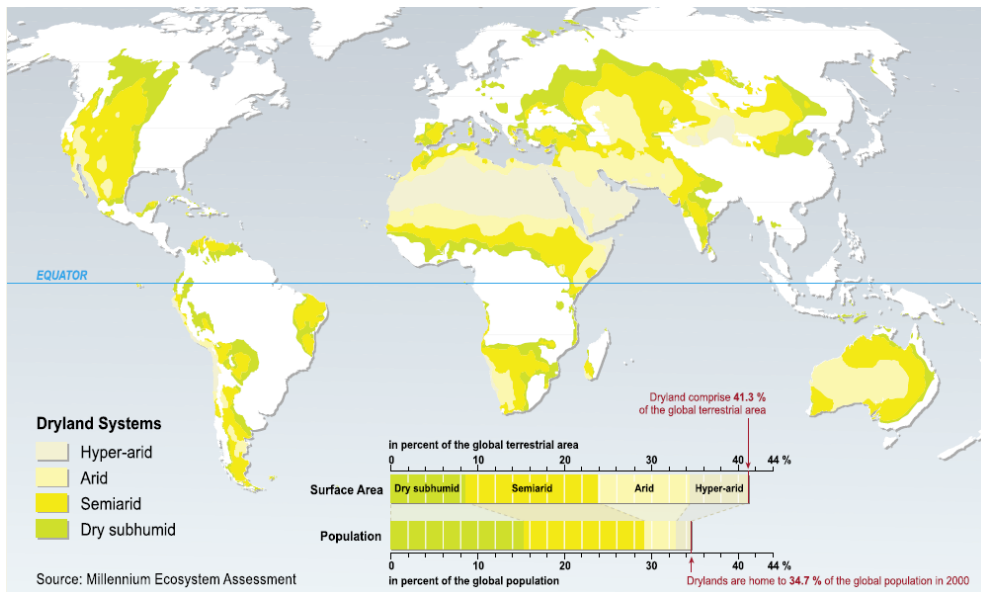
Figure 4. Drylands subtypes extension in the global land surface.
Source: Ecosystems and human well-being: desertification synthesis
by Board M.E.A. (2005).

In this regard, water scarcity corresponds to the main limitation that constrains photosynthesis as well as respiration in arid regions (Tang and Baldocchi, 2005), while, in temperate ecosystems, solar radiation density (Michaelis and Menten, 1913) and temperature (Lloyd and Taylor, 1994) are the most important limiting factors of biological activity. Hence, the main difference between drylands and temperate ecosystems stems from the limiting factors that drive their structure and functioning. In this sense, the well-known dependency between the C cycle and its driving factors in medium-latitude ecosystems has been widely used to discriminate between photosynthesis and respiration when measuring net CO_2 exchange at ecosystem scale (Reichstein et al., 2005) with EC technique. However, the use of these partitioning techniques

is limited in drylands given their reliance on hydric resources (Noy-Meir, 1973) and moreover, due to the occurrence of non-biological processes.

In this context, several studies have demonstrated the influence of these non-biological processes in the ecosystem-atmosphere CO_2 exchange, especially, under extreme drought conditions during summer months, when, in turn, biological activity is substantially reduced. Firstly, the CO_2 fluxes related to geochemical weathering that have been reported are low (i.e. < 1 µmol m^{-2} s^{-1}; Hamerlynck et al., 2013; Roland et al., 2013; Serrano-Ortiz et al., 2010). Secondly, the photodegradation process has been related to CO_2 effluxes (Rutledge et al., 2010) over the dry season in arid ecosystems, nevertheless, the magnitude of the observed C loss was below 0.2 µmol m^{-2} s^{-1} (Brandt et al., 2009; Rutledge et al., 2010). In contrast, subterranean ventilation has been linked to more sizeable CO_2 release of one to two orders of magnitude higher (Kowalski et al., 2008; Rey et al., 2012; Serrano-Ortiz et al., 2009).

Overall, drylands functioning has been recently recognized as determinant in the inter-annual variability of the global C budget (Ahlström et al., 2015; Poulter et al., 2014). However, more research is needed in order to address key unresolved questions related to drylands C cycle. On one hand, an increase in the number of monitored ecosystems located in drylands would be beneficial to acquire representative estimates of drylands' C balance worldwide. Additionally, the continuity of these measurements is crucial in order to quantify how climate fluctuations, antecedent conditions and disturbances affect net C exchange and its component processes (Baldocchi, 2008). On the other hand, relevant and specific issues related to drylands' functioning are still in a preliminary research status. Firstly, the influence of land degradation in the C sequestration capacity of drylands has never been quantified at ecosystem-level by using the EC technique. Secondly, further research focused on the link

between precipitation distribution and magnitude and drylands' C balance is indispensable in order to build more accurate terrestrial C models. Finally, non-biological processes, and concretely, subterranean ventilation, which has been traditionally neglected, must be deeply investigated given its potential outstanding role in drylands' C balance.

5. JUSTIFICATION

To deeply understand the global C cycle is a precondition to develop accurate terrestrial C models that will allow us to identify the feedback mechanisms between terrestrial biosphere and global change that may reduce the mitigation role of biosphere against global warming. However, besides their great global extension, drylands' are underrepresented in global long-term monitoring infrastructures designated to directly measure biosphere-atmosphere CO_2 exchange. Thus, our principal aim is to investigate the relevant processes involved in the C balance of drylands and especially, of semiarid ecosystems, which correspond to the drylands' subtype with the largest global extension. Concretely, this thesis is spatially framed in two experimental sites of Cabo de Gata-Níjar Natural Park (Almeria), which is located in Southeastern Spain, the most arid region of Europe where ecosystems are subjected to high aridity conditions and degradation processes. Overall, the eddy covariance technique, in combination with other methodologies, results in a quite suitable method to quantify C balance of the semiarid ecosystems of study by integrating all subsystems (i.e. soil, plants, and microorganisms) into a whole ecosystem-scale assessment.

6. OBJECTIVES AND THESIS OUTLINE

The aims of this thesis can be summarized in three main specific objectives:

- to evaluate the effect of land degradation processes on the C balance of semiarid ecosystems. Thus, a comparison between C sequestration capacities of two semiarid ecosystems showing a differing degradation status has been developed in **Chapter 1**, entitled "**Can land degradation drive differences in the C exchange of two similar semiarid ecosystems?**";

- to quantitatively and qualitatively assess the response of semiarid ecosystems to rain pulses, which has been carried out in **Chapter 2**, entitled "**Enhancement of the net CO_2 release of a semiarid grassland in southeast Spain by rain pulses**";

- to investigate the relevance and driving factors of subterranean ventilation, a non-biological and poor known process that potentially can contribute to the net CO_2 exchange of semiarid ecosystems. Hence, the study is described in **Chapter 3**, entitled "**Subterranean ventilation of allochthonous CO_2 governs net CO_2 exchange in a semiarid Mediterranean grassland**".

Accordingly, the general goal of this thesis is to improve the knowledge of C cycle in drylands by quantifying the C balance of semiarid ecosystems and exploring the relevance of its involved processes as well as its dependency with land degradation processes and water resources.

MATERIAL AND METHODS

1. EXPERIMENTAL SITES DESCRIPTION

The study area of the present research is located in the southeast of Spain, which represents the driest part of Europe. The two experimental sites investigated, Balsa Blanca and Amoladeras, are located within the Cabo de Gata-Níjar Natural Park (Almería, Spain; Fig. 1).
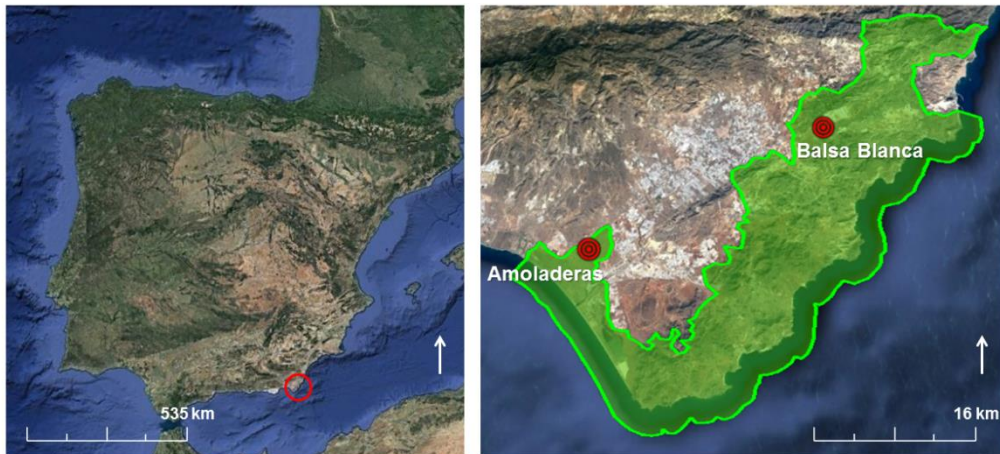
Figure 1. Location of the study area. Green area represents the Cabo de Gata-Níjar Natural Park.

The experimental sites are quite similar, in terms of climate and ecosystem type. The climate of both sites is a desert climate, according to Köppen classification (Bwh; Kottek et al., 2006), with a mean annual temperature of 18°C and mean annual precipitation of approximately 220 mm, and prevailing wind directions are Northeast and Southwest. The ecosystem type corresponds to "espartal", a Mediterranean semiarid grassland where the dominant species is *Machrocloa tenacissima* (Fig. 2). This perennial tussock grass is very well adapted to semiarid and arid conditions owing to its shallow root system and physiological tolerance and avoidance strategies against hydric stress (Haase et al., 1999; Pugnaire et al., 1996). *Machrocloa* sp. can be found in vast territories within the Western Mediterranean region, given its great ecological amplitude (Maestre, 2007). Concretely, in the Northwest Africa the area corresponding to

"espartal" ecosystem type represents 6,000,000-8,000,000 ha in the Northwest Africa (Le Houérou, 1986) and 409,000 ha in the Iberian Peninsula (Ministerio de Medio Ambiente, 1999). This species usually shows patchy distribution resulting in unequal availability of nutrients and water resources in drylands, which corresponds to the well-documented "islands of fertility" (Charley and West, 1975; Cross and Schlesinger, 1999; Maestre et al., 2007).

Regarding the functioning of both experimental sites, the growing season usually begins in late autumn and ends in early spring, when the temperature starts to rise and water resources have not yet become scarce (Serrano-Ortiz et al., 2014). In addition, a long drought period with high temperatures, absence of precipitation and high incident radiation causes a prolonged period of hydric stress, usually from May to September-October, when first rainfall events occur, after the dry season. Additionally, water inputs derived from relevant dewfall episodes have been previously reported (Uclés et al., 2014) in the area, which may rehydrate soil and plants during night and early morning hours.

Figure 2. "Espartal" ecosystem in Cabo de Gata-Níjar Natural Park. Photograph author: Ana López Ballesteros.

Apart from this, the experimental sites show some differences explained below.

1.1. AMOLADERAS EXPERIMENTAL SITE

The study site of Amoladeras (N36.8336°, W2.2523°; Fig. 1) is located at an altitude of 65 m above sea level and 3.6 km from the Mediterranean Sea. Typical soils, classified as Calcaric Lithic Leptosol (World Reference Base for Soil Resources, 2006), are thin (0.10 m of maximum soil depth), alkaline (pH above 8), and include petrocalcic horizons (Weijermars, 1991). Texture is sandy loam with sand (58.4%), silt (27%), and clay (14.5%) and with a bulk density of 1.11 g cm^{-3}. Ground cover fractions consist on bare soil (8.1%), gravel (21.1%), rock (14%), litter (10.5%) and biological soil crust (23.1%) and vegetation (23.1%). The vegetation distribution is patchy, and the main plant species are *Chamaerops humilis, Rhamnus lycoides, Pistacia lentiscus, Asparagus horridus, Olea europea* var. *sylvestris, Rubia peregrina* and *Machrocloa tenacissima,* which is clearly the most abundant (>50% of total plant cover; Rey et al., 2011).

1.2. BALSA BLANCA EXPERIMENTAL SITE

The experimental site of Balsa Blanca (N36.9394°, W2.0340°; Fig. 1) is an alpha grassland located at an altitude of 208 m above sea level and situated 6.3 km from the Mediterranean Sea. Prevailing soils, classified as Mollic Calcaric Lithic Leptosol (World Reference Base for Soil Resources, 2006), are thin (0.20 m of maximum soil depth), alkaline (pH above 8), and include petrocalcic horizons (Weijermars, 1991). Texture is sandy loam with sand (61%), silt (23%), and clay (16%) with a bulk density of 1.25 g cm^{-3}. Ground cover consists of bare soil (0.3%), gravel (8.6%), rock (1.5%), litter (8.1%) and biological soil crust (18.2%) and vegetation (63.2%). Although there are other species such as *Chamaerops humilis*, *Rhamnus lycoides*, and *Pistacia lentiscus*,

the dominant species is *Machrocloa tenacissima* (>50% of total plant cover; Rey et al., 2011).

These two experimental sites represent different degradation stages according to the ecosystem classification performed by Escribano et al. (2002) and based on soil characteristics and ground cover fractions (Cammeraat, 1996; Dregne, 2002). Therefore, Balsa Blanca could represent a low degradation status while Amoladeras could exemplify a more developed degradation status (Rey et al., 2011).

2. APPLIED METHODOLOGIES

2.1. EDDY COVARIANCE MONITORING STATIONS

Two eddy covariance (EC) monitoring stations were installed in Amoladeras and Balsa Blanca in July 2007 and June 2006, respectively. The characteristics of both locations are ideal to feasibly use the EC technique, since both areas are quite flat and the surface is very homogeneous, what assures that the area sampled by the EC tower (footprint) is representative of the whole ecosystem area (fetch). The EC technique represents the principal methodology of this thesis, since all chapters of the results section include EC results.

All data acquired are shared with the research community through the European Fluxes Database Cluster (http://www.europe-fluxdata.eu/), which is an international initiative whose goals are to harmonize and integrate databases generated through a wide variety of European projects focused on GHGs flux measurements. Sites codes of our experimental sites within this database are "ES-Amo" and "ES-Agu", for Amoladeras and Balsa Blanca, respectively.

Figure 3. Eddy covariance stations of Balsa Blanca (right) and Amoladeras (left) experimental sites. Photograph author: Enrique P. Sánchez-Cañete.

2.1.1. INSTRUMENTATION AND DATA ACQUISITION

The fundamental instrumentation of the EC stations are two fast-response sensors that allow the measurement of turbulent fluxes. On one hand, the infrared gas analyzer (IRGA) measures the trace gas (such as CO_2) and water vapor densities and its functioning is based on Beer-Lambert law. On the other hand, the sonic anemometer measures the speed of sound, from which sonic temperature is derived, and the 3-D wind speed. Additionally, other ambient variables were also measured in order to interpret and analyze turbulent fluxes. Detailed information regarding measured variables, sensors used and installation height in both experimental sites can be found in Table 1.

Regarding data acquisition, the core variables needed for turbulent flux calculation (CO_2 and water vapor densities, air pressure, 3-D wind speed and sonic temperature) were measured and logged at a frequency of 10 Hz (i.e. raw data), while measurements of ambient variables (Table 1 and 2) were registered as half-hourly averages. Data acquisition systems consisted on dataloggers (CR3000, CR10 and CR10X, Campbell Scientific, Logan, UT, USA).

2.1.2. EDDY COVARIANCE DATA PROCESSING

The whole scheme of EC data processing comprises several stages: data pre-processing, flux calculation, flux correction and flux quality check and assurance. Additionally, every stage includes several processing steps, as depicted in Table 2. Most of these processing steps were performed using the EddyPro® software (version 5.2.1; LI-COR, Inc. 2014).

Variable	Sensor	Sensors height	
		Amoladeras	**Balsa Blanca**
Eddy Covariance system			
A three-axis sonic anemometer (CSAT-3, CSA)	Wind speed (3-D) and sonic temperature	3.05 m	2.90 m
An open-path infrared gas analyzer (Li-Cor 7500, Lincoln, NE, USA)	Pressure, CO_2 and H_2O vapour densities	3.05 m	2.90 m
Meteorological and soil measurements			
Two PAR sensors (Li-190, Li-Cor, Lincoln, NE, USA)	Photosynthetic Photon Flux Density	1.40 m	1.50 m
A net radiometer (NR Lite, Kipp&Zonen, Delft, Netherlands)	Net Radiation	1.70 m	1.50 m
A thermohygrometer (HMP35-C, CSI)	Air temperature and air humidity	3.62 m	1.50 m
Two heat flux plates (HFP01SC, Hukseflux, Delf, Netherlands)	Soil heat flux	-0.08 m	-0.08 m
Two water content reflectometers (CS616, CSI)	Subsoil Water Content	-0.05, -0.15 and -1.50 m	-0.05 and -1.50 m
Two soil temperature probes (TCAV, CSI)	Subsoil temperature	-0.05, -0.15 and -1.50 m	-0.05 and -1.50 m
CO_2 sensor (GMP-343, Vaisala, Inc., Finland)	Subsoil CO_2 molar fraction	-0.05 m	-0.05 m
CO_2 sensor (GMM222, Vaisala, Inc., Finland)	Subsoil CO_2 molar fraction	-0.15 and -1.50 m	-1.50 m
A tipping bucket (0.2 mm) rain gauge (785 M, Davis Instruments Corp., Hayward, CA, USA)	Rainfall	1.30 m	1.40 m

Table 1. Sensors used to measured variables and their installation height in Amoladeras and Balsa Blanca experimental sites. CSI is an abbreviation of "Campbell Scientific, Logan, UT, USA".

Processing stages	Processing steps
Data pre-processing	- *Despiking* - Statistical flagging
Data processing	- Coordinates rotation - Flux calculation - Random uncertainty estimation
Data post-processing: Flux correction	- WPL correction - Spectral corrections
Data post-processing: Quality check and assurance	- Quality flagging - Flux data screening

Table 2. Processing scheme applied to the EC data used in the present study.

2.1.2.1. DATA PRE-PROCESSING

This data processing stage is based on the publication of Vickers and Mahrt (1997). It entails raw data (10 Hz) preparation prior to flux calculation and includes several statistical tests that are used to detect, and occasionally eliminate, anomalies in the time series of the core variables (Table 3). The unique processing step that implies elimination of anomalous raw data is the *despiking* process. It involves the detection and removal of spikes, which consist on one to three consecutive outranged values (out of plausibility ranges) found in every 5min time window within the time series of the core variables. The plausibility ranges used are defined in Table 3.

25

Core variables	Plausibility range (σ units)
Horizontal wind speed (u)	5
Vertical wind speed (w)	3.5
Cross-stream wind speed (v)	3.5
Sonic temperature (T_s)	3.5
CO_2 density (ρ_c)	3.5
H_2O density (ρ_v)	8

Table 3. Plausibility ranges, in terms of standard deviation (σ) units, of the core variables used in the *despiking* process.

Additionally, a set of statistical tests were performed to detect drop-outs, excessive skewness and kurtosis, presence of long-duration outranged values and insufficient variables fluctuations. The outputs of these tests were used to flag half-hourly fluxes based on their raw data statistical characteristics. In the post-processing stage and concretely, in the data screening process, the statistical outputs used were the number of spikes and the excessive skewness and kurtosis flag. The upper and lower limits used for detecting excessive skewness and kurtosis (for all the core variables), which, in turn, can be derived from instrument malfunction, are defined in Table 4.

Limits	Value
Skewness lower limit	-1
Skewness upper limit	1
Kurtosis lower limit	2
Kurtosis upper limit	5

Table 4. Ranges of skewness and kurtosis used to flag half-hourly averages of the core variables.

2.1.2.2. FLUX CALCULATION

This processing stage includes coordinates rotation for tilt correction and flux calculation based on Reynolds decomposition.

Firstly, coordinates rotation is performed in order to assure that the vertical component of the wind speed used for flux calculation is actually perpendicular to the surface. The method we used is the double-rotation method (McMillen, 1988; Kowalski et al., 1997), which, briefly, consists on the transformation of the original coordinates (derived from the anemometer position) by maximizing the horizontal component of the wind speed, u, and hence, nullifying v and w wind speed components over the time period defined by the flux averaging length. This method has been recommended for homogeneous and flat surfaces, such as grasslands.

Secondly, the high-frequency raw data registered at EC stations, after spikes removal, statistical flagging and coordinates rotation, are used to calculate CO_2, water vapor, sensible and latent heat flux densities, commonly and hereinafter termed as "fluxes".

In this regard, the turbulent flux of a scalar magnitude, for instance, the CO_2 density, can be defined as the amount of CO_2 that moves through a unit of area perpendicular to the movement direction per unit of time. Then, the velocity component of the movement direction would cause the transport and consequently, the flux itself. Hence, flux calculation is based on the interaction of vertical wind speed (w, m s^{-1}) and CO_2 molar density (ρ_c, mmol m^{-3}), being both variables directly measured by EC systems.

Reynolds decomposition (also termed as "block average") is commonly used to describe turbulent transport and is based on the following equation:

$$\xi = \bar{\xi} + \xi'$$
(Eq. 1)

where any measured variable ξ can be decomposed as the sum of its averaged value $\bar{\xi}$ and its fluctuation ξ', an instantaneous value with regard to the mean or

averaged value. Therefore, when we have a product of variables, for example w and ρ_c, we should operate as follows:

$$w\rho_c = (\bar{w} + w')(\bar{\rho_c} + \rho'_c) =$$

$$= \overline{w}\overline{\rho_c} + \overline{w}\rho'_c + w'\overline{\rho_c} + w'\rho'_c \qquad \text{(Eq. 2)}$$

However, to estimate a flux value, it is more suitable to use an averaged value instead of a punctual value, since the latter usually shows great variability given the chaotic nature of turbulence. Consequently, by averaging Eq. 2, the expression takes the form:

$$\overline{w\rho_c} = \overline{\overline{w}\overline{\rho_c}} + \overline{\overline{w}\rho'_c} + \overline{w'\overline{\rho_c}} + \overline{w'\rho'_c} \qquad \text{(Eq. 3)}$$

In the expression above, all the terms including averaged fluctuations are null, since negative and positive fluctuations compensate each other, resulting in an averaged fluctuation of zero. Thus, the simplified version of Eq. 3 is described below as:

$$\overline{w\rho_c} = \overline{\overline{w}\overline{\rho_c}} + \overline{w'\rho'_c} \qquad \text{(Eq. 4)}$$

where the averaged scalar flux ($\overline{w\rho_c}$) can be decomposed as the sum of a mean transport ($\overline{\overline{w}\overline{\rho_c}}$) and a turbulent transport ($\overline{w'\rho'_c}$), being the latter the dominant term.

In this way, uncorrected turbulent flux of the measured trace gas, in our case CO_2, can be calculated, in our system, as follows:

$$F_{c\_uncorr} = 10^3 \, \overline{w'\rho_c'} \qquad \text{(Eq. 5)}$$

where F_{c_uncorr} (μmol m^{-2} s^{-1}) is the uncorrected averaged turbulent CO_2 flux and $\overline{w'\rho_g'}$ is the covariance between vertical wind speed (m s^{-1}) and the CO_2 molar density fluctuations (mmol m^{-3}) over the averaging period, which equates

to 30 minutes, based on international research community recommendations (Aubinet et al., 1999).

Similarly, uncorrected water vapor flux, latent heat flux, evapotranspiration flux and sensible heat flux were calculated based on the following equations:

$$F_{v\_uncorr} = \overline{w'\rho_v'} \qquad \text{Eq. (6)}$$

where F_{v_uncorr} (mmol m^{-2} s^{-1}) is the uncorrected averaged turbulent flux of water vapor and $\overline{w'\rho_v'}$ is the covariance between vertical wind speed (m s^{-1}) and the molar density of water vapor (mmol m^{-3}).

$$LE_{uncorr} = 10^{-3} F_{v\_uncorr} \lambda M_{H2O} \qquad \text{Eq. (7)}$$

where LE (W m^{-2}) is the uncorrected latent heat flux, F_{v_uncorr} (mmol m^{-2} s^{-1}) is the uncorrected averaged turbulent flux of water vapor, λ is the specific evaporation heat (J kg^{-1}) and M_{H2O} is the molecular weight of water (kg mol^{-1}).

$$ET_{uncorr} = 10^{-3} F_{v\_uncorr} M_{H2O} \qquad \text{Eq. (8)}$$

where ET is the uncorrected evapotranspiration flux (kg m^{-2} s^{-1}), F_v (mmol m^{-2} s^{-1}) is the averaged turbulent flux of water vapor and M_{H2O} is the molecular weight of water (kg mol^{-1}).

$$H_{uncorr} = \overline{\rho_a} c_p \overline{w'T_s'} \qquad \text{Eq. (9)}$$

where H_{uncorr} is the uncorrected sensible heat flux (W m^{-2}), $\overline{\rho_a}$ is the half-hourly averaged moist air density (kg m^{-3}), c_p is the moist air heat capacity at constant pressure (J kg^{-1} K^{-1}) and $\overline{w'T_s'}$ is the covariance between vertical wind speed (m s^{-1}) and sonic temperature (K).

For all fluxes defined above, half-hourly covariances, variances, averages and fluxes were calculated only when missing raw data were less than 10% over every half-hourly period. Additionally, random uncertainty was estimated for CO_2, water vapor, latent and sensible heat fluxes according to (Finkelstein and Sims, 2001). This uncertainty is a consequence of analyzing a continuous process by means of discrete samples (half-hourly averaged fluxes) and cannot be avoided.

2.1.2.3. FLUX CORRECTION

The main two flux corrections that were applied at the post-processing stage were spectral corrections and density-fluctuation corrections.

Firstly, spectral corrections includes both low and high frequency corrections and must be applied because most EC systems cannot measure effectively in the lowest (high-pass filtering) and highest frequency ranges (low-pass filtering). On one hand, the low-pass filtering corresponds to the impossibility to measure very small eddies and is related to the limited sampling frequency, the use of linear methods for detrending and the physical separation between sonic anemometer and the IRGA. To correct spectral bias in the high frequency range we used the method proposed by Moncrieff et al. (1997). On the other hand, the high-pass filtering results in missing measurements of very large eddies and is related to the selected averaging period. To correct spectral bias in the high frequency range we used the method proposed by Moncrieff et al. (2004). Additionally, EC tower height also provokes spectral biases. Tall EC towers has lower low-frequency range losses since can measure larger eddies while small EC towers has lower high-frequency range losses and can registered fluctuations derived from smaller eddies.

Secondly, the density-fluctuation correction applied to trace gas fluxes, such as CO_2 flux, must be performed in order to exclude variations of the trace gas density due to changes in the sampled air density derived from temperature or water vapor fluctuations. This correction has been applied according to Webb et al. (1980). The correction takes the form:

$$F_c = F_{c\_uncorr} + \overline{\rho_c}\left[\mu\frac{F_{v\_uncorr}}{\overline{\rho_d}} + \left(1 + \mu\frac{\overline{\rho_c}}{\overline{\rho_d}}\right)\frac{\overline{w'T_s'}}{\overline{T_s}}\right] \qquad \text{Eq. (10)}$$

where F_c (µmol m^{-2} s^{-1}) is the corrected CO_2 flux, F_{c_uncorr} (µmol m^{-2} s^{-1}) is the uncorrected averaged turbulent CO_2 flux, $\overline{\rho_c}$ (µmol m^{-3}) is the averaged CO_2 density, µ is the ratio between dry air molar mass and water vapor molar mass (1.6077), F_{v_uncorr} (µmol m^{-2} s^{-1}) is the uncorrected averaged turbulent water vapor flux, $\overline{\rho_d}$ (µmol m^{-3}) is the dry air density , $\overline{w'T_s'}$ (K m s^{-1}) is the covariance between vertical wind speed and sonic temperature and $\overline{T_s}$ (K) is the averaged sonic temperature. The first term of Eq. 10 corresponds to the calculated CO_2 flux, the second term represents the water vapor dilution correction and the third term denotes the thermal expansion-compression correction. When correcting the water vapor flux only the thermal expansion-compression correction term is applied.

Similarly, sensible heat flux was corrected for humidity effects according to van Dijk et al. (2004). The equation takes the form:

$$H = H_{uncorr} - \overline{\rho_a}c_p\alpha\left(\overline{T_s}\frac{ET}{\overline{\rho_a}} + Q\,\overline{w'T_s'}\right) \qquad \text{Eq. (11)}$$

where H is the corrected sensible heat flux (W m^{-2}), H_{uncorr} is the uncorrected one (Eq. 9), $\overline{\rho_a}$ is the half-hourly averaged moist air density (kg m^{-3}), c_p is the moist air heat capacity at constant pressure (J kg^{-1} K^{-1}), α=0.51, $\overline{T_s}$ is the half-hourly averaged sonic temperature (K), ET is the evapotranspiration flux (kg m^{-2}

s^{-1}) with the thermal correction applied, Q is the specific humidity (kg kg^{-1}) and $\overline{w'T_s'}$ is the covariance between vertical wind speed (m s^{-1}) and sonic temperature (K).

2.1.2.4. FLUX QUALITY CHECK AND ASSURANCE

Finally, in order to assure the analysis of the best quality flux data in the results section, we performed both quality check and post-processing data screening.

On one hand, the aim of the quality check process is to filter out those data corresponding to periods when stationarity and turbulence conditions are not sufficient and hence, measurements can correspond to inaccurate fluxes. This process is based on the "*steady state test*" and the "*developed turbulence conditions test*" (Foken and Wichura, 1996). Briefly, the *steady state test* is based on the comparison of the covariances calculated over 30-min period and shorter intervals within this period (frequently 5 min). Accordindly, when the difference between both covariances is below 30% , a half-hourly averaged flux is considered to be steady state (Mauder and Foken, 2004). The *developed turbulence conditions test* consists on the flux-variance similarity where the ratio of the standard deviation of a turbulent parameter and its turbulent flux (measured parameter) is a function of the stability (modelled parameter). In this regard, well developed turbulence coincides with periods when the difference between measured and modelled parameters is lower than 30% (Mauder and Foken, 2004). As a result, individual quality flags derived from every test are combined to provide a single quality flag per flux (F_c, F_v and H). The final flagging system applied is the described by Mauder and Foken (2004), which consists on quality flags from "0", for the best quality fluxes (differences <30% for both tests), to "2", for those fluxes that must be excluded from the analysis (differences >30% for both tests). Intermediate quality fluxes show a quality

flag of "1" (differences <30% for one test). In order to estimate annual carbon balances of our experimental sites, we used fluxes whose quality flags were "0" and "1", however, when analyzing specific processes we only used the best quality flux data (i.e. quality flag of "0").

On the other hand, the main goal of the post-processing flux data screening process was to exclude erroneous data corresponding mainly to instrument malfunction prior to analysis. This method was applied to F_c, F_v and H fluxes and its core variables (ρ_c, ρ_v and T_s). The screening process was based on the outputs of several previous processing steps, such as pre-processing statistical tests, flux calculation and random uncertainty estimation as half-hourly outputs related to every flux value. Therefore, flux data were excluded from subsequent analysis when:

(i)   excessive skewness and kurtosis was detected in the raw data (ρ_c, ρ_v and T_s) through its statistical output flag,

(ii)   in case of T_s, the number of spikes detected was above 100,

(iii)   random uncertainty estimated for F_c, F_v and H fluxes exceeded 4 μmol m^{-2} s^{-1}, 10 mmol m^{-2} s^{-1} and 50 W m^{-2}, respectively, and

(iv)   variances of ρ_c, ρ_v and T_s exceeded 0.1 (μmol m^{-3})^2, 100 (mmol m^{-3})^2 and 5 K^2, respectively.

2.2.   ADDITIONAL METHODOLOGIES

Some additional methodologies were occasionally used together with the EC technique in order to answer specific scientific questions (results section). Concretely, flux chambers were used in the first chapter of the results section, subsoil CO_2 sensors were used in all chapters and MODIS Land Products were used in the third chapter of the results section. A detailed description of these methodologies can be found below.

2.2.1. FLUX CHAMBERS

Flux chambers are a wide-used methodology that permits the measurement of isolated components of ecosystem-atmosphere gas exchange, such as plant- or soil-atmosphere gas exchange. The flux chambers utilized in this thesis are closed, dynamic, portable and non-steady state, since ambient variables, such as relative humidity or temperature, change over the measurement length (Reicosky et al., 1990). Concretely, when measuring the CO_2 flux derived from either plants or soil plots, the system directly registers the accumulated CO_2 molar fraction inside the chamber volume (where plants and soil plots are enclosed) over a certain period by using an IRGA. To estimate the CO_2 fluxes, we firstly corrected CO_2 molar fraction data for dilution effect (Hubb, 2012), which is provoked by water addition during the closure time, as follows:

$$X_c = \frac{X\prime_c}{1 - X_v \, 10^{-3}} \qquad \text{Eq. (12)}$$

where X_c is the corrected CO_2 molar fraction (ppm), $X\prime_c$ is the uncorrected CO_2 molar fraction (ppm) and X_v is the water vapor molar fraction (ppt). Hence, through this correction we convert CO_2 molar fraction referred to moist air to CO_2 molar fraction referred to dry air.
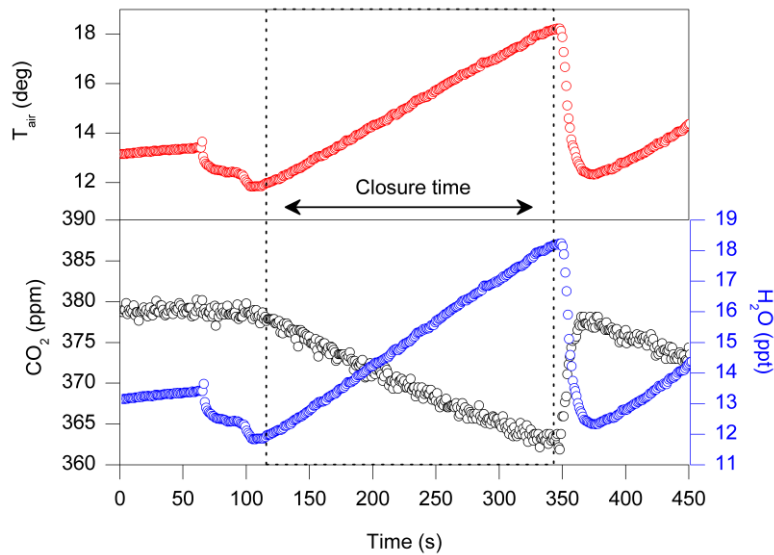
Figure 4. Variation in air temperature (T_{air}), CO_2 and H_2O molar fractions over the closure time, when data used for flux estimation is registered.

Afterwards, we estimated CO_2 fluxes based on the variation of corrected CO_2 molar fraction over time (Fig. 4), concretely, from the initial slopes of corrected CO_2 molar fractions of the confined air versus time to better assess the pre-deployment and less disturbed CO_2 flux (Livingston and Hutchinson, 1995), by using either linear or quadratic regression for the best regression fit.

In this regard, the quadratic regression was also used because, as said above, these closed chambers are non-steady state and during the closure time the air conditions in the confined volume are disturbed related to its pre-deployment status, what may produce a non-linear effect on CO_2 molar fraction variation over closure time (Kutzbach et al., 2007; Wagner et al., 1997). Hence, the closure time must be defined by minimizing disturbance on ambient conditions but also minimizing flux random errors derived from short closure times (Pérez-Priego et al., 2015).

Finally, the CO_2 flux calculation was performed based on Ideal Gas law, according to Pérez-Priego et al. (2015), by using the following equation:

$$F_c = \frac{\partial X_c}{\partial t} \frac{(P-e)\,V}{R\,T_{air}}$$

Eq. (13)

where F_c is the CO_2 flux (µmol m^{-2} s^{-1}), $\frac{\partial X_c}{\partial t}$ is the initial slope of the corrected CO_2 molar fraction (ppm s^{-1}), P is the ambient pressure (Pa), e is the partial pressure of water vapor (Pa), V is the chamber volume, R is the ideal gas constant (8.314 m^3 J mol^{-1} K^{-1}) and T_{air} (K).

2.2.1.1. SOIL CHAMBERS

Manual and portable opaque soil chamber systems (EGM-4, PP-systems, Hitchin, UK) were used to measure soil CO_2 effluxes, also termed as "soil respiration" (R_{soil}). Soil plots were delimited by inserting PVC collars of 0.0087 m^2 area on the soil and measurements were acquired by placing the opaque chamber on the collars over 120s, when ambient pressure, T_{air}, CO_2 and water vapor molar fractions were recorded every 3 seconds.

Figure 4. Soil respiration chambers in Balsa Blanca (Almería). Photograph author: Ana López Ballesteros.

2.2.1.2.CANOPY CHAMBERS

A transparent hand-made closed chamber, hereinafter termed as "canopy chamber", was used to measure plant-atmosphere gas exchange and ecosystem-atmosphere gas exchange, which is equivalent to what EC technique measures but at a smaller spatial scale and hence, includes both plant and soil patches. Chamber dimensions were 0.5x0.5x0.6 m and chamber walls consisted on transparent film sheets (NRS90 clear, Llumar®, Solutia Inc., Düsseldorf, Germany) of 75 µm thick that were attached to the structural aluminum frame. The chamber system includes an Infrared Gas Analyzer (IRGA; Li-840, Li-cor, Lincoln, NE, USA) to measure the CO_2 and water vapor molar fractions, two small fans (8.9 cm diameter) to homogenize the air within the chamber volume, a thermocouple (PT100) to measure the confined air temperature and a datalogger (CR1000, Campbell Sci., Logan, UT, USA) to record all measured variables at a frequency of 1 Hz.
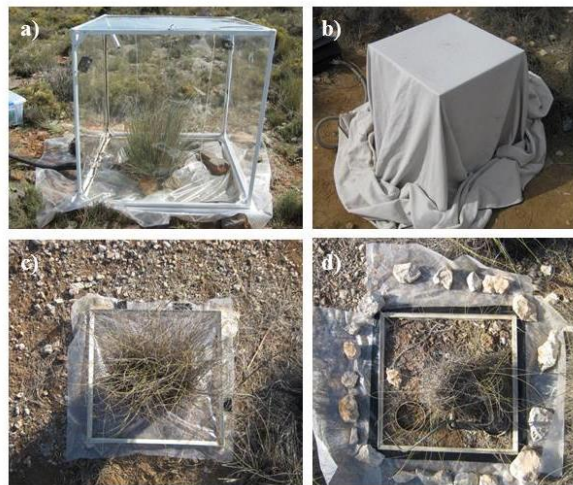
Figure 5. Canopy chamber measuring **a)** under light conditions and **b)** under dark conditions. Chamber collars used to measure **c)** plant-atmosphere gas exchange and **d)** ecosystem-atmosphere gas exchange. Photograph author: Ana López Ballesteros.

Several variables were measured with this canopy chamber. On one hand, plant-atmosphere gas exchange was measured when soil effluxes were excluded by placing a plastic sheet between the plant base and the basal aluminum collar (Fig. 5c).

Hence, we measured aboveground net primary productivity (ANPP) under light conditions (Fig. 5a) and aboveground respiration ($R_{aboveground}$) under dark conditions, which were kept by covering the chamber with an opaque and reflective material (Fig. 5b). On the other hand, when soil effluxes were not excluded (Fig. 5d), net ecosystem CO_2 exchange (NEE) and ecosystem respiration (R_{eco}) were measured under light and dark conditions, respectively. The chamber system was ventilated prior any measurement to minimize the difference between initial and natural air conditions.

2.2.2. SUBSOIL CO_2 MEASUREMENTS

Subsoil CO_2 molar fractions were measured at several depths. On one hand, a deep profile (Fig. 6a) of temperature (107 temperature sensor, Campbell Scientific, Logan, UT, USA), soil water (CS616, Campbell Scientific, Logan, UT, USA) and CO_2 sensors (Fig. 6b; GMP-343, Vaisala, Inc., Finland) was installed in every experimental site at 0.15 and 1.5 m.

On the other hand, shallow measurements were obtained at 0.05 m belowground by means of CO_2 sensors (GMM222, Vaisala, Helsinki, Finland). Sampling frequency was 1 Hz and 5 and 30 min averages were stored in dataloggers (CR23X, CR1000 and CR3000, Campbell Sci., Logan, UT, USA).
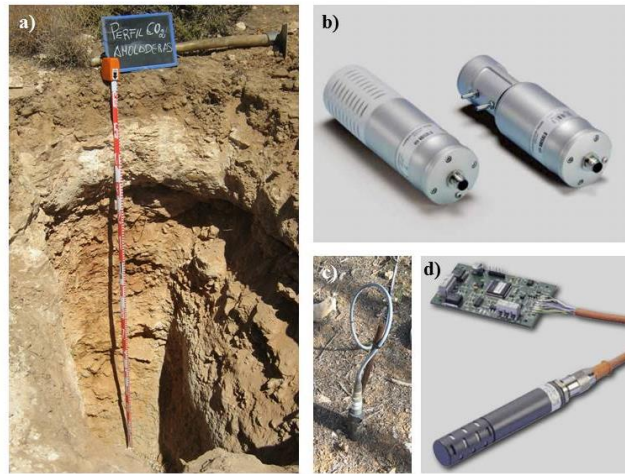
Figure 6. Measurements of CO_2 molar fractions performed in (**a**) a deep profile where the (**b**) subsoil CO_2 probes were installed (GMP-343, Vaisala, Inc., Finland) and in (**c**) the shallowest soil layer where (**d**) subsoil CO_2 probes were installed (GMM222, Vaisala, Helsinki, Finland). Photographs authors: Enrique P. Sánchez-Cañete and Ana López Ballesteros.

Regarding data processing, the CO_2 molar fraction readings were corrected for variations in soil temperature and atmospheric pressure, since the Vaisalas´ IRGA takes constant values instead of the actual ones. Then, the correction takes the form:

$$X_c = X'_c \frac{P_{ct}}{P} \frac{T_{soil}}{T_{soil\_ct}} \qquad \text{(Eq. 13)}$$

where X_c is the corrected CO_2 molar fraction (ppm or μmol mol^{-1}), X'_c is the uncorrected CO_2 molar fraction (ppm or μmol mol^{-1}), P is the atmospheric pressure (kPa) and T_{soil} is the soil temperature (K). The subscript "ct" denotes the constant values used by the IRGA for T and P (298.73 K and 101.13 kPa, respectively).

The soil CO_2 efflux ($R_{soil\_vaisala}$) was estimated, only for the shallow measurements, according to the gradient method described by Sánchez-Cañete

and Kowalski, (2014), where the gas transport due to molecular diffusion is defined by Fick's Law as follows:

$$R_{soil\_vaisala}(z) = -D_s\,\rho_a\,\frac{\partial X_c}{\partial z} \qquad \text{(Eq. 14)}$$

where $R_{soil\_vaisala}(z)$ is the soil CO_2 efflux (µmol m^{-2} s^{-1}), ρ_a is the moist air density (µmol m^{-3}), $\frac{\partial X_c}{\partial z}$ (m^{-1}) is the vertical gradient of the corrected CO_2 molar fraction (X_c; ppm or µmol mol^{-1}) within a depth z (m) and D_s is the effective diffusion coefficient of the CO_2 in the soil (m^2 s^{-1}) calculated as follows:

$$D_s = D_a\,\xi \qquad \text{(Eq. 15)}$$

where D_a (m^2 s^{-1}) is the diffusivity coefficient of CO_2 in air and ξ is the relative gas diffusion coefficient also named as the gas tortuosity factor, estimated, according to Moldrup et al. (2000), as:

$$\xi = \frac{(\Phi - \theta)^{2.5}}{\Phi} \qquad \text{(Eq. 16)}$$

where Φ (m^3 m^{-3}) is the soil porosity and θ is the volumetric soil water content (m^3 m^{-3}).

2.2.3. MODIS LAND PRODUCTS

We used datasets of the Enhanced Vegetation Index (EVI) acquired by the Moderate Resolution Imaging Spectroradiometer (MODIS), which is on board the Earth Observing System-Terra platform, in order to track vegetation dynamics in both experimental sites. The nominal resolution of EVI products (code "MOD13Q1") is 250 m at nadir and temporal resolution corresponds to 16-day compositing periods. The spatial coordinates used for Amoladeras and Balsa Blanca were 36.8340°N, -2.2526°E and 36.9394°N, -2.0341°E, respectively.

The EVI is a three-band vegetation index encompassing blue, red and NIR spectral reflectance information and has been widely used to track temporal variation of vegetation structure (Gao et al., 2000), such as Leaf Area Index (LAI).

RESULTS

CHAPTER 1:

CAN LAND DEGRADATION DRIVE DIFFERENCES IN THE C EXCHANGE OF TWO SIMILAR SEMIARID ECOSYSTEMS?

Ana López-Ballesteros, Cecilio Oyonarte, Andrew S. Kowalski, Penélope Serrano-Ortiz, Enrique P. Sánchez-Cañete, M. Rosario Moya, Francisco Domingo

ABSTRACT

The concept of land degradation stems from the loss of an ecosystem's biological productivity, which in turn relies on several degradation processes, such as long-term loss of natural vegetation, depletion of soil nutrients, soil compaction or water and wind erosion, to which drylands are especially vulnerable. Currently, drylands occupy more than one third of the global terrestrial surface and will probably expand under future climate change scenarios. Drylands´ key role in the global C balance has been recently demonstrated, but the effects of land degradation on C sequestration by these ecosystems needs further research. In the present study, we compare net carbon exchange, together with satellite data and meteorological, ambient and vadose zone (CO_2, water content and temperature) variables, between two nearby (~23 km) experimental sites representing "natural" (i.e. site of reference) and "degraded" grazed semiarid grasslands located in SE Spain, via eddy covariance measurements over 6 years, with highly variable precipitation magnitude and distribution. Results show a striking difference in the annual C balances with an average release of 196 ± 40 and -23 ± 20 g C m^{-2} yr^{-1} for the "degraded" and "natural" sites, respectively. At the seasonal scale, differing patterns in net CO_2 fluxes were detected over both growing and dry seasons. As expected, during the growing seasons, greater net C uptake over longer periods was observed in the "natural" site, however, much greater net C release was measured in the "degraded" site during drought periods. We tested differences in all monitored meteorological and soil variables and found it most relevant that CO_2 at 1.50 m belowground was around 1000 ppm higher in the "degraded" site. Thus, we believe that subterranean ventilation of this vadose zone CO_2, previously observed at both sites, largely drives the differences in C dynamics between them, especially during the dry season maybe due to enhanced subsoil-atmosphere interconnectivity in the "degraded" site. Overall, the 12 site-years of

data allow direct exploration of the roles of climate and land degradation in the biological and non-biological processes that ultimately control the C sequestration capacity of semiarid ecosystems.

1. INTRODUCTION

The concept of land degradation stems from the loss of an ecosystem's biological productivity, which in turn relies on several degradation processes such as long-term loss of natural vegetation, deterioration of soil quality, depletion in biodiversity or water and wind erosion (UNCCD, 1994). Arid, semiarid and dry sub-humid areas, commonly known as drylands, have been recognized as areas vulnerable to land degradation processes. Overall, drylands occupy more than one third of Earth´s land surface and are inhabited by more than 2 billion people (Safriel et al., 2005), and concretely, the semiarid ecoregion comprises a major fraction, 37% of global dryland area, where the dominant biome is grassland (Safriel et al., 2005). Drylands have expanded globally for the last sixty years at an estimated annual rate of 5.8 million hectares in mid latitudes alone (Lal, 2001), and are projected to expand under future climate change scenarios (Feng and Fu, 2013; Cook et al., 2014). Furthermore, the Mediterranean region has been recognized as an especially vulnerable region (Gao and Giorgi, 2008), where major expansions of semiarid areas will occur (Feng and Fu, 2013).

Over recent decades, most research focused on land degradation has been based on remote sensing and earth observation techniques. Much of these investigations has aimed to refine methodological issues in order to accurately track land degradation in vulnerable areas, reduce uncertainties and explain inconsistencies among studies. For instance, a wide array of satellite-derived data, such as vegetation indices, normalized surface reflectance, brightness temperature or biomass-net primary production derivatives (Mbow et al., 2015), has been utilized to appraise desertification effects in the Sahel (Mbow et al., 2015; Fensholt et al., 2013) and also in other African countries such as Kenya (Omuto, 2011), Somalia (Omuto et al., 2010), South Africa (Thompson et al.,

2009) or Zimbabwe (Prince et al., 2009). Likewise, desertification in the Mediterranean region has been studied through satellite imagery, concretely, in Greece (Bajocco et al., 2012), Israel (Shoshany and Karnibad, 2015) and the Iberian Peninsula (del Barrio et al., 2010). Additionally, some global assessments based on modelling approaches have focused on the global loss of net primary production derived from land degradation (Zika and Erb, 2009) or the effect of desertification on climate (Wang et al., 2016). However, although drylands´ key role in the global carbon (C) balance has been demonstrated (Poulter et al., 2014; Ahlström et al., 2015), very few investigations have directly quantified how land degradation processes disturb the C sequestration capacity of drylands (Lal, 2001), which is one of the most important ecosystem services (Watanabe and Ortega, 2011).

In this regard, the few C-related desertification studies conducted over last decade have centered on soil C dynamics. Concretely, soil organic carbon (SOC) inventories have been used to explore the effects of climate, human activities and grazing pressure in desertification-prone areas of China (Feng et al., 2006) and Brazil (Schulz et al., 2016). Similarly, other investigations have evaluated soil degradation processes by means of soil CO_2 effluxes together with other biometric measurements in drylands found in China (Hou et al., 2014; Wang et al., 2007), Chile (Bown et al., 2014) and southeast Spain (Rey et al., 2011; Rey et al., 2017). However, the degradation processes associated with desertification affect several subsystems as well as their interactions at multi-spatial and temporal scales. For instance, adverse effects on soil quality involve depletion of soil fertility, but also reduce soil water storage (Mainguet and Da Silva, 1998), which, in turn, can constrain seed germination and vegetation reestablishment, modify climax vegetation, disrupt biogeochemical cycles, alter water and energy balances, and consequently lead to a loss of ecosystem resilience (Lal, 2001). This cascade of disturbances may result in a reduction of

the C sequestration capacity of a given ecosystem, which is clearly a symptom of the loss of biological productivity, resulting in a positive feedback to global warming. Therefore, a quite suitable and holistic approach is to integrate all subsystems effects into a whole ecosystem-scale assessment when quantifying the C loss derived from land degradation. However, the use of this integrative method is mostly lacking in the available literature.

The present study is located in an area, the southeast of Spain, that has been recognized as a hotspot of land degradation owing to the synergistic interaction of sociological and climatic factors (Puigdefábregas and Mendizabal, 1998), where, furthermore, rainfall has trended downward at ca. 3 mm yr^{-1} since 1900 (Oñate-Rubalcaba, 1993). Our core aim is to evaluate how dryland degradation affects the dynamics of net ecosystem-atmosphere C exchange of two semiarid grasslands that represent differing degradation status by means of meteorological and satellite measurements, subsoil CO_2 sensors and the eddy covariance (EC) technique (Baldocchi et al., 1988). This technique allows us to directly quantify the net exchange of energy, water and CO_2 flux densities (hereinafter fluxes) between an ecosystem (including all of its subsystems, i.e. soil, plants, microorganisms, vadose zone...) and the atmosphere at a high frequency (from minutes to hours). Owing to the high temporal resolution of the EC method, we can assess the effect of land degradation as a slow change or disturbance legacy in the studied ecosystems and how, in turn, it influences the capacity of these ecosystems to absorb fast changes or short-term disturbances, such as droughts. Accordingly, our main hypothesis is that the degree of land-degradation affects net ecosystem C sequestration capacity through its impact on some or all of the processes that compose the overall ecosystem C balance: photosynthesis, ecosystem respiration (biological processes) and subterranean ventilation – a non-biological process that provokes the transfer of CO_2-rich air from subsoil to atmosphere under drought and high turbulence conditions. In

this context, as subterranean ventilation has been measured in both experimental sites (Rey et al., 2012; López-Ballesteros et al., 2017), we also hypothesize a significant role of this process in the monitored ecosystems. Hence, our specific objectives are: (1) to compare C sequestration capacity of two semiarid ecosystems showing a differing degradation status, (2) to study involved processes (biological *vs* non-biological) and influencing factors that can drive potential differences in the net C exchange of studied ecosystems, and (3) to evaluate whether degradation can modulate ecosystem responses against short-term disturbances. To do this, we analysed 12 site-years of EC data, Enhanced Vegetation Index (EVI) time series and monitored ambient variables registered over the same period (2009-2015) at both sites. Additionally, we used subsoil CO_2, moisture and temperature data obtained during 2014-2015.

2. MATERIAL AND METHODS

2.1. EXPERIMENTAL SITES DESCRIPTION

The two experimental sites are Amoladeras (N36º50'5''W2º15'1'') and Balsa Blanca (N36°56'26.0'' W2°01'58.8''). As stated previously, both are located in Cabo de Gata-Níjar Natural Park (Almería, Spain) and show similar climate and ecosystem type (detailed in Material and Methods section, p. 20). In this regard, in Cabo de Gata-Níjar Natural Park, a great fraction of agricultural areas that were abandoned over 1957-1994 resulted in "espartal" ecosystems (Alados et al., 2011; Alados et al., 2004), which corresponds to the ecosystem type of both experimental sites.

Regarding the topographic, geologic and edaphic characteristics, both sites are located on an alluvial fan, where the main geological materials consist of quaternary conglomerates and Neogene-Quaternary sediments cemented by lime (caliche) (Rodríguez-Fernández et al., 2015) and slopes of 2-6% (Rey et al., 2017) so no significant runoff occurs. Additionally, both sites present petrocalcic horizons. However, altitude and soil type differ. While Balsa Blanca (hereinafter BB) is located at an altitude of 208 m and has Mollic Lithic Leptosols (Calcaric), Amoladeras (hereinafter AMO) is situated closer to the sea level, at 65 m, and presents less developed soils, Lithic Leptosol (Calcaric; Table 1).

	Amoladeras	Balsa Blanca
Site characteristics		
Location	Almeria N36º50'5'' W2º15'1''	Almeria N36º56' 0'' W2º1'58''
Altitude (m)	65	208
Climate	Subtropical, dry, semiarid	Subtropical, dry, semiarid
Annual T	18	18
Annual P	220	220
Predominant sp.	*Machrocloa tenacisima*	*Machrocloa tenacissima*
Surface fractions		
Vegetation cover (%)	23.1 ± 2.4*	63.2 ± 5.2*
Litter (%)	10.5 ± 2.0	8.1 ± 1.9
Biological crust (%)	23.1 ± 2.8	18.2 ± 3.8
Bare soil (%)	8.1 ± 0.1*	0.3 ± 0.3*
Gravel (%)	21.1 ± 0.1*	8.6 ± 2.5*
Rock (%)	14.0 ± 1.2*	1.5 ± 0.5*
Soil properties		
Soil type	Lithic Leptosol (Calcaric)	Mollic Lithic Leptosol (Calcaric)
Maximum soil depth (cm)	10	20
Soil texture class	Sandy loam	Sandy loam
Clay (%)	14.6	16.1
Silt (%)	27.0	22.8
Sand (%)	58.4	61.1
Bulk density (g cm^{-3})	1.11± 0.04	1.25 ± 0.09
SOC (kg m^{-2})	1.24	4.64
Carbonates (%)	14	2

Table 1. Site characteristics, surface fractions and soil properties of both experimental sites studied. Asterisks denote significant differences (p-value<0.05). Adapted from Rey et al. (2011).

Overall, as stated by Rey et al. (2011), these two experimental sites represent different degradation stages owing to their differing soil characteristics and surface fractions (Table 1). While BB has more deep and fertile soils and higher vegetation cover, AMO shows thinner and poorer soils and has half of Balsa Blanca´s vegetation cover. Therefore, in accordance to Rey et al. (2011; 2017), we considered that BB represents the "natural" site, being, currently, a

representative ecosystem of the area, while AMO represents a "degraded" site with respect to BB.

2.2. METEOROLOGICAL AND EDDY COVARIANCE MEASUREMENTS

The net ecosystem-atmosphere exchange of water vapour, CO_2 and sensible and latent heat were measured in terms of fluxes via the eddy covariance (EC) technique. Thus, an EC station was installed at each experimental site, AMO and BB (with site codes "Es-Amo" and "Es-Agu" of the European Database Cluster <u>http://www.europe-fluxdata.eu</u>), where ambient and micrometeorological variables (detailed in Table 1 of Material and Methods section; p. 42) were monitored continuously since 2009. The EC footprint (i.e. actual measured area) is well within the fetch (i.e. distance to a change in surface characteristics) at both sites. Regarding data processing, the half-hourly averaged fluxes were calculated from raw data collected at 10 Hz using EddyPro 5.1.1 software (Li-Cor, Inc., USA). Flux calculation, flux corrections and quality assessment were performed according to López-Ballesteros et al. (2016).

Additionally, flux measurements acquired under low-turbulence conditions were excluded from the analysis by using a friction velocity (u_*) threshold according to the approach proposed by Reichstein et al. (2005). The average u_* thresholds for the whole study period (i.e. 2009–2015) were 0.11 and 0.16 m s^{-1}, for AMO and BB, respectively. Furthermore, over the six years of measurements at both sites, data gaps due to low-turbulence conditions, instrument malfunction and theft were unavoidable and not randomly distributed, as noted by Ma et al. (2016). Therefore, the total annual fractions of missing half-hourly net CO_2 fluxes accounted for 33 ± 3 % and 29 ± 6 % of night-time data and 8 ± 6 % and 14 ± 5 % of day-time data, for AMO and BB, respectively. Missing data were gap-filled by means of the marginal distribution approach proposed by Reichstein et al. (2005) and errors derived from the gap-

filling procedure were calculated from the variance of the gap-filled data, as explained by López-Ballesteros et al. (2016). The annual cumulative C balance was estimated, when possible, by integrating gap-filled half-hourly net CO_2 fluxes of good quality (0 and 1 quality flags, according to Mauder and Foken, 2004) over a hydrological year.

In order to test the validity of both EC stations, we assessed the energy balance closure (Moncrieff et al., 1997) by computing the linear regression of half-hourly turbulent energy fluxes, sensible and latent heat fluxes (H+LE; W m^{-2}) against available energy, net radiation less the soil heat flux (R_n-G; W m^{-2}) with the whole six-years database. The resulting slopes were 0.873 ± 0.002 (R^2 = 0.907) and 0.875 ± 0.001 (R^2 = 0.920) for AMO and BB, respectively.

2.3. ENHANCED VEGETATION INDEX DATA SERIES

We used Enhanced Vegetation Index (EVI) data acquired by the Moderate Resolution Imaging Spectroradiometer (MODIS), which is on board the Earth Observing System-Terra platform, in order to track vegetation dynamics at both experimental sites. The nominal resolution of EVI products (code "MOD13Q1") is 250 m at nadir and temporal resolution corresponds to 16-day compositing periods. The spatial coordinates used for AMO and BB were N36.8340°, E-2.2526° and N36.9394°, E-2.0341°, respectively. The EVI is a three-band vegetation index encompassing blue, red and NIR spectral reflectance information and has been widely used to track temporal variation of vegetation structure (Gao et al., 2000).

2.4. VADOSE ZONE MEASUREMENTS

Subsoil CO_2 molar fraction, temperature and volumetric water content were measured at 0.05 m and 1.50 m below the surface (detailed in Table 1 of Material and Methods section; p. 41) from January 2014 to August 2015 at both

experimental sites. In the case of the shallower CO_2 sensor, it was installed vertically with an in-soil adapter (211921GM, Vaisala, Inc., Finland) to avoid water entrance. Subsoil CO_2 molar fractions were sampled every 30 s and 5 min averages were stored in a data logger (CR3000 and CR1000, CSI; for AMO and BB, respectively). The deeper CO_2 sensor was equipped with a soil adapter for horizontal positioning (215519, Vaisala, Inc., Finland), consisting of a PTFE filter to protect to the CO_2 sensor from water. It was buried in the summer of 2013 and the measurements were made every 30 s and stored as 5 min averages in a datalogger (CR1000 and CR23X Campbell Sci., Logan, UT, USA, for AMO and BB, respectively). All CO_2 molar fraction records were corrected for variations in soil temperature and atmospheric pressure.

2.5. STATISTICAL ANALYSIS

All meteorological and soil variables monitored at each site were compared through computation of the non-parametric two-sided Wilcoxon summed rank test in order to detect those factors/variables influencing potentially distinct ecosystem functioning between sites. This test was chosen because variables used satisfied the independence and continuity assumptions but not all were normally distributed. The confidence level used was 95% and the effect size was evaluated using an estimator based on confidence intervals that corresponded to the median of the difference between the samples (Amoladeras minus Balsa Blanca) and was expressed as an absolute value (Diff) and as a standarized value (Diff$_{st}$; dimensionless), which was obtained by using the sample values of every site divided by its standard deviation in order to be able to compare results among different variables. This analysis was performed by using three different periods: the whole study period, the period from May to September and the period from May to September during only daytime. These periods were selected given their demonstrated coincidence with high relevance of non-

57

biological processes. All calculations were performed using R software version 3.2.5.

Additionally, in order to include the relationship between pressure and subsoil CO_2 variations as a potential factor influencing net CO_2 exchange (Sánchez-Cañete et al., 2013), we firstly calculated, separately for each site, Spearman correlation coefficients to determine the time step (6, 12, 24 or 72 hours) with the highest correlation between the differential transformation of pressure and the subsoil CO_2 molar fraction at 1.50 m.

3. RESULTS

3.1 . AMBIENT CONDITIONS OVER THE STUDY PERIOD

Over the study period, the wettest hydrological year was 2009/2010, with annual precipitation of ~500 mm (ca. twice the annual average precipitation for both sites over the study period, Fig. 1). On the contrary, the driest year was 2013/2014, with annual precipitation of ~100 mm for both sites, less than half the annual average precipitation registered at Amoladeras (AMO) and Balsa Blanca (BB). Generally, the months with precipitation higher than 20 mm occurred from the beginning of autumn until midwinter, however, in case of 2009/2010, 2010/2011, 2012/2013 and 2014/2015, relevant precipitation events were registered during spring months. By contrast, in 2013/2014, precipitation was always below 20 mm with the exception of November and December, for both sites, and June, in the case of AMO (Fig. 1a). Commonly, while maximum precipitation usually occurred from November to February, there was a remarkable drought period over summer months (June-August) when it scarcely ever rained (Fig. 1).

Regarding air temperature (T_{air}) patterns, monthly averaged T_{air} ranged from 9.6 and 8.1 °C to 27.6 and 27.9 °C in AMO and BB, respectively, over the entire study period. Based on half-hourly averaged data, minimum and maximum T_{air} values registered were 0.1 and 37.9 °C in AMO, and -1.3 and 39.9 °C, in BB, respectively. On one hand, those months with T_{air} above 15 °C usually corresponded to April-November, approximately. Additionally, August was the month with the highest average T_{air} at both sites, with T_{air} ranges of 25.2 - 27.6 °C at AMO and 24.9 - 27.9 °C at BB, respectively (Fig. 1), over the study period. On the other hand, the lowest monthly average T_{air} usually occurred in January but sometimes also in December and February, with 11.2 – 12.3 °C at AMO and 8.1 - 14.1 °C at BB.
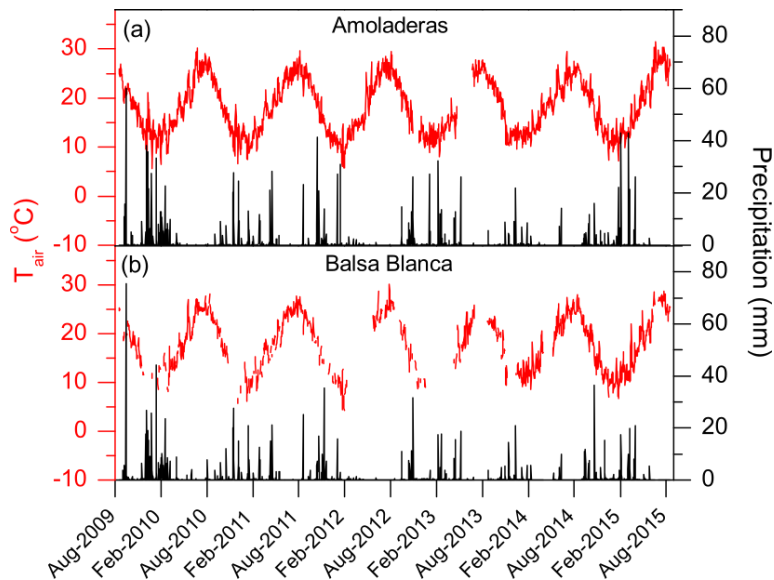

Figure 1. Daily averages of air temperature (T_{air}) and precipitation in **(a)** Amoladeras and **(b)** Balsa Blanca.

3.2 . ANNUAL CARBON BALANCES

The comparison of the annual carbon (C) balance among sites was only possible for three hydrological years, 2009/2010, 2010/2011 and 2012/2013, due to long-term data gaps existing in BB during other years. The annual cumulative net CO_2 exchange was always positive for AMO (i.e., net C release), whereas BB was neutral or even acted as a C sink over the three years (Fig. 2). For example, in 2009/2010, the net C uptake measured in BB equated to 32 ± 10 g C m^{-2} while in AMO, a total amount of 185 ± 10g C m^{-2} was released to the atmosphere (Fig. 2a). The year with the largest difference between sites was 2010/2011, with annual C release of 240 ±8 and -38 ±10 g C m^{-2} in AMO and BB, respectively (Fig. 2b). Likewise, 2011/2012 was the year when the lowest CO_2 release was measured in AMO with 163 ± 7 g C m^{-2} while a neutral C balance was measured in BB with 0 ± 8 g C m^{-2} (Fig. 2c).

Overall, a positive and saturating trend was observed at both sites during autumn months until December-February when cumulative net CO_2 release start to decline. The autumn net CO_2 release (i.e., positive values) was usually higher in AMO than in BB, excepting for 2012/2013, and the declining slope was always higher in BB, meaning greater net C uptake rates. Although the pattern of the cumulative net CO_2 exchange showed differences between sites over autumn, winter and spring months, stronger discrepancies were found during summer droughts. Concretely, from April-May until August, BB showed neutral behavior while a remarkable positive trend was observed in AMO, denoting a large net CO_2 release.
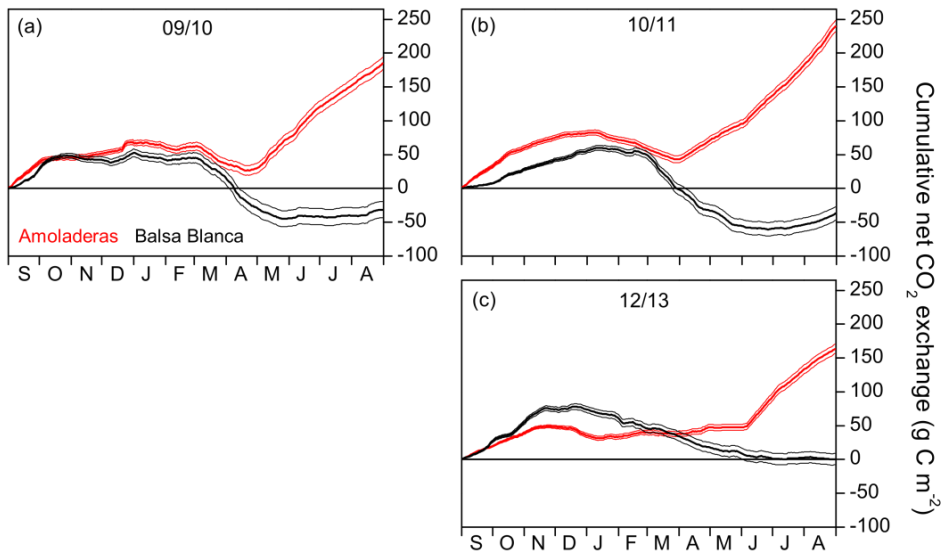
Figure 2. Cumulative annual net CO_2 exchange over the three hydrological years without long-periods of missing data in both experimental sites, Amoladeras (red lines) and Balsa Blanca (black lines). Negative values denote net carbon uptake while positive values denote net carbon release. Thin lines indicate uncertainty derived from the gap-filling procedure.

3.3 . SEASONAL AND DIURNAL NET CO_2 EXCHANGES

Long-term data loss occurred in BB during the springs of 2011/2012, 2013/2014 and 2014/2015 and summers of 2013/2014 and 2014/2015, when annual C balances could not be estimated. However, by observing the available seasonal data, it is noticeable that, maximum and minimum seasonal net CO_2 exchanges were very different between sites (Fig. 3). On one hand, maximum seasonal net CO_2 uptake was measured during winter (December-February) in AMO and over spring (March-May) in BB, when peaking net CO_2 uptake fluxes equated to -31 g C m^{-2} (winter 2011/2012) and -105 g C m^{-2} (spring 2010/2011) in AMO and BB, respectively. Additionally, net CO_2 uptake was only observed during three winters in the case of AMO, whereas it was frequently measured during both winter and spring in BB. On the other hand, cumulative net CO_2 release to the atmosphere occurred over all types of seasons in AMO, but

acutely in summer, when maximum seasonal net CO_2 release was always observed ranging from 111 to 153 g C m^{-2}. In contrast, in BB, the highest CO_2 effluxes usually occurred in autumn ranging from 25 to 74 g C m^{-2}, although significant CO_2 release was also observed in winter 2013/2014 and the summers of 2009/2010-2011/2012.
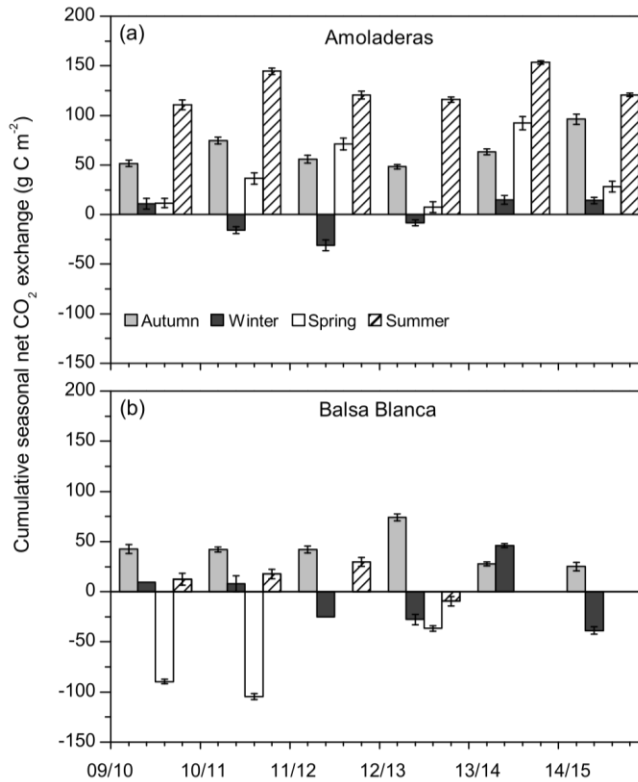
Figure 3. Cumulative seasonal net CO_2 exchange over the study period in both experimental sites. Negative values denote net carbon uptake while positive values denote net carbon release. In case of Balsa Blanca, lacking bars correspond to long-term data losses (>50% data).

Comparing daily-scale net CO_2 exchange and evapotranspiration (ET) fluxes with punctual Enhanced Vegetation Index (EVI) data, we can notice some similarities in the general patterns of both sites (Fig. 4). Roughly, there was a common annual pattern at both sites in which the highest values of EVI coincided with maximum net CO_2 uptake rates (i.e. negative net CO_2 fluxes),

which in turn, corresponded to peaking ET fluxes. Additionally, a decreasing trend in EVI over the 6 years of study was also noticeable for both sites. However, some inter-site and inter-annual differences were evident (Fig. 4).
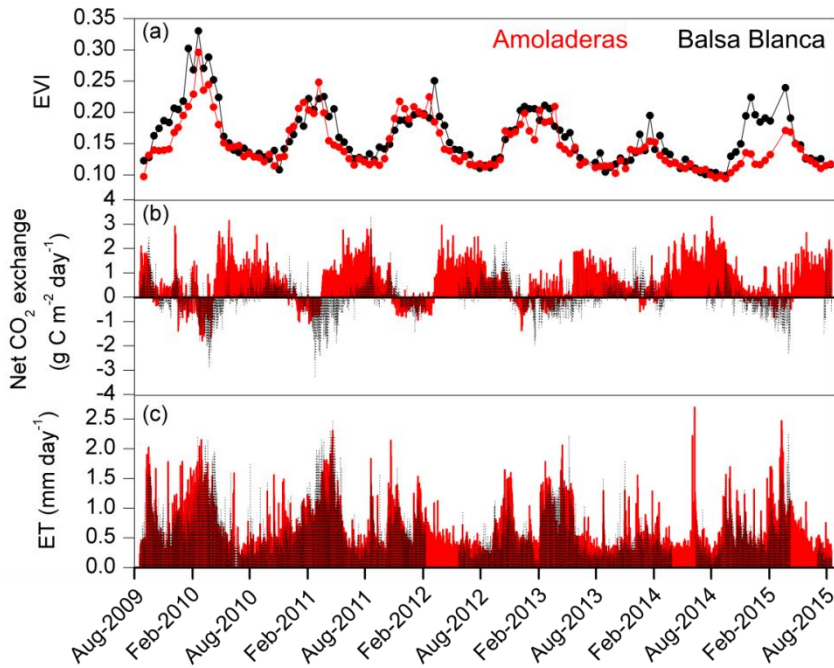
Figure 4. Time series of **(a)** Enhanced Vegetation Index (EVI), **(b)** daily net CO_2 exchange and **(c)** daily evapotranspiration fluxes measured in Amoladeras (red lines and dots) and Balsa Blanca (black lines and dots) over six hydrological years (2009-2015). Long-term data losses correspond to periods of several months when ET and CO_2 fluxes are absent.

On one hand, there were two main differences between sites. Firstly, extreme net CO_2 release was measured uniquely in AMO during summer months (June-August), when maximum net CO_2 fluxes ranging from 31 to 68 g C m^{-2} were measured (Fig. 4b). Over the study period, the monthly net CO_2 exchange of AMO during dry seasons was up to one hundred times higher than in BB (in August 2013), since monthly net CO_2 fluxes measured in BB were much lower, from -8 to 16 g C m^{-2} (Fig. 4b). Besides the striking differences in summer net CO_2 exchange between sites, minor discrepancies were also found

63

in ET fluxes and EVI for the same drought periods. In this regard, monthly averaged ET over the dry season equated to 13 ± 4 and 10 ± 4 mm for AMO and BB, respectively, and EVI was on average 4% higher in BB than in AMO (Fig. 4a,c). The second inter-site difference was the greater net CO_2 uptake over longer periods measured in BB. Concretely, the period during which the ecosystems acted as C sinks lasted on average 38 days longer in BB than in AMO annually (Table 3). Accordingly, the annual amount of C fixation ranged from 6-59 g C m^{-2} at AMO and 15-129 g C m^{-2} at BB, respectively, with the annual averaged net C uptake in BB 162% higher than at AMO (Table 3). Consequently, peaking EVI values were usually observed during March-April for both sites, however, over winter and spring months (growing period), EVI measured at BB was 3 - 37% higher than AMO, with the largest inter-site differences in 2009/2010 and 2014/2015 (Fig. 4a). Likewise, monthly averaged ET fluxes measured at BB over winter and spring months (December-May) were from 3 to 24% larger than those measured at AMO. Additionally, the growing period of the driest year (2013/2014) corresponded to the lowest monthly ET fluxes and the least difference between sites.

On the other hand, differences in the inter-annual variability of EVI, carbon and water fluxes were also observed; however, due to long-term data losses at BB, accurate and comparative inter-annual analysis could not be done with carbon and water fluxes. In this sense, 2009/2010 and 2013/2014 were the years with maximum and minimum annual precipitation and EVI observations, respectively, for both sites. Concretely, in 2009/2010, EVI observations were 28% and 20% higher than the six-year averaged values in BB and AMO, respectively. In case of the driest year, 2013/2014, growing season (winter-spring) EVI was reduced 35% and 28% in BB and AMO, respectively. Nevertheless, the largest difference between sites in winter-

spring EVI observations was found in 2014/2015, following the driest year, when BB showed a pattern very similar to those registered over the years previous to the dry spell, while AMO still presented EVI values 21% below the six-year average (Fig. 4a).

3.4 . DIFFERENCES IN METEOROLOGICAL AND SOIL VARIABLES BETWEEN SITES

Results from the two-sided Wilcoxon summed rank test (Table 4) showed significant differences (p-value < 0.05) between sites in most of the monitored meteorological variables. The few exceptions were the friction velocity (u_*), when using the whole study period, the maximum wind speed registered every half-hour (WS_{max}), when analyzing May-September data, and the wind speed (WS) and precipitation when assessing daytime May-September data (Table 4). The great amount of observations (n ranged from 21410 to 205751) produced highly significant results (Table 4). Hence, the standardized difference between the samples ($Diff_{st}$) allowed us to quantitatively explore the differences between sites. Relevant differences ($Diff_{st}>1$) were found only for pressure when using all databases, due to the distinct altitude of monitored sites.

Variables	All periods		May - September		May - September Daytime	
	$Diff_{st}$	n	$Diff_{st}$	n	$Diff_{st}$	n
PPFD ($\mu mol\ m^{-2}\ s^{-1}$)	0.0009*	205751	0.0009*	84491	0.1378*	38963
Net radiation ($W\ m^{-2}$)	-0.0457*	197924	-0.0476*	81019	-0.1205*	38963
T_{air} (°C)	0.0310*	182240	0.1935*	77866	0.0502*	37480
VPD (hPa)	0.0783*	166918	0.1370*	71474	-0.0938*	34430
RH (%)	-0.1636*	197649	-0.1031*	80950	0.1784*	38935
u_* ($m\ s^{-1}$)	-0.0054	166346	-0.0563*	71194	-0.1340*	34284
WS ($m\ s^{-1}$)	0.1628*	166359	0.0793*	71195	0.0165	34285
WS_{max} ($m\ s^{-1}$)	0.1001*	165458	0.0124	70635	-0.0796*	33994
Pressure (hPa)	**1.6999***	166359	**1.8696***	71195	**1.8633***	34285
Precipitation (mm)	-1.95E-05*	204892	-4.84E-05*	83860	5.32E-05	38963

Table 4. Results of the two-sided Wilcoxon summed rank test used to assess differences among meteorological variables measured at each experimental site over all periods, from May to September and from May to September during daytime, separately. Medians of the difference between the samples (Amoladeras minus Balsa Blanca) in standarized terms ($Diff_{st}$) and number of observations are detailed. Significant results (p-value<0.05) are denoted with asterisks, and bold values represent those variables with $Diff_{st}$ between sites above 1.

Regarding soil variables, important differences ($Diff_{st}$>1) between sites were detected in subsoil CO_2 molar fraction measured at 1.50 m depth ($CO_{2,\ 1.50m}$) for all periods, and during May-September months even when using only daytime data (Table 5). Concretely, $CO_{2,\ 1.50m}$ was always higher in AMO, from 889 to 1109 ppm (Table S1, S2 and S3). Additionally, volumetric water content at 0.05m depth ($VWC_{0.05m}$) was also higher in AMO compared to BB but only during summer months (Table 5), when absolute differences were very small, ranging from 0.028 to 0.037 $m^3\ m^{-3}$ (Tables S1, S2 and S3). In contrast, subsoil CO_2 molar fraction measured at 0.05 m depth ($CO_{2,\ 0.05m}$) was from 89 to 150 ppm higher in BB when analyzing dry season (May-September) daytime data (Table 5, S1, S2 and S3).

| Variables	All periods		May - September		May - September Daytime	
	$Diff_{st}$	n	$Diff_{st}$	n	$Diff_{st}$	n
$CO_{2,\ 0.05m}$ (ppm)	-0.4027*	46340	-0.6578*	21413	**-1.1396***	9816
$CO_{2,\ 1.50m}$ (ppm)	**1.1196***	50133	**1.3517***	24347	**1.3062***	11385
$T_{0.05m}$ (°C)	0.0927*	46337	-0.1160*	21410	-0.2119*	9813
$T_{1.50m}$ (°C)	0.1476*	50137	-0.0591*	24350	-0.0834*	11385
$VWC_{0.05m}$ (m^3 m^{-3})	0.8265*	52353	**1.2724***	25231	**1.2839***	11303
$VWC_{1.50m}$ (m^3 m^{-3})	-0.8385*	53865	0.0674*	24570	0.0547*	11462

Table 4. Results of the two-sided Wilcoxon summed rank test used to assess differences among meteorological variables measured at each experimental site over all periods, from May to September and from May to September during daytime, separately. Medians of the difference between the samples (Amoladeras minus Balsa Blanca) in standarized terms ($Diff_{st}$) and number of observations are detailed. Significant results (p-value<0.05) are denoted with asterisks, and bold values represent those variables with $Diff_{st}$ between sites above 1.

The temporal dynamics of subsoil CO_2 molar fractions revealed similar annual patterns between sites; generally however, $CO_{2,\ 0.05m}$ was higher in BB, from 6 to 88%, while $CO_{2,\ 1.50m}$ was always greater in AMO, from 31 to 97% (Fig. 5). On one hand, the maximum monthly averaged values of $CO_{2,\ 0.05m}$ were registered in autumn, concretely, in November and October with 642 and 1120 ppm in AMO and BB, respectively, whereas minimum values occurred in September and August with 373 and 400 ppm at each site (Fig. 5a). On the other hand, peaking monthly averaged values of $CO_{2,\ 1.50m}$ occurred in July for both sites, with 2751 and 1602 ppm in AMO and BB, respectively, although relatively high $CO_{2,\ 1.50m}$was also measured during November in BB. On the contrary, minimum values were observed in December and February, with 1364 and 735 ppm in AMO and BB, respectively (Fig. 5b).
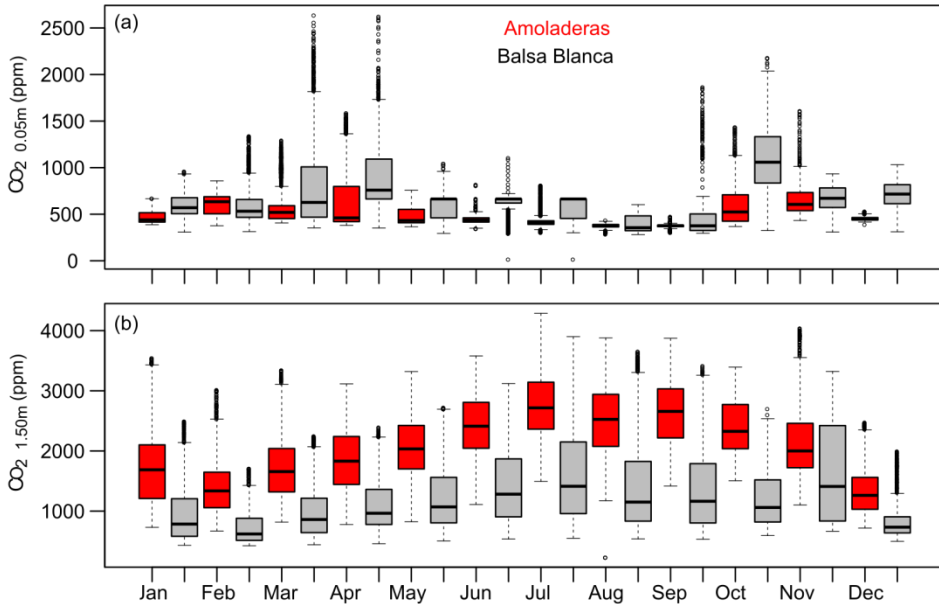
Figure 5. Box-and-whisker plots of CO_2 molar fractions measured at **(a)** 0.05 m and **(b)** 1.50 m belowground in Amoladeras (red boxes) and Balsa Blanca (grey boxes) from January 2014 to August 2015. The box extends from the first (Q1) to the third quartiles (Q3) and the central line represents the median (50% percentile). Dots represent outliers; upper whisker is located at the smaller of the maximum value and Q3 + 1.5 IQR (Interquartile Range), and lower whisker is located at the larger of the minimum value and Q1 − 1.5 IQR.

Finally, results of the Spearman correlation analysis between pressure and belowground CO_2 at 1.50 m depth ($CO_{2,\ 1.50m}$) showed a negative relationship between both variables. Additionally, although most of the coefficients were significant (p-value<0.05), higher correlations were found in AMO compared to BB (Table 6). Spearman correlation coefficients (r_s) were maxima at 12 h intervals for $CO_{2,\ 1.50m}$ and pressure increments (dP_{12h}) at AMO, and and at 6 h intervals for $CO_{2,\ 1.50m}$ and pressure increments (dP_{6h}, respectively) at BB, with r_s equal to -0.87 and -0.63, respectively.

	Amoladeras					Balsa Blanca				
	P	dP_{6h}	dP_{12h}	dP_{24h}	dP_{72h}	P	dP_{6h}	dP_{12h}	dP_{24h}	dP_{72h}
$CO_{2,\,1.50m}$	**-0.66**	-0.33	-0.46	-0.56	-0.55	**-0.33**	-0.51	**-0.53**	**-0.62**	-0.45
$dCO_{2,\,1.50m\_6h}$	-0.1	**-0.84**	-0.5	-0.26	-0.01	-0.07	**-0.63**	-0.19	-0.13	-0.04
$dCO_{2,\,1.50m\_12h}$	-0.08	-0.57	**-0.87**	-0.55	-0.05	-0.03	-0.46	-0.50	-0.31	-0.03
$dCO_{2,\,1.50m\_24h}$	-0.13	-0.47	-0.78	**-0.85**	-0.15	-0.04	-0.40	-0.59	-0.58	-0.04
$dCO_{2,\,1.50m\_72h}$	-0.28	-0.28	-0.49	-0.64	**-0.74**	-0.13	-0.28	-0.43	-0.57	**-0.48**

Table 6. Spearman correlation coefficients (r_s) for every paired simple correlation among maximum quality net CO_2 exchange fluxes ($\mu mol\ m^{-2}\ s^{-1}$), absolute and differential pressure (hPa) at 6, 12, 24 and 72 hours time-step and absolute and differential CO_2 molar fraction measured at 1.50 m below ground (ppm) at the same time-steps. Bold values represent the highest correlation coefficients while shaded ones denotes non-significant relationships (p-value>0.05).

4. DISCUSSION

Our results verify that land-degradation affects the C sequestration capacity of semiarid ecosystems, since relevant differences between sites were observed during the growing season, when greater net C uptake over longer periods was observed in the "natural" site (BB). However, contrary to what we previously hypothesized, much greater net C release was measured at the "degraded" site (AMO) over drought periods due to the predominance of subterranean ventilation (López-Ballesteros et al., 2017). In fact, the great difference in annual C budgets between sites (Fig. 1) was largely related to this process resulting in an average release of 196 ± 40 and -23 ± 20 g C m^{-2} yr^{-1} for the "degraded" (AMO) and "natural" (BB) sites, respectively. In this regard, the ecosystems' functioning could be divided into three different phases. The first phase corresponded to the autumn months, when the first rainfall events after the dry summer (i.e. rain pulses) activated the soil microbiota triggering respiratory CO_2 emissions as previously measured at the same experimental sites (López-Ballesteros et al., 2016; Rey et al., 2017). During this phase, maximum CO_2

release was observed at BB, however higher CO_2 release was usually measured at AMO (Fig. 3), maybe due to the greater hydric stress experienced prior to rewetting, the differences in microbial communities (Rey et al., 2017), and the greater pool of soil inorganic carbon (Emmerich, 2003; Table 1). The second phase comprised the growing period, when plants photosynthesized and also respired along with microorganisms under milder temperatures and better hydric conditions. During this phase, larger net CO_2 uptake was measured in BB, concretely 162% more than in AMO (Table 3) due to the higher vegetation cover and more fertile soils (Table 1) of the "natural" site. Moreover, this result was supported by the lower ET and EVI values obtained in AMO during winter and spring months of the whole study period (Fig. 4). The third phase consisted of the dormancy period when water scarcity and high temperatures constrained biological activity. During this period, as stated previously, a neutral C balance was observed in BB while extreme CO_2 release was measured in AMO.

In order to detect potential factors driving the observed differences in the C balances, we checked whether soil and meteorological variables differed between sites. Our results demonstrated that some factors typically influencing gross primary production (GPP) and ecosystem respiration (R_{eco}), and hence net ecosystem CO_2 exchange, such as photosynthetic photon flux density (PPFD; Michaelis and Menten, 1913), precipitation (Berner et al., 2017; Jongen et al., 2011), vapor pressure deficit (VPD; Lasslop et al., 2010) and soil and air temperature (Lloyd and Taylor, 1994), did not differ between sites (Table 4, 5). Conversely, some differences were found for shallow soil volumetric water content ($VWC_{0.05m}$) during dry seasons (Table 5), when $VWC_{0.05m}$ was two times higher in AMO than in BB, but absolute differences were slight, from 0.028 to 0.037 m^3 m^{-3} (Tables S1,S2 and S3). Hence, although the important influence of soil moisture in both GPP and R_{eco} is known (Tang and Baldocchi, 2005), we believe that differences in $VWC_{0.05m}$ are not relevant enough to cause

the differing ecosystems' functioning observed over the drought period. Additionally, we think that this inter-site difference in $VWC_{0.05m}$ could be instrumental, or due to the spatial variability of $VWC_{0.05m}$ derived from the heterogeneity of soil morphological characteristics, since we only used one sensor at each site.

Similarly, important differences were not detected in several variables linked to subterranean ventilation, such as the friction velocity (u_*; Kowalski et al., 2008), wind speed (WS; Rey et al., 2012), half-hourly maximum wind speed (WS_{max}) and net radiation, which has been positively correlated to ventilative CO_2 fluxes (López-Ballesteros et al., 2017), when using the analysis periods when this process is supposed to be relevant, namely daytime hours during the dry seasons (Table 4). In contrast, inter-site differences were found in net radiation (Table 4). However, although no turbulence and wind speed inter-site differences were found, interconnectivity of soil pores and fractures is probably higher at AMO (Table 1) due to its higher gravel and rock fractions (Table 1), which could lead to an enhanced penetration of eddies within the vadose zone (Pérez-Priego et al., 2013).

Apart from that, outstanding differences between sites were observed in subsoil CO_2 molar fractions measured at 0.05 and 1.50 m depths ($CO_{2, 0.05m}$ and $CO_{2, 1.50m}$, respectively; Table 5). On one hand, $CO_{2, 0.05m}$ was generally higher in BB given its lower degradation level, which probably promotes a higher microbial activity supported by higher vegetation density and soil fertility (Table 1) especially during spring (Fig. 5), as pointed also by Oyonarte et al. (2012). On the other hand, $CO_{2, 1.50m}$ values were acutely higher in AMO, by up to 1000 ppm compared to BB (Tables S1, S2 and S3). Therefore, we suggest that $CO_{2, 1.50m}$ is the main factor responsible for the inter-site differences in net CO_2 fluxes over the dry season. However, not only the amount of subsoil CO_2

matters but also how effective is its transport, since both determine the net CO_2 release from the vadose zone to the atmosphere. In this context, Oyonarte et al. (2012) found, in the same study area (Cabo de Gata-Níjar Natural Park), that soils with degradation symptoms, such as lower SOC, depleted biological activity, coarser texture and worse structure, showed higher soil CO_2 effluxes over the dry season. Additionally, soil CO_2 effluxes measured during summer months correlated positively with the fraction of rock outcrops, suggesting that deteriorated soil physical conditions actually enhanced vertical transfer of CO_2-rich air from subsoil to the atmosphere (Oyonarte et al., 2012). In fact, correlation analysis between $CO_{2, 1.50m}$ and atmospheric pressure (Table 6) showed a stronger relationship between both variables at AMO. In this sense, ecosystem degradation could provoke a greater exposure of subsoil CO_2 to the pressure effect, as described by Sánchez-Cañete et al. (2013), probably due to a higher fraction of bare soil, coarser structure, differing porosity type and/or thinner soil depth (Table 1).

Regarding EVI data, these results have allowed us to complement our findings based on CO_2 fluxes, especially when EC data losses occurred. For instance, the declining trend observed from 2009/2010 until the end of the study period, for both sites, was not noticeable from EC data alone (Fig. 4). This long-term decrease in EVI may be related to a gradual drying following the wettest year (2009/2010), when extraordinarily high precipitation (twice the annual average precipitation for both sites over the study period) occurred. This EVI pattern also denotes a pulse-like behaviour of ecosystem vegetation over the inter-annual time scale. Moreover, in addition to demonstrating that degradation can influence the biological activity of ecosystems' vegetation, EVI results also showed that degradation level can modulate how an ecosystem responds to a short-term change. A clear example is the dry spell experienced in 2013/2014, when a reduction in EVI was measured during the growing season in both sites,

i.e. 35% and 28% in BB and AMO, respectively. However, a year later (2014/2015), EVI values below the six-year average were observed only at AMO (21% lower; Fig. 4a). Accordingly, the "natural" site (BB) seemed to be more stable than the "degraded" site (AMO) against the short-term disturbance, since the effect of drought persisted in AMO even during the following year, while BB recovered to a pre-perturbation state within the same period (Fig. 4a). As a result, ecosystem resilience, defined by Holling (1973) as the amount of disturbance that a system can withstand without changing state, was lessened by long-term disturbances such as degradation, making degraded ecosystems more vulnerable to climate extremes (Reichstein et al., 2013). In this sense, mitigation policies to confront land degradation should be focused on prevention programs since ecosystem restoration does not recover complete ecosystem functionality (Lal, 2001; Moreno-Mateos et al., 2017). Moreover, even after several decades, relict degradation legacies can remain (Alados et al., 2011).

5. CONCLUSIONS

The present study can be seen as a step forward to better understanding the effect of land degradation on the intricate network of multi-scale processes, factors and structures that define ecosystems' biological productivity and ultimately control their C balances. Despite some limitations, such as long-term data gaps, this research demonstrates that continuous ecosystem-scale EC observations remain crucial to comprehend how climate and land use change can modify the C sequestration capacity of ecosystems. In fact, annual average release of 196 ± 40 and -23 ± 20 g C m^{-2} yr^{-1} for the "degraded" and "natural" (i.e. site of reference) sites were measured, respectively. Additionally, larger net CO_2 uptake over longer periods was observed at the "natural" site, concretely an amount of C 162% higher compared to the "degraded" site, whereas much

greater net CO_2 release was measured at the "degraded" site during drought periods. Future research should be based on the continuity of long-term monitoring stations, such as eddy covariance stations, in order to calibrate and validate satellite data, reduce uncertainties in the relationships between ecosystem productivity, land degradation and climate change and finally, to improve the predictive ability of current terrestrial C models.

SUPPLEMENTARY MATERIAL

Table S1. Results of the two-sided Wilcoxon summed rank test used to assess differences between meteorological variables measured at each experimental site over the all periods. Medians of the absolute (Diff) and standardized differences (Diff and $Diff_{st}$) between the samples (Amoladeras minus Balsa Blanca), p-values and number of observations (n) are detailed.

Variables	All periods			
	Diff	$Diff_{st}$	p-value	n
PPFD ($\mu mol\ m^{-2}\ s^{-1}$)	0.4701	0.0009	0	205751
Net radiation ($W\ m^{-2}$)	-8.8620	-0.0457	0	197924
T_{air}(°C)	0.1928	0.0310	6.42E-10	182240
VPD (hPa)	0.5358	0.0783	4.38E-104	166918
RH (%)	-3.1947	-0.1636	6.39E-244	197649
u_* ($m\ s^{-1}$)	-0.0016	-0.0054	0.1214	166346
WS ($m\ s^{-1}$)	0.3621	0.1628	0	166359
WS_{max}($m\ s^{-1}$)	0.4327	0.1001	5.53E-132	165458
Pressure (hPa)	19.0061	1.6999	0	166359
Precipitation (mm)	-0.0001	-1.95E-05	0.0003	204892
$CO_{2,\ 0.05m}$ (ppm)	-93.8644	-0.4027	0	46340
$CO_{2,\ 1.50m}$ (ppm)	888.9239	1.1196	0	50133
$T_{0.05m}$ (°C)	0.9215	0.0927	5.51E-21	46337
$T_{1.50m}$ (°C)	0.5780	0.1476	1.43E-51	50137
$VWC_{0.05m}$ ($m^3\ m^{-3}$)	0.0372	0.8265	0	52353
$VWC_{1.50m}$ ($m^3\ m^{-3}$)	-0.0123	-0.8385	0	53865

Variables	May - September			
	Diff	$Diff_{st}$	p-value	n
PPFD (μmol m^{-2} s^{-1})	0.5230	0.0009	8.11E-147	84491
Net radiation (W m^{-2})	-10.9546	-0.0476	4.78E-167	81019
T_{air}(°C)	0.8378	0.1935	1.53E-145	77866
VPD (hPa)	1.1136	0.1370	4.50E-90	71474
RH (%)	-2.0229	-0.1031	1.21E-38	80950
u_* (m s^{-1})	-0.0186	-0.0563	8.47E-31	71194
WS (m s^{-1})	0.1720	0.0793	1.84E-31	71195
WS_{max}(m s^{-1})	0.0498	0.0124	0.0749	70635
Pressure (hPa)	18.6707	1.8696	0	71195
Precipitation (mm)	0.0000	-4.84E-05	4.29E-05	83860
$CO_{2, \, 0.05m}$ (ppm)	-89.2404	-0.6578	9.99E-207	21413
$CO_{2, \, 1.50m}$ (ppm)	1109.1440	1.3517	0	24347
$T_{0.05m}$ (°C)	-0.8057	-0.1160	3.04E-16	21410
$T_{1.50m}$ (°C)	-0.1570	-0.0591	3.13E-07	24350
$VWC_{0.05m}$ (m^3 m^{-3})	0.0286	1.2724	0	25231
$VWC_{1.50m}$ (m^3 m^{-3})	0.0011	0.0674	3.51E-18	24570

Table S2. Results of the two-sided Wilcoxon summed rank test used to assess differences between meteorological variables measured at each experimental site from May to September. Medians of the absolute (Diff) and standardized differences (Diff and $Diff_{st}$) between the samples (Amoladeras minus Balsa Blanca), p-values and number of observations (n) are detailed.

Variables	May – September Daytime				Table S3. Results of the two-sided Wilcoxon summed rank test used to assess differences between meteorological variables measured at each experimental site from May
	Diff	Diff$_{st}$	p-value	n	
PPFD (μmol m^{-2} s^{-1})	64.3400	0.1378	5.62E-42	38963	
Net radiation (W m^{-2})	-21.9460	-0.1205	4.80E-34	38963	
T_{air}(°C)	0.1939	0.0502	1.39E-06	37480	
VPD (hPa)	-0.7579	-0.0938	3.87E-20	34430	
RH (%)	2.9921	0.1784	1.45E-65	38935	
u_* (m s^{-1})	-0.0430	-0.1340	3.76E-87	34284	
WS (m s^{-1})	0.0356	0.0165	0.1341	34285	
WS$_{max}$(m s^{-1})	-0.2920	-0.0796	5.83E-14	33994	
Pressure (hPa)	18.4085	1.8633	0	34285	
Precipitation (mm)	0.0000	5.32E-05	0.9875	38963	
$CO_{2,\,0.05m}$ (ppm)	-149.513	-1.1396	0	9816	
$CO_{2,\,1.50m}$ (ppm)	1046.358	1.3062	0	11385	
$T_{0.05m}$ (°C)	-1.473	-0.2119	2.70E-21	9813	
$T_{1.50m}$ (°C)	-0.220	-0.0834	4.75E-07	11385	
VWC$_{0.05m}$ (m^3 m^{-3})	0.028	1.2839	0	11303	
VWC$_{1.50m}$ (m^3 m^{-3})	0.001	0.0547	1.05E-09	11462	

to September during daytime. Medians of the absolute (Diff) and standardized differences (Diff and Diff$_{st}$) between the samples (Amoladeras minus Balsa Blanca), p-values and number of observations (n) are detailed.

CHAPTER 2:

ENHANCEMENT OF THE NET CO$_2$ RELEASE OF A SEMIARID GRASSLAND IN SE SPAIN BY RAIN PULSES

Ana López-Ballesteros, Penélope Serrano-Ortiz, Enrique P. Sánchez-Cañete, Cecilio Oyonarte, Andrew S. Kowalski, Óscar Pérez-Priego, Francisco Domingo

ABSTRACT

Occasional rain events occur over the dry season in semiarid ecosystems and cause immediate, large increases in the net CO_2 efflux, which gradually decrease over a few days following the rain event. In a semiarid grassland located in SE Spain, these precipitation pulses represent only 7% of dry season length but provoked approximately 40% of the carbon emitted during the dry seasons over 2009-2013. We performed a manipulation experiment to decompose the net ecosystem pulse response into its biological processes in order to quantify how much of a role photosynthesis and aboveground respiration play compared to soil respiration. Experimental results showed that while soil respiration was the dominant component of the net CO_2 flux (net ecosystem CO_2 exchange, NEE) over the irrigation day and the day after (80% of NEE), plant photosynthesis remained inactive until 2 days after the pulse, when it appeared to become as prevalent as soil respiration (approximately 40% of NEE). Additionally, aboveground respiration was generally secondary to soil respiration over the whole experiment. However, statistical results showed that aboveground carbon exchange was not significantly affected by the rain pulse, with soil respiration being the only component significantly affected by the rain pulse.

1. INTRODUCTION

Arid and semiarid ecosystems comprise nearly a third of the total land surface (Okin, 2001; Schlesinger, 1990) and play a pivotal role in the global carbon (C) balance (Ahlström et al., 2015; Metcalfe, 2014; Poulter et al., 2014), owing to their dynamic behavior modulated by precipitation events. In this regard, rain pulses are common and stochastic water inputs that strongly determine arid land structure and function (Ehleringer et al., 1999; Lázaro et al., 2001; Noy-Meir, 1973), especially after an extended period of hydric stress. In Mediterranean regions, occasional summer and early autumn storms fit this concept due to their brevity and unpredictable nature (Cleverly et al., 2013; Lázaro et al., 2001) and even can be recognized as a transition phase between dry and growing seasons.

Some studies have examined regional-scale rain pulse responses using satellite imagery and climatic data. For example, Li et al. (2013) found correlations between the magnitude of rain events and the photosynthetic activity increase in two different arid ecosystems. Conversely, Zhang et al. (2013) concluded that the combination of heavy rainfalls with dry periods led to a reduction in primary production. Measurements of CO_2 exchanges at the ecosystem scale also highlighted an enhancement of C release triggered by rain pulses under dry conditions (Jenerette et al., 2008; Ross et al., 2012; Williams et al., 2009). However, deeper knowledge is needed in order to understand the mechanisms by which rain pulses affect the biological processes that compose the overall net ecosystem response.

In this sense, most research has focused on either soil processes (Fan et al., 2012; Leon et al., 2014; Sponseller, 2007; Unger et al., 2010) or plant physiological responses (Balaguer et al., 2002; Padilla et al., 2015; Pugnaire et al., 1996). Accordingly, few studies have simultaneously and separately tracked

the effect of rain pulses on the overall components of the ecosystem C balance in order to disentangle all the processes composing the total effect on net ecosystem CO_2 exchange (NEE) (Huxman et al., 2004a; Unger et al., 2012).

In this study, we have assessed the relevance of rain pulses over the dry season C balance of a semiarid grassland located in southeast Spain through the analysis of eddy covariance (EC) data from 2009 to 2013. In addition, given the complexity of C dynamics in these regions, we simulated a realistic rain pulse in order to delve into the short-term response of the distinct biological processes that compose the overall rewetting effect on NEE, monitoring aboveground and belowground C exchanges. For this purpose, we have integrated novel methodologies, such as transient-state canopy chambers, soil chambers, and subsoil continuous CO_2 sensors, to directly measure aboveground net primary productivity (ANPP), soil respiration (R_{soil}), aboveground respiration ($R_{aboveground}$), and plot-scale NEE (i.e., NEE_{plot}).

We hypothesize that rain pulses during the dry season provoke a relevant net C release by enhancing soil respiration processes, commonly known as the Birch effect (Birch, 1959; Carbone et al., 2011; Huxman et al., 2004a; Jarvis et al., 2007; Leon et al., 2014; Sponseller, 2007; Thomey et al., 2011; Unger et al., 2010; Wohlfahrt et al., 2008). Furthermore, since Balaguer et al. (2002) stated that the relevant species (Machrocloa *sp.*) has the ability to respond to punctual, infrequent, and random rain pulses, we expect activation of plant photosynthesis following rain events, regardless of pulse magnitude (Lázaro et al., 2001; Sala and Lauenroth, 1985), although this C assimilation may be offset or even exceeded by soil respiratory emissions.

Accordingly, our objectives are as follows: (i) to quantify the contribution of rain pulse events to dry season NEE in this semiarid grassland, (ii) to detect differing NEE responses depending on the magnitude of rain pulses, and (iii) to

determine if soil respiration, as well as plant photosynthesis (i.e., belowground and aboveground processes, respectively), activates following the rain events.

2. MATERIAL AND METHODS

2.1. EXPERIMENTAL SITE DESCRIPTION

This study was carried out at the experimental site of Balsa Blanca (N36°56′26.0″, W2°01′58.8″), a semiarid grassland located in the Cabo de Gata-Níjar Natural Park (Almería, Spain). Detailed information concerning the characteristics of this experimental site can be found in Material and Methods section (pp. 20, 22-23).

### 2.2. METEOROLOGICAL AND EDDY COVARIANCE MEASUREMENTS AND DATA PROCESSING

In this study, we used meteorological and flux data from 2009 to 2013, acquired by an eddy covariance (EC) tower and complementary sensors (detailed in Table 1 of Material and Methods section; p. 42) installed in Balsa Blanca (site code "Es-Agu" of the European Database Cluster, http://www.europe-fluxdata.eu/). The CO_2, water vapor, and sensible heat fluxes were calculated from raw data acquired at 10 Hz and processed with EddyPro 5.1.1 software (Li-Cor, Inc., USA). Processing steps included spike removal, double axis rotation, correction for sensor separation, spectral corrections for high- and low-frequency ranges (Moncrieff et al., 2005, 1997), Reynolds averaging, and correction for density fluctuations (Webb et al., 1980). Half-hourly averaged fluxes were rejected if missing raw data records exceeded 10% or more of the total records of any of the three components of wind velocity and/or CO_2 concentration. Quality of EC flux data was assured by selecting quality control flags 0 and 1 from EddyPro outputs (Mauder and Foken, 2006)

and by rejecting the remaining anomalous flux data associated with dust, rain, or dew events. In addition, averaging periods with low turbulence were filtered out based on a friction velocity (u_*) threshold estimated for each year by using the approach proposed by Reichstein et al. (2005). The averaged u_* threshold for all the analyzed period (i.e., 2009–2013) was 0.15 m/s. The resulting fraction of daily and nocturnal missing NEE_{EC} data averaged for all years were 33 ± 13% and 74 ± 9%, respectively. However, assessment of the effect of rain pulses on NEE at ecosystem scale was performed with EC data for the drought period (defined below), and in addition, 70% of total rain pulses occurred during daytime, resulting in less missing NEE_{EC} data, approximately 25 ± 11%.

The net ecosystem carbon balances (NEE_{EC}) for both the year and the dry season were estimated by integrating the half-hourly CO_2 fluxes. Missing values were filled using the marginal distribution sampling technique (Reichstein et al., 2005). Random uncertainty and errors in NEE_{EC} values introduced by the gap-filling process were calculated from the variance of the gap-filled data. The variance of the measured data was calculated by introducing artificial gaps and repeating the standard gap-filling procedure. Twice the standard deviation of sums of total data was taken as our NEE_{EC} error for the several time periods we used. Positive values of NEE_{EC} imply net CO_2 release to the atmosphere, while negative values represent net CO_2 uptake.

Regarding the rain pulse response analysis with EC data, dry seasons were defined as periods when a minimum volumetric soil water content (VWC_{soil}) of approximately 0.025 $m^3 m^{-3}$ was observed, which usually began in the middle of July and ended in early November (Fig. 1).
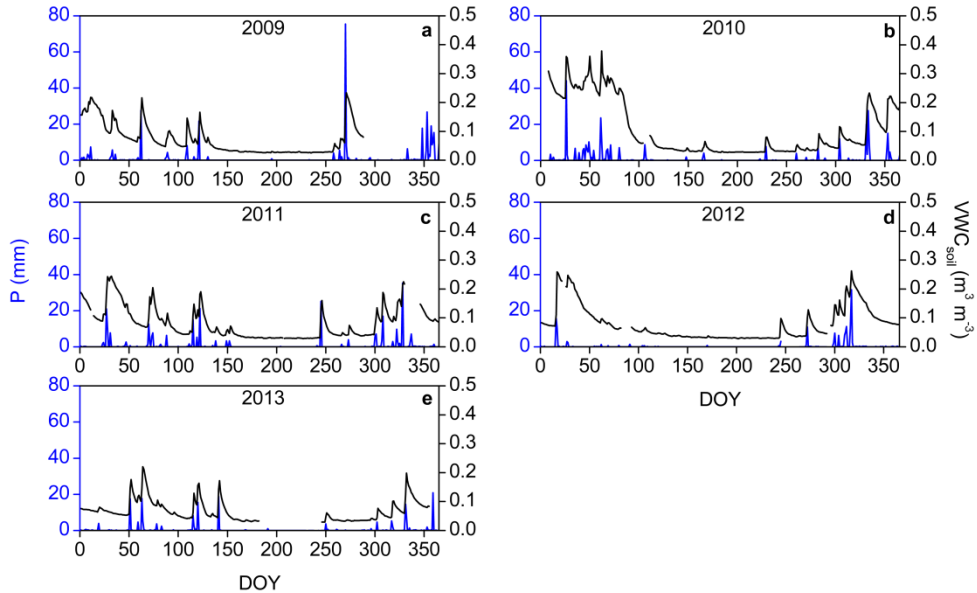
Figure 1. Time series of daily averaged soil water content (VWC$_{soil}$; m^3 m^{-3}, black line) and precipitation (P; mm, blue line) in Balsa Blanca, for every year from 2009 to 2013.

Additionally, we considered that precipitation pulses were those precipitation events observable by VWC$_{soil}$ sensors, which corresponded to >1 mm rainfall. We assessed the ecosystem response to rain pulse via the analysis of net ecosystem CO$_2$ fluxes during 7 days, from 1 day before the precipitation pulse to 5 days afterward. We excluded from our EC data analyses those half-hourly averaged EC values that corresponded to the moments when rainfall occurred in order to ensure the quality of the analyzed data. This period was selected after observing that the effect of most of rain pulses on NEE$_{EC}$ disappears after 5 days.

2.3. RAIN PULSE EXPERIMENT

2.3.1. EXPERIMENTAL OVERVIEW

This section summarizes the experimental design; details for individual measurement systems appear in the subsections of the following section.

Eight plots of 0.25 m^2 containing a tussock grass of medium size and its surrounding soil area were randomly selected and demarcated in order to monitor aboveground, belowground, and net CO_2 exchanges during the rainfall manipulation experiment (Fig. 2).
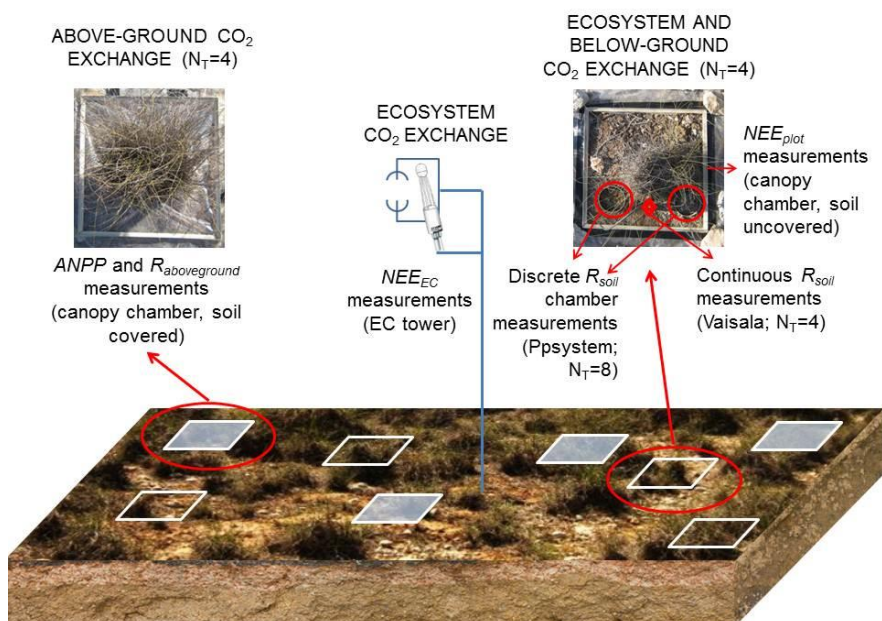
Figure 2. Diagram of the different methodologies used in this study in order to measure carbon exchanges at several spatial scales.

On the other hand, the remaining four plots were selected to measure soil as well as net CO_2 exchanges (R_{soil} and NEE_{plot}, respectively; Fig. 2, top right), where NEE_{plot} fluxes were measured using the canopy chamber and discrete and continuous R_{soil} measurements were acquired by means of two different methodologies: soil respiration chambers were located on two PVC collars per plot (10 cm height, 10.5 cm diameter) to acquire discrete R_{soil} measurements, and volumetric soil CO_2 molar fraction, soil temperature, and volumetric soil water content were continuously measured by means of a CO_2 probe (GMM222, Vaisala, Helsinki, Finland), a temperature sensor (Decagon Devices, Inc., Pullman, WA, USA), and a ECH_2O sensor (EC-20, Decagon Devices, Inc.,

Pullman, WA, USA), respectively, in each of the four plots where the soil remained uncovered. These sensors were located at 5 cm depth, and data were collected every 5 min. All soil sensors were placed within the experimental plots 1 month before the experiment in order to allow partial soil structure recovery. Soil properties alteration related to water channeling alongside the instrument was not observed during the experiment.

The experiment was conducted from 25 August (experiment day 1) to 29 August (experiment day 3) 2014, when meteorological conditions were similar and representative of the dry summer season in southeast Spain; concretely, no rainfall was registered since 24 June 2014. During day 1, the day prior to watering, we monitored aboveground, belowground, and net ecosystem CO_2 exchanges at the plot scale in order to characterize the ecosystem status under dry conditions. On day 0, the rain pulse was simulated in the early morning, when each plot was irrigated with 3.75 L of evenly distributed water with low mineralization, which corresponds to a precipitation event of 15 mm. Chamber measurement frequency was not constant during the whole experiment period. During the first two days (days 1 and 0), flux measurements were carried out approximately every hour in order to characterize diurnal variability before and immediately after the rain event. However, during days 1-3, measurements were carried out before solar noon since the photosynthetic activity of this species reached its maximum in early morning and became negligible around the central hours of the day (Haase et al., 1999; Pugnaire et al., 1996; Ramírez, 2006). All the instrumentation was calibrated 1 month before the experiment.

2.3.2. CANOPY AND SOIL CHAMBERS MEASUREMENTS

2.3.2.1. CANOPY CHAMBER

A transparent transitory-state closure chamber ("canopy chamber") was used to measure ANPP, $R_{aboveground}$ and NEE_{plot}. Chamber dimensions were 50x50x60 cm and dark conditions, when measuring $R_{aboveground}$, were kept by covering with an opaque and reflective material to avoid light within the canopy chamber. The chamber system includes the following instrumentation: an Infrared Gas Analyzer (IRGA; Li-840, Li-cor, Lincoln, NE, USA), two small fans (8.9 cm diameter), a thermocouple (PT100), and a datalogger (CR1000, Campbell Sci., Logan, UT, USA). For each set of measurements, light conditions measurements (i.e. ANPP and NEE_{plot} fluxes) were acquired approximately 1 h before dark conditions measurements in order to minimize plant perturbations. We chose this approach because it is portable and allows rapid and accurate canopy flux measurements. More detailed information about canopy chamber design and methodology is given by Pérez-Priego et al. (2015).

2.3.2.2. SOIL CHAMBER

A manual and portable opaque soil chamber system (EGM-4, PP-systems, Hitchin, UK) was used to acquire discrete measurements of soil CO2 effluxes ($R_{soil\_ppsystem}$). For each measurement, the soil chamber was placed on a PVC collar during 120s and CO_2 and water vapor molar fractions were recorded every 3 seconds.

2.3.2.3. FLUX CALCULATION

For both chamber systems, the CO_2 fluxes were estimated from the initial slopes of CO_2 molar fractions of the confined air versus time, by using either linear or quadratic regression (Kutzbach et al., 2007; Pérez-Priego et al., 2010; Wagner et al., 1997) for the best regression fit. The raw values of CO_2

molar fraction were previously corrected for dilution (Hubb, 2012) from CO_2 molar fractions referred to wet air. Finally, the flux density was calculated using the ideal gas equation as explained by Pérez-Priego et al. (2015). We rejected measurements acquired just after water addition to exclude data corresponding to the degasification process, namely, the displacement of CO_2-rich air from soil pores to the atmosphere due to water infiltration (Inglima et al., 2009; Ma et al., 2012; Marañón-Jiménez et al., 2011; Wohlfahrt et al., 2008; Xu et al., 2004).

2.3.3. CONTINUOUS SOIL CO_2 FLUXES

The subsurface CO_2 molar fraction was continuously measured in each plot by CO_2 sensors (GMM222, Vaisala, Helsinki, Finland). Each probe was encased in a vertical PVC pipe open at the bottom, buried to a depth of 5 cm and sealed on the upper part by a rubber gasket. Sampling frequency was 1 Hz and 5 min averages were stored in a data-logger (CR3000, Campbell Sci., Logan, UT, USA). The CO_2 molar fraction readings were corrected for variations in soil temperature and atmospheric pressure. The soil CO_2 efflux ($R_{soil\_vaisala}$) was estimated according to the gradient method described by Sánchez-Cañete and Kowalski (2014).

2.3.4. STATISTICAL ANALYSIS

We applied different statistical tests to analyze the effect of the rain pulse over the different CO_2 fluxes measured at ecosystem and plot scales. On one hand, the one-way ANOVA test was applied to EC data in order to analyze the time response of the semi-arid grassland C balance after rain pulses. On the other hand, we used the repeated-measurements ANOVA test to evaluate the effect of irrigation, in terms of time (i.e. days before and after rain pulse) as the fixed factor, over NEE_{plot}, ANPP, R_{soil} and $R_{aboveground}$ since we directly measured every flux component in four plots over the five days of the

experiment. For all the repeated-measurements ANOVA analysis, the Mauchly sphericity test indicated that the sphericity assumption was not fulfilled, therefore we used the Huynh-Feldt approach to correct degrees of freedom. Additionally, in both cases, we investigated the differences between pairs of groups (i.e. CO_2 fluxes) via Bonferroni post-hoc test. The statistical parameters obtained were F-ratio ($F(DF_M, DF_R)$), together with the model and residual degrees of freedom (DF_M and DF_R, respectively), P-value and partial eta-squared (η^2_p).

3. RESULTS

3.1. EDDY COVARIANCE FLUXES AND RAIN PULSE EVENTS

Eddy covariance CO_2 fluxes in Balsa Blanca reveal that, although annual NEE_{EC} varies widely from acting as a carbon (C) source or C sink over the period 2009-2013, net CO_2 emissions occur during the dry season for all years (Table 2). In fact, during the dry season, more than 80% of all days correspond to daytime C emissions. Additionally, precipitation pulses systematically provoke greater net emission of CO_2 over the short term (days to weeks; Fig. 3).

Year	Annual NEE_{EC}	Dry season NEE_{EC}	Total rain pulses dry season	Total rainfall dry season	NEE_{EC} after rain pulses	$\dfrac{C_{\text{rain pulse}}}{C_{\text{dry season}}}$
-	g C m^{-2}	g C m^{-2}	-	mm	g C m^{-2}	%
2009	43 ± 8	51 ± 4	7	89	30 ± 2	58
2010	-42 ± 8	37 ± 6	6	24	17 ± 2	46
2011	-67 ± 7	48 ± 4	4	36	17 ± 2	36
2012	67 ± 7	73 ± 4	5	20	30 ± 2	41
2013	-23 ± 7	22 ± 4	1	4	2 ± 1	9
Avg ± SD	-4 ± 57	46 ± 19	5 ± 2	35 ± 33	19 ± 12	38 ± 18
CV (%)	-1297	41	50	94	60	48

Table 2. Contribution of carbon emitted during five days subsequent to rain pulse events (> 1 mm) over the total carbon emitted during the dry season (DOY=200-310). Uncertainty of NEE_{EC} is related to gap-filling procedure. Average, standard deviation and coefficient of variation (Avg, SD and CV, respectively) are presented in the last three rows. Positive values indicate carbon release while negative values mean carbon uptake.

As shown in Table 2, an important amount of the total C emitted during the dry season corresponds to CO_2 released in the first 5 days following precipitation. On average, although precipitation pulse responses represent only 7% of the dry season length, ca. 40% of the C emitted during the dry season corresponds to ecosystem CO_2 release registered after these precipitation events.

In this regard, in 2009, the highest number of pulse events together with the highest amount of total rainfall resulted in a release of 58% of total C emitted during post-pulse episodes comprising just 11% of the dry season period. Similarly, in 2010, 2011 and 2012, a relevant number of rain events caused 36-46 % of the total C emission during 6-10% of the dry season period, while in 2013, far fewer and smaller rain pulses occurred, which corresponded to 9% of the total C emitted over just 2% of the dry season. Regarding inter-annual variability (Table 2), annual NEE_{EC} shows the highest coefficient of variation (CV=1297) compared to NEE_{EC} during dry season (CV=41) and after rain

93

pulses (CV=60), and also compared to the fraction of C loss following rain events over the total C amount emitted during dry season. Total amount of rainfall corresponding to rain pulses is also highly variable among years (CV=94).
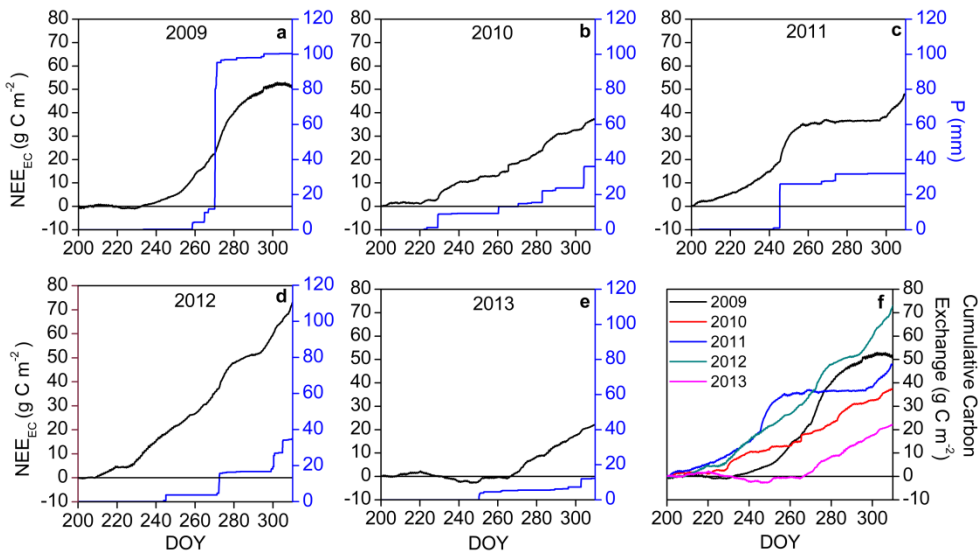

Figure 3. Cumulative dry season (DOY=200-310) net ecosystem carbon exchange measured with eddy covariance tower (NEE$_{EC}$; g C m^{-2}) and cumulative precipitation (P; mm) in Balsa Blanca, for every year from 2009 to 2013.

In Figure 3, we can notice that moderate and large precipitation pulses provoked sudden and great increases in C emissions that returned to neutral progressively over several days after watering, as can be seen for some of the rain pulses occurring in 2010, 2011 and 2012 (Fig. 3b, 3c and 3d, respectively). Additionally, in 2009, when the highest rain pulse occurred (83 mm) over 2009-2013, we also detect net C uptake several weeks after precipitation (negative slope; Fig. 3a). In contrast, small rain pulses triggered slight increases in C emission rates, as occurred in 2010 and 2013 (Fig. 3b, 3e). Overall, rain pulses influence the pattern of net C emission over the dry season for 2009-2013 by increasing C release rates (Fig. 3f).

It is evident that rain pulse magnitude is an important factor that determines the NEE_{EC} response (Fig. 3, 4). Based on our results, high-magnitude rain pulses ($\geq$ 20 mm) can enable net CO_2 uptake since they generate a reserve of available water for several days enabling plants to up-regulate and then carry out photosynthesis. For instance, the 83-mm rain pulse of September 27th, 2009 (Fig. 4a) provoked CO_2 release during the subsequent 7 days, but then NEE_{EC} became neutral and afterwards started - on the 10th day after abundant rainfall - to show diurnal net assimilation patterns with maximum uptake rates of approximately 4 $\mu mol\ m^{-2}\ s^{-1}$.
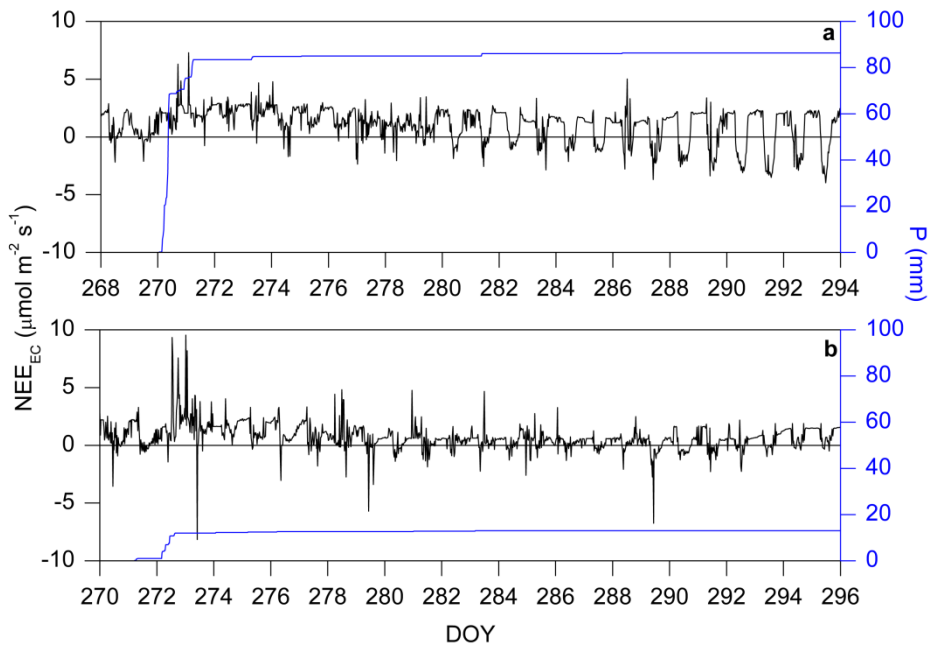
Figure 4. Half-hour averages of net ecosystem carbon exchange (NEE_{EC}; $\mu mol\ m^{-2}\ s^{-1}$, black line) and accumulated precipitation (P; mm, blue line). Upper graph **(a)** shows an extreme rain pulse (27th September 2009), and **(b)** a small rain pulse (28th September 2012). Positive values indicate CO_2 release and negative values mean CO_2 uptake.

In contrast, low-magnitude rain pulses (< 10 mm), such as that of September 28th, 2012 (Fig. 4b), do not trigger net CO_2 uptake. However, this far lesser

rainfall also readily provoked net emission of CO_2 of approximately 3 µmol m^{-2} s^{-1} over a seven day interval until NEE$_{EC}$ returned to near-neutral levels.

Consequently, the overall effect of precipitation pulses on the C balance of our semi-arid site depends on the amount of rainfall in each pulse. In this context, the rain pulse magnitude distribution (Fig. 5) highlights the higher occurrence of low-magnitude rain pulses (i.e. < 10 mm) that commonly trigger net CO_2 emission, as shown before.
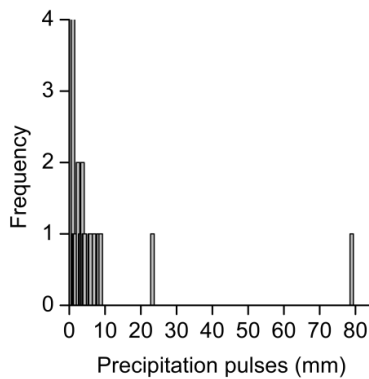
Figure 5. Absolute frequency distribution of magnitudes of rain pulses occurring during the dry season (DOY=200-310) over a 5 years period (2009-2013).
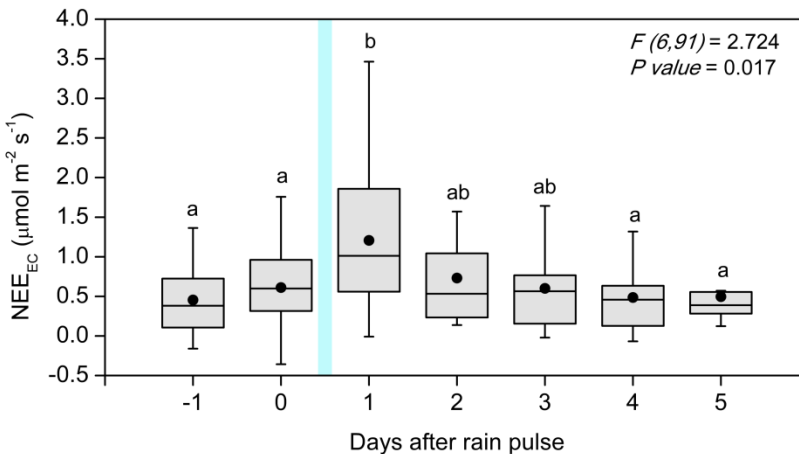
Figure 6. Box-and-whisker plots of diurnal ecosystem responses after an averaged rain pulse of 5 ± 5 mm (blue bar) in terms of net ecosystem carbon exchange measured with eddy covariance (NEE$_{EC}$; µmol CO_2 m^{-2} s^{-1}). Every flux data point corresponds to the diurnal average of half-hour NEE$_{EC}$ fluxes after every rain pulse occurred during the drought periods (DOY=200-310) of years 2009-2013. Positive values indicate CO_2

96

release. Results of one-way ANOVA test (F-ratio and P-value) and post-hoc Bonferroni test (letters above the box charts) are shown in the graph; the significance level is 95% (α=0.05).

In fact, when we examine the short-term effect of rain pulses over the measured NEE_{EC} for the whole study period (i.e. dry seasons of 2009-2013) at the diurnal time scale (Fig. 6), we see that net *C* emission predominates, reaching its maximum during the first 24h after the rain pulse. During subsequent days, NEE_{EC} decreases in magnitude and reaches values quite similar to those occurring the day before water input. The high variability of NEE_{EC} is related to the great amount of data used to calculate each averaged value, which corresponds to variable-magnitude rain pulses happening at different moments over the dry season (Fig. 6). However, the ANOVA test results show that NEE_{EC} is significantly affected by rain pulses at the short-term ($F_{(6,91)}$=2.724; P-value=0.017), for the overall rain pulses that occurred over the whole study period (2009-2013). In addition, based on Bonferroni test results, there is a significant difference between the day after the rain pulse (day 1), when the highest ecosystem CO_2 flux rate occurs, compared to the rest of the days.

3.2. RAIN PULSE MANIPULATION EXPERIMENT

On one hand, we analyze the pulse response evolution for every NE*E* component based on the plot-scale flux measurements acquired during the manipulation experiment. Generally, during the whole five–day experiment, R_{soil} measured with soil respiration chambers (i.e. $R_{soil\_PPsystem}$) and R_{soil} measured with soil CO_2 concentration sensors ($R_{soil\_vaisala}$) agreed by showing similar CO_2 flux values and patterns (Fig. 7), so hereinafter we will occasionally refer to both variables as if they were the same (i.e. R_{soil}). During the pre-pulse day (day -1), average NEE was low but positive (0.25 μmol m^{-2} s^{-1}), with R_{soil} being the predominant component comprising 61% of the NEE magnitude (Fig. 8c).
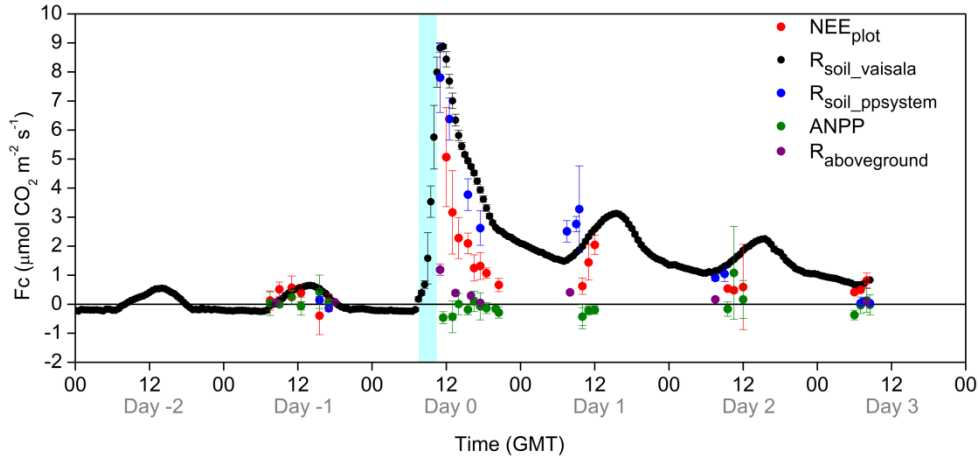
Figure 7. Averaged (n=4) CO_2 fluxes (Fc; μmol m^{-2} s^{-1}) of: net ecosystem carbon exchange at plot scale (NEE$_{plot}$; red data points), above-ground net primary production (ANPP; green data points), above-ground respiration (R$_{aboveground}$) and below-ground or soil respiration fluxes, obtained with soil chambers (R$_{soil\_ppsystem}$; blue data points) and with soil CO_2 concentration sensors (R$_{soil\_vaisala}$; black data points), all measured during the five days of the experiment (25-29 August 2014), one before and 4 after the simulated rain pulse of 15 mm (blue bar on day 0). Positive values indicate CO_2 release while negatives values mean CO_2 uptake. Error bars are ±SD.

On day 0, we irrigated each plot with 15mm and afterwards, *NEE* was one order of magnitude higher than on the previous day (ca. 10 μmol m^{-2} s^{-1}) and, likewise R$_{soil}$ was the prevailing component constituting 82% of the overall net *C* release, while R$_{aboveground}$ only comprised 13% (Fig.8d). On day 1 (*i.e.* first day after the pulse), *NEE* decreased 64%, with R$_{soil}$ and R$_{aboveground}$ prevalent as on day 0. Contrary to previous days, on day 2, despite the great variability measured among plots, the contribution of the average *ANPP* became as important as R$_{soil}$, each comprising 40% of *NEE* (Fig. 8b). Additionally, R$_{aboveground}$ increased its prevalence up to 17%. Finally, on day 3 of the experiment, *NEE* became neutral (ca. 0.64 μmol m^{-2} s^{-1}), similar to the pre-pulse day.
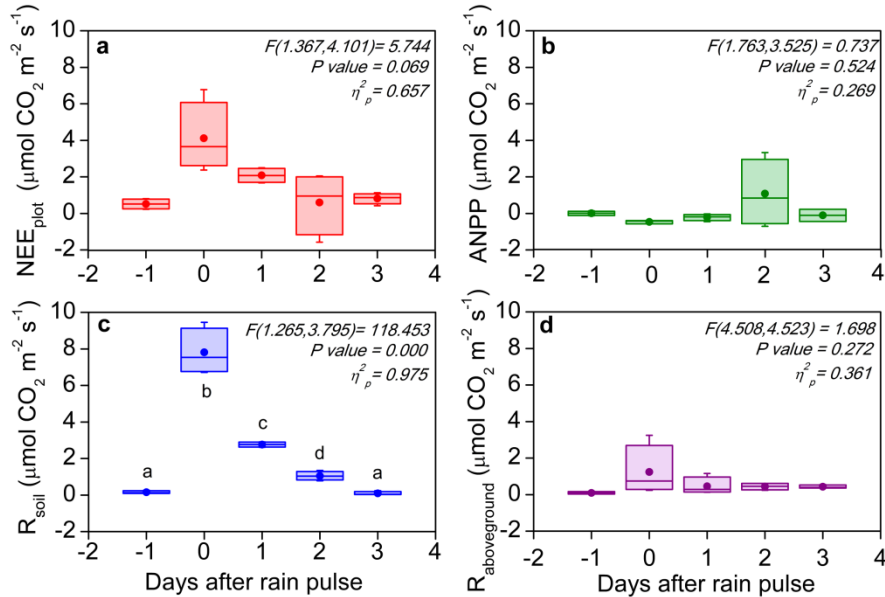
Figure 8. Box-and-whisker plots of CO_2 fluxes (µmol m^{-2} s^{-1}) of: **(a)** net ecosystem carbon exchange at plot scale (NEE$_{plot}$; red box charts), **(b)** above-ground net primary production (ANPP; green box charts), **(c)** below-ground or soil respiration (R$_{soil}$; blue box charts) measured with chambers, and **(d)** above-ground respiration (R$_{above-ground}$) for the five-days long rain pulse manipulation experiment. Results of the one-way ANOVA test for repeated measurements (F-ratio and P-value) and the post-hoc Bonferroni test (letters above the box charts) are shown in every graph (n=4). For all the statistical analysis, the significance level is 95% (α=0.05) and Huynh-Feldt approach has been used to correct degrees of freedom.

Additionally, we elucidate whether the *NEE* components were significantly affected by rain pulses at the daily time scale (Fig. 8). In this sense, results of the repeated-measurements ANOVA test applied to plot-scale NEE, ANPP, R$_{soil}$ and R$_{aboveground}$ showed that only R$_{soil}$ was significantly affected by irrigation ($F_{(1.27, 3.80)}$=118.45; P-value=0.000; η^2_p=0.98; Fig. 8c). In fact, the Bonferroni test results demonstrated that daily *R$_{soil}$* fluxes were statistically different among days 0-2 (Fig. 8c), while day -1 and day 3 were not different. On the other hand, NEE was also statistically affected at a lower significance level of 90% ($F_{(1.37, 4.10)}$=5.74; P-value=0.069; η^2_p=0.49; Fig. 8a). Additionally, we found significant differences between day -1 and the day after irrigation (day 1) as well as between day 1 and 3, but also at a lower significance

level of 90%. In contrast, ANPP (F(1.76, 3.53)=0.74; P-value =0.52; η^2_p=0.27) and $R_{aboveground}$ (F(1.51, 4.52)=1.70; P-value =0.27; η^2_p=0.36) were not significantly affected by the rain event (Fig. 8b and 8d).

The relationship between the common driving factors that determine CO_2 flux magnitudes over the experiment is modulated by soil water availability. Air temperature as well as soil temperature influence R_{soil} (i.e. $R_{soil\_ppsystem}$) only when soil is moist (Fig. 9a and 9b). In fact, we can observe two distinct groups of points, one where R_{soil} fluxes are close to zero even for high soil temperatures of around 35-45ºC (Fig. 9b), and another where an hysteretic pattern may correspond to the days after irrigation (Fig. 9a and 9b). Similarly, light sensitivity of ANPP fluxes uniquely exists in a few particular moments after irrigation, as very low values of ANPP are registered for a wide range of incident photosynthetically photon flux densities (PPFD; Fig 9c). Accordingly, NEE_{plot} measurements are more affected by increments in soil volumetric water content (VWC_{soil}), as well as R_{soil}, given the scant plant photosynthetic response to water addition.
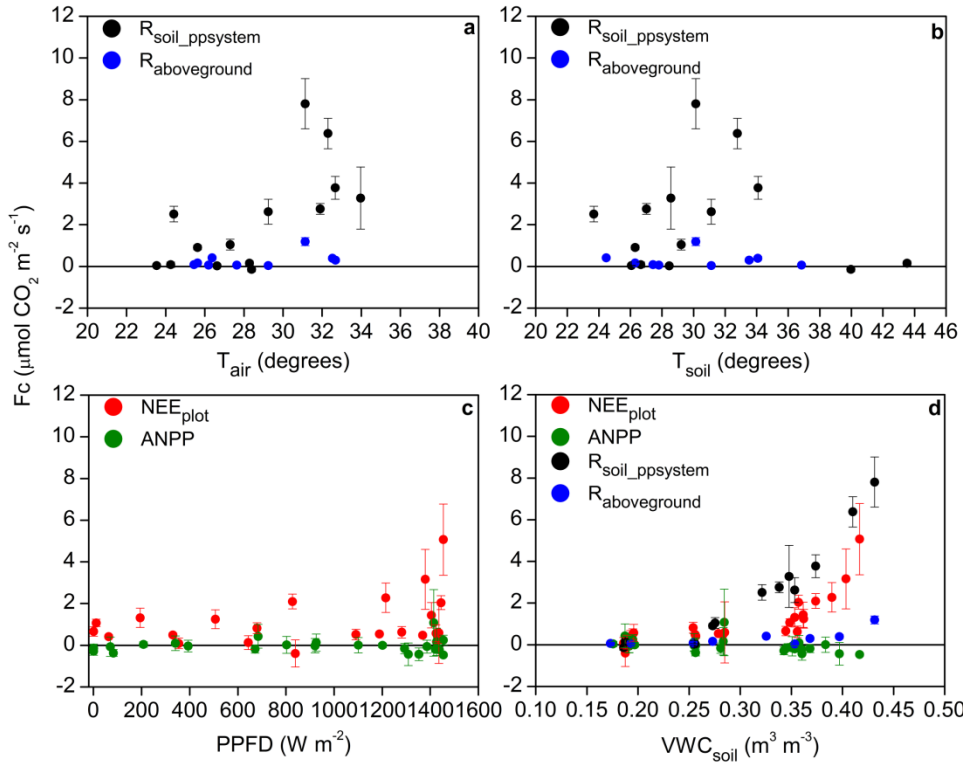
Figure 9. Relationship between meteorological variables and CO_2 fluxes measured during the five days-long experiment performed in Balsa Blanca from the 23th August to 29th August 2015. Half-hour averages of: **(a)** air temperature (T_{air}) versus above-ground respiration ($R_{aboveground}$) and soil respiration measured with chamber systems ($R_{soil\_ppsystem}$); **(b)** soil temperature (T_{soil}) versus above-ground respiration ($R_{aboveground}$) and below-ground or soil respiration measured with chamber systems ($R_{soil\_ppsystem}$); **(c)** photosynthetically photon flux density (PPFD) versus inverse of above-ground net primary production (ANPP) and net ecosystem exchange (NEE_{plot}), and **(d)** volumetric soil water content (VWC_{soil}) versus all punctual measured CO_2 fluxes (NEE_{plot}, ANPP, $R_{soil\_ppsystem}$ and $R_{aboveground}$). All flux data are averages of 4 measurements. Positive values indicate CO_2 release while negative values are CO_2 uptake. Error bars are ±SD.

4. DISCUSSION

4.1. PRECIPITATION PULSE RESPONSE OF ECOSYSTEM C EXCHANGE

At the annual time scale, we have determined that drought conditions systematically entail C emission (Fig. 3f), and concretely, Balsa Blanca emits *ca.* 50 g C m^{-2} year^{-1} during the dry season (Table 2). This has been also observed in other semi-arid and arid ecosystems (Aires et al., 2008; Baldocchi, 2008; Cleverly et al., 2013; Huxman et al., 2004b; Wohlfahrt et al., 2008; Yan et al., 2011), especially in grass-dominated arid and semi-arid ecosystems like Balsa Blanca (Scott et al., 2012). This C loss stems from: (1) significant GPP reduction (Scott et al., 2012), (2) the presence of minimal but significant ecosystem respiration (Cable et al., 2012; Ma et al., 2012) and (3) the sudden increase in soil respiration (R_{soil}) when low- and medium-size rain pulses occur (Barron-Gafford et al., 2011), as shown in this study (Fig. 3). In this sense, we have quantified that, annually, 40% of the C emitted during the dry season corresponds to C released during the five days subsequent to rain pulses, a period encompassing only 7% of the dry season length.

The effect of a precipitation pulse on a semi-arid ecosystem C balance depends on the specific rain pulse attributes, such as magnitude (mm), which has been proposed to be one of the most determining factors affecting the ecosystem response (Huxman et al., 2004b). Similar to previous studies in Mediterranean grasslands (Aires et al., 2008), we have found different responses after a small and a large rain pulse in our semi-arid grassland. The selected large rain pulse (Fig. 4a), which in total exceeded 80 mm, triggered net CO_2 assimilation, while the smaller one (ca. 13 mm; Fig. 4b) did not correspond to a sufficient water supply to stimulate plant photosynthesis. Nonetheless, some studies suggest that a rain pulse of this magnitude could elicit net C uptake

(Huxman et al., 2004b), while others state that small or even medium-size rain events (e.g., 10-15mm) only can provoke C release (Aires et al., 2008; Lauenroth and Bradford, 2012).
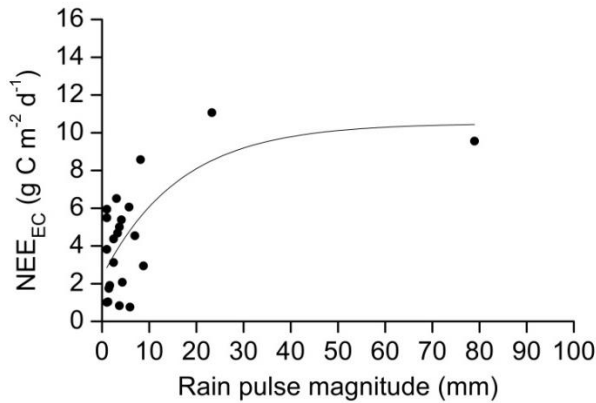
Figure. 10. Rain pulse magnitudes versus cumulative net carbon ecosystem exchange measured with eddy covariance tower (NEE_{EC}) measured over the five days after every rain pulse registered during the dry season from 2009 to 2013. Coefficient of determination (R^2) equates to 0.38.

As observed in other water-limited ecosystems (Baldocchi, 2008; Cleverly et al., 2013; Huxman et al., 2004a; Mayor et al., 2011; Schwinning and Sala, 2004), most of the rain pulses registered in Balsa Blanca correspond to small or medium-size precipitation events (<10 mm; Fig. 5). Hence, precipitation events that occurred over the 2009-2013 dry seasons statistically enhanced net CO_2 emissions at the short term during the dry season, concretely, during five days after the rain pulse (Fig. 6). Nevertheless, similar to other results (Parton et al., 2012), the relationship between the rain pulse magnitude and triggered net *C* emission during the dry season is complex, and thus, it is difficult to find a robust correlation (Fig. 10). Additionally, it is important to notice the possible underestimation in NEE caused by the exclusion of half-hourly EC fluxes that corresponded to the moments when rainfall occurred, but given the brevity of

the rainfall episodes, generally 0.5 – 1 hour, the error caused by gap-filled data is minimal.

Accordingly, the decomposition of NEE becomes crucial to understand the complex ecosystem response composed of several biotic processes and, consequently, to provide quantitative evidence of whether photosynthesis as well as soil respiration activate after irrigation.

4.2. SHORT TERM PULSE RESPONSE OF NEE COMPONENTS

On one hand, our experimental results revealed that, despite differences in the contribution of the NEE components among days of experiment, only R_{soil} was significantly affected by the addition of 15mm.

During the pre-pulse and third day of experiment, we observed similar and low R_{soil} rates (i.e. 0-1 µmol m^{-2} s^{-1}). Such slight soil respiration rates have been related to the lack of soil moisture that inhibits heterotrophic respiration (Baldocchi, 2008; Cable et al., 2012; Yan et al., 2011), and to the limitation of substrates due to GPP reduction (Cleverly et al., 2013), given the link between productivity and ecosystem respiration (Janssens et al., 2001; Migliavacca et al., 2011). Nevertheless, despite the absence of water in the soil, minimum daily respiration rates have been observed whose diurnal pattern shows a maximum at noon (Ma et al., 2012; Scott et al., 2010), similar to our results.

During the pulse day (day 0) we measured the highest R_{soil} and irrigation explained the 98% of the R_{soil} variance (η^2_p=0.98). Under drought conditions, many studies have also reported an immediate increase in R_{soil} following rain pulses (Carbone et al., 2011; Huxman et al., 2004a; Jarvis et al., 2007; Leon et al., 2014; Sponseller, 2007; Thomey et al., 2011; Wohlfahrt et al., 2008), as observed in this study (Fig. 6). This effect on R_{soil} has been attributed to the

Birch effect, which corresponds to the activation of soil respiration with the consequent mineralization of organic matter and C release (Birch, 1959).

Then, two days after water addition, R_{soil} effluxes decrease significantly compared to day 0. The progressive decline of R_{soil}, after the first peak following a rain pulse, may be related to the depletion of water in soil pores as well as the reduction in soil labile organic matter. In this regard, prior to the rainfall event, the process of photodegradation can provide the amount of organic carbon needed to allow this peak in soil respiration, since it is known that there is accumulation of dead biomass around *Machrocloa* sp. tussocks (Maestre et al., 2009) that is susceptible to partial degradation under conditions of high UV radiation, dry soil and high temperature during drought periods (Ma et al., 2012; Rutledge et al., 2010).

On the other hand, contrary to our hypothesis, above-ground processes (i.e. ANPP and $R_{aboveground}$) were not significantly affected by the rain pulse. Despite the higher contribution of $R_{aboveground}$ (13%) and ANPP (40%) over NEE, on day 0 and day 2, respectively, neither variable was significantly pulse-affected due the great variability among plot values. However, for larger rain pulses, Pugnaire et al. (1996) detected the activation of the photosynthetic apparatus of *Machrocloa* sp. after a simulated rain pulse of 31 mm, double the amount of water added in our study. Consequently, we suggest that, after prolonged drought, only large rainfall amounts (≥20 mm) are able to break the dormancy period where *Machrocloa* sp. plants remain photosynthetically inactive. This might be related to any of many morphological and physiological strategies of this species against drought that lead to the insufficient presence of active leaves to carry out photosynthesis. These include: low elasticity of cell walls (Pugnaire and Haase, 1996), regulation of stomatal conductance (Haase et al., 1999), photoinhibition (Balaguer et al., 2002; Pugnaire et al., 1996),

photoprotection (Pugnaire and Haase, 1996), photorespiration (Balaguer et al., 2002; Bohnert and Jensen, 1996; Foyer and Noctor, 2000; Wingler et al., 2000), leaf folding (Rychnovská, 1964), leaf pigment loss (Ramírez, 2007) and leaf angle modification (Valladares and Pugnaire, 1999). Additionally, Huxman et al. (2004b) highlighted the relevance of infiltration depth as a factor determining plant activation after rain pulses but, in our case, this cannot play a key role because *Machrocloa* sp. is a shallow-rooted species (Maestre et al., 2007).

Finally, regarding our study results, negative values of nocturnal R_{soil} fluxes estimated from the vaisala probes ($R_{soil\_vaisala}$; Fig. 7) were detected during previous days before irrigation and turned into positive after irrigation (Fig. 6). Similar results were found by means of both a multi-chamber soil respiration monitoring system and soil CO_2 Vaisala probes located in the soil subsurface within a Chihuahuan desert shrubland that also features a caliche horizon (Hamerlynck et al., 2013). They observed negative nocturnal soil CO_2 effluxes under drought conditions that became positive during the monsoon season. These authors related these negative soil fluxes to processes of carbonate dissolution, which might also happen in Balsa Blanca where there is a petrocalcic horizon too. On the other hand, at some specific moments throughout the experiment, we found that the difference between R_{soil} and ANPP exceeds measured NEE by ca. $1\mu mol\ m^{-2}\ s^{-1}$. This fact might be due to the accuracy of the different sensors and methodologies used to acquire these flux measurements. Apart from that, we can conclude from our experiment results that the highest increase in CO_2 emission occurs in a short-time period, (from minutes to a few hours; Fig. 7) following the rain pulse, and sometimes (for small rain pulses) this emission peak may be smoothed in a half-hourly averaged EC value.

4.3. GENERAL DISCUSSION

In our study, we highlight the strength of EC data to measure the long-term effect of rain pulses on NEE as well as to assess its high inter-annual variability (Table 2). However, by using solely the EC technique we cannot track biological processes composing the overall NEE, and hence, we present the experimental results to complement EC results at the short-term. However, the experiment was limited in order to determine the threshold magnitude needed to trigger photosynthesis (due to the short duration and the unique rain pulse magnitude simulated). Nevertheless, we have demonstrated that C emission is significant (Table 2) during the dry season and highly modulated by the rain pulses that enhance this C loss (Fig. 3, Fig. 6) through the activation of soil respiration (Fig. 7, 8c).

Overall, future climate projections point to decreases in water availability via decreases in rain events and total precipitation in some regions (Beier et al., 2012; IPCC; 2007) including the Mediterranean basin (Solomon et al., 2009). Concurrently, this indicates an alteration of rainfall distribution that likely implies variation in the size, frequency and intensity of future rain pulses (Cleverly et al., 2013; IPCC; 2012) in such arid and semi-arid regions. In this regard, the occurrence of stochastic precipitation pulses within long dry periods might mostly provoke the activation of soil respiration processes in arid and semi-arid ecosystems. Hence, a precipitation distribution characterized by low-frequency and low-magnitude events would lead to C release, while anomalous high-magnitude and low-frequency events might cause intermittent C uptake over several days, as shown in this study. In contrast, high-frequency events may support continuous photosynthetic activity as well as soil respiration, with the overall biological activity being proportional to the amount of stored water in the soil (up to saturation). In this way, the capability of semi-arid ecosystems

to act as C sinks would be enhanced. Nevertheless, more research is still needed to accurately characterize the dimension and sense of C balance variability in drylands regarding their response to climate change. This is especially so when the aim of building applicable modeling approaches in drylands is considered as imperative in order to predict, mitigate, and adapt to future climatic and environmental scenarios.

5. CONCLUSIONS

Rain pulses, occurring during the dry season, are a frequent form of water input in semi-arid ecosystems and an important climatic factor affecting the *C* balance of water-limited ecosystems. In the studied semi-arid grassland, the net CO_2 emitted to the atmosphere triggered by rain pulse events contributed from 9 to 58% to the total net CO_2 release measured with eddy covariance, despite comprising just 2 to 11% of the dry season period length for five study years (2009-2013). The main biological process determining the NEE response after a rain pulse is soil respiration, given the higher occurrence of small and medium-sized rain events that may be not sufficient to enable plant photosynthesis. However, net C uptake patterns can be observed when infrequent and large rainfall events occur. The manipulation pulse experiment results showed that only R_{soil} was significantly affected by the rain pulse. However, the contribution of the different components to the overall NEE changed over the experiment days. In this regard, R_{soil} was distinctly dominant during the pulse day and the day afterwards (ca. 80% of the NEE), whereas ANPP seemed to become more prevalent during the second day following irrigation (ca. 40% of NEE), despite the great variability in the measurements.

Global estimations of temperature and precipitation regimes point to an increase of drought periods and extreme precipitation events that might imply an

increase in the net CO_2 emission in semi-arid regions. Therefore, the characterization of the responses of biological components of the C balance to rain pulses becomes crucial in order to improve current climatic modeling schemes and also to design proper mitigation policies.

CHAPTER 3:

SUBTERRANEAN VENTILATION OF ALLOCHTHONOUS CO_2 GOVERNS NET CO_2 EXCHANGE IN A SEMIARID MEDITERRANEAN GRASSLAND

Ana López-Ballesteros, Penélope Serrano-Ortiz, Andrew S. Kowalski, Enrique P. Sánchez-Cañete, Russell L. Scott, Francisco Domingo

ABSTRACT

Recent research highlights the important role of (semi-)arid ecosystems in the global carbon (C) cycle. However, detailed process based investigations are still necessary in order to fully understand how drylands behave and to determine the main factors currently affecting their C balance with the aim of predicting how climate change will affect their structure and functions. Here, we explore the potential biological and non-biological processes that may compose net CO_2 exchange in a semiarid grassland in southeast Spain by means of eddy covariance measurements registered over six hydrological years (2009-2015). Results point out the great importance of subterranean ventilation, an advective transport process causing net CO_2 release, especially during drought periods and under high-turbulence conditions. Accordingly, extreme CO_2 release, far exceeding that found in the literature, was measured over the whole study period (2009-2015) averaging 230 g C m^{-2} $year^{-1}$; this occurred mostly during the dry season and was very unlikely to correspond to concurrent biological activity and variations of *in situ* organic C pools. Underground CO_2 concentrations corroborate this finding. In this regard, the potential origins of the released CO_2 could be geological degassing and/or subterranean translocation of CO_2 in both gaseous and aqueous phases. However, future research is needed in order to understand how CO_2 transport and production processes interact and modulate drylands' terrestrial C balance. Overall, the present study exposes how subterranean ventilation and hydrogeochemistry can complicate the interpretation of the terrestrial C cycle.

1. INTRODUCTION

Anthropogenic emissions of carbon dioxide (CO_2) have been rising since the beginning of the industrial era, increasing concentrations from 277 parts per million (ppm) to approximately 400 ppm (Dlugokencky & Tans, 2015; Joos & Spahni, 2008). The major role of the biosphere as a natural CO_2 sink is extensively known given that the oceans and terrestrial ecosystems combined remove around 50% of the anthropogenically emitted CO_2 (Le Quéré et al., 2009). Thus, it is crucial to understand the processes, feedbacks and driving factors that modulate the carbon (C) sink capacity of natural ecosystems given their implications for future climate. In this context, recent studies have determined that drylands' C balance strongly affects the inter-annual variability of C dynamics at a global scale (Ahlström et al., 2015, Metcalfe, 2014, Poulter et al., 2014). Hence, given the wide presence of arid and semiarid ecosystems (Okin, 2001; Schlesinger, 1990), more research is needed in order to understand how these ecosystems behave, in terms of processes and climatic forcing factors that are involved in their C cycle.

During the last decade, research related to drylands' C balance has demonstrated that biotic processes, such as photosynthesis and plant and soil respiration, occasionally play a secondary role in the ecosystem-atmosphere CO_2 exchange (Serrano-Ortiz et al., 2012). In fact, under drought conditions when biological activity is substantially reduced, non-biological processes, such as photodegradation (Rutledge et al., 2010), geochemical weathering (Emmerich, 2003), and subterranean ventilation (Kowalski et al., 2008), may influence surface C exchanges during daytime hours. In this regard, estimates of CO_2 fluxes corresponding to photodegradation of senescent organic matter equate to 0.015 and 0.179 μmol m^{-2} s^{-1}, based on microcosm measurements under natural solar radiation (Brandt et al., 2009) and eddy covariance (EC) and

chamber measurements (Rutledge et al., 2010), respectively. Likewise, short-term estimates of geochemical weathering, concretely calcite precipitation, are estimated to correspond to very low CO_2 effluxes (Hamerlynck et al., 2013; Roland et al., 2013) of ca. 0.05 µmol m^{-2} s^{-1} (Serrano-Ortiz et al., 2010). In contrast, subterranean ventilation (also termed "atmospheric or pressure pumping"), conceived as the advective transport of CO_2-rich air from the vadose zone to atmosphere (Sánchez-Cañete et al., 2013), likely results in much more sizeable CO_2 effluxes.

Recent studies have demonstrated the relevance of subterranean ventilation for the net CO_2 exchange of some Mediterranean ecosystems. Based on EC measurements, several studies have highlighted the outstanding role of subterranean ventilation in El Llano de los Juanes, a sub-humid karstic shrubland located at Sierra de Gádor (Almería, Spain; Kowalski et al., 2008, Pérez-Priego et al., 2013, Sanchez-Cañete et al., 2011, Serrano-Ortiz et al., 2009). Likewise, significant CO_2 release was attributed to ventilation processes, especially under unstable conditions, in Balsa Blanca, a semiarid grassland located in Almería (Rey et al., 2013, Rey et al., 2012, Sánchez-Cañete et al., 2013). Additionally, several studies developed in temperate and alpine ecosystems also found evidence of soil ventilation induced by wind or pressure fluctuations (i.e. non-difussive gas transport) via isotope measurements (Bowling & Massman, 2011, Frisia et al., 2011), buried CO_2 sensors (Frisia et al., 2011, Hirsch et al., 2004, Maier et al., 2012, Maier et al., 2010, Seok et al., 2009, Takle et al., 2004), radon measurements (Fujiyoshi et al., 2009), ground-penetrating radar (Comas et al., 2007, Comas et al., 2011) and soil flux chambers (Redeker et al., 2015, Subke et al., 2003).

This study presents the first EC measurements of net CO_2 exchange at Amoladeras, a semiarid grassland located in SE Spain, over 2009 to 2015 (six hydrological years). We explore the driving biophysical processes governing the

116

net exchange, paying special attention to subterranean ventilation whose relevance may be pronounced for this ecosystem with a very long dry season and only scant biotic activity limited to the winter season. Thus, we hypothesize that the biological activity in this experimental site is constrained to very short periods when water is available, so that photosynthesis and respiration flux rates are low due to the sparse plant cover and the prolonged and extreme meteorological conditions registered over the seasonal summer drought period. Accordingly, we expect outstanding contributions from ventilation processes to the net CO_2 exchange, especially during the dry season and in the daytime hours. Our main objectives are:

1. To quantify the net CO_2 exchange at seasonal and annual scales;

2. To determine the prevalence of biological *vs.* non-biological processes in the net CO_2 exchange during growing and dry seasons over the study period (2009-2015); and

3. To quantitatively explore the magnitude of subterranean ventilation, as well as its relation with potential driving factors.

2. MATERIAL AND METHODS

2.1. EXPERIMENTAL SITE DESCRIPTION

This experimental site of the present study is Amoladeras (N36.8336°, W2.2523°; Fig. 1), a semiarid grassland located in the Cabo de Gata-Níjar Natural Park (Almería, Spain). Detailed information concerning the climate and ecosystem characteristics of this experimental site can be found in Material and Methods section (pp. 20-22).

Figure 1. Amoladeras experimental site (Almería, Spain).

Regarding its geological characteristics, this experimental site is located on an alluvial fan, where the main geological materials consist of plio-quaternary marine conglomerates and Neogene-Quaternary sediments that formed after the last volcanic events (7.5 million of years ago; Braga-Alarcón et al., 2003; Baena-Pérez et al., 1977). There is a nearby fault system, the Carboneras Fault Zone, whose last displacement in the Southern part is dated to 6 million of years ago (Rutter et al., 2012; see Appendix A for more geological information). An unconfined aquifer extends 165 km^2 at approximately 50 m below the surface (Carrasco et al., 1988).

2.2. METEOROLOGICAL AND EDDY COVARIANCE MEASUREMENTS

This study is based on micrometeorological data acquired by an eddy covariance (EC) tower and complementary sensors (detailed in Table 1 of Material and Methods section; p. 42) installed at Amoladeras (site code "Es-Amo" of the European Database Cluster (http://www.europe-fluxdata.eu) in 2009. The EC footprint is well within the fetch, even under the lowest turbulence conditions. The net CO_2, water vapor, and sensible heat fluxes were calculated from raw data collected at 10 Hz by using EddyPro 5.1.1 software (Li-Cor, Inc., USA). Data processing and quality assessment were performed according to López-Ballesteros et al., (2016). Furthermore, based on the approach proposed by Reichstein et al. (2005), the averaged u_* threshold for all the analyzed period (i.e., 2009–2015) was 0.11 m s^{-1}, which was used to filter out those measurements corresponding to low-turbulence conditions. The resulting annual fractions of missing EC flux data were 8 ± 5 % and 33 ± 3 % for daytime and nighttime data, respectively. The validity of our EC system was assessed via energy balance closure (Moncrieff et al., 1997). The linear regression of half-hourly turbulent energy fluxes, sensible and latent heat fluxes (H+LE; W m^{-2}) against available energy, net radiation less the soil heat flux (R_n-G; W m^{-2}), resulted in a slope of 0.873 ± 0.002 (R^2 = 0.907), which is similar to the average imbalance measured in EC systems within FLUXNET global network (i.e. 20%; Wilson et al., 2002).

2.3. ESTIMATION OF THE ANNUAL CUMULATIVE CO_2 BALANCE

Cumulative CO_2 balances, for the six hydrological years within study period (2009-2015), were estimated by integrating the half-hourly CO_2 fluxes (F_c) with quality flags equal to 0 and 1 (Mauder & Foken 2004). Missing values were gap-filled using the marginal distribution sampling technique (Reichstein et al., 2005) and random uncertainty and errors in F_c values introduced by the gap-

filling process were calculated from the variance of the gap-filled data, as explained by López-Ballesteros et al., (2016). Negative values of F_c represent net CO_2 uptake while positive values denote net CO_2 emission/release to the atmosphere. In this regard, we emphasize that, in the present study, the concept of "emission" entails production and subsequent transport to the atmosphere (usually via diffusive transport) whereas "release" refers to the escape of gas to the atmosphere, regardless of when or how it has been produced.

2.4. SEASONAL VARIABILITY OF NET CO_2 EXCHANGE AND DRIVING PROCESSES

In order to analyze the time series of net CO_2 exchange at smaller time scales (i.e. seasonal) we split our database into growing and dry season periods. To do that, we chose two ambient variables, the Bowen ratio (β; ratio of sensible to latent heat fluxes) and volumetric soil water content (SWC; m^3 m^{-3}), to discern between dormancy (β > 4 and SWC ≤ 0.1) and biologically-active periods (the rest), hereinafter referred to as the dry and growing season, respectively. The same variables have been used in other Mediterranean ecosystems (Pérez-Priego et al., 2013, Serrano-Ortiz et al., 2009), but with site-adapted thresholds. Evidence that appropriate criteria were chosen is shown in Fig. 2.
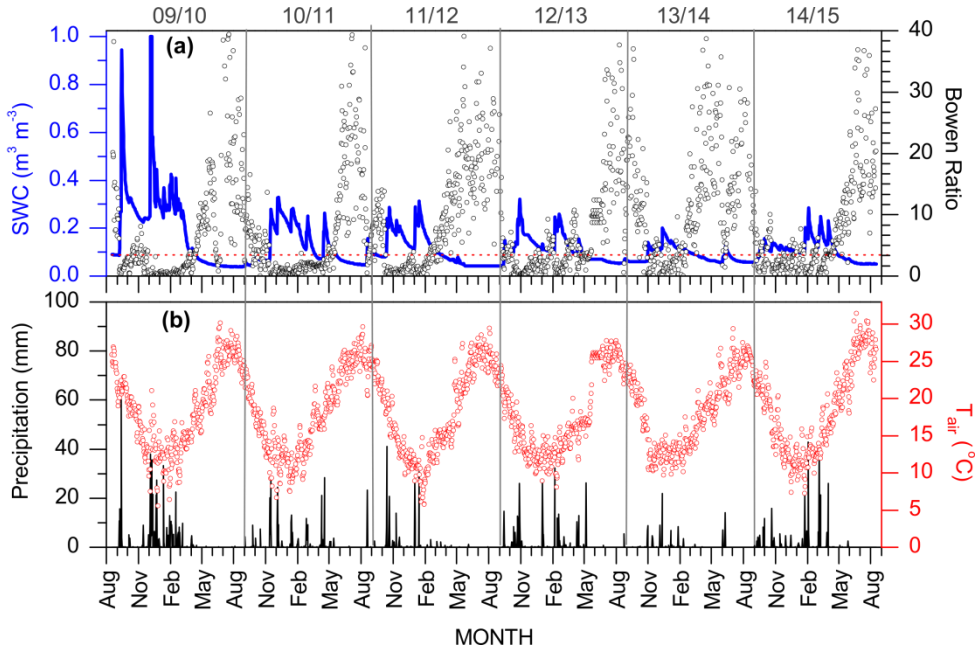
Figure 2. Daily averaged volumetric soil water content at -0.08m (SWC) and Bowen ratio are represented by blue line and gray dots, respectively. Threshold values for both variables used to define criteria to split data into growing and dry season are denoted by dashed red line in the upper panel. Daily precipitation (black lines) and daily averaged air temperature (T_{air}; red dots) are shown in the lower panel.

Accordingly, over the growing season we explored the biological processes that presumably control the net CO_2 exchange via light-curve fitting, based on the rectangular hyperbolic model described by the following equation (Michaelis & Menten, 1913):

$$F_c = GPP_{max} \cdot PPFD/(k + PPFD) + R_d \qquad \text{(Eq. 1)}$$

where F_c represents daytime ($R_n > 10$ W m^{-2}) half-hourly net CO_2 fluxes (μmol m^{-2} s^{-1}; quality flag=0), and the fitting coefficients are GPP_{max} (μmol m^{-2} s^{-1}), which represents gross primary productivity at infinite light, k (μmol m^{-2} s^{-1}), which is the level of Photosynthetic Photon Flux Density (PPFD; μmol m^{-2} s^{-1}) corresponding to half of the GPP_{max}, and R_d (μmol m^{-2} s^{-1}), which indicates

121

daytime ecosystem respiration. Additionally, we studied the temperature-dependency of ecosystem respiration.

In the dry season, on the other hand, with the aim of determining the relevance of subterranean ventilation in this ecosystem, we examined the linear relationship between friction velocity (u_*), which can be viewed as a proxy for turbulence intensity, and daytime ($R_n > 10$ W m^{-2}) half-hourly net CO_2 fluxes (F_c; quality flag=0), excepting those corresponding to rainfall events.

2.5. SUBSOIL CO_2 MEASUREMENTS

Subsoil CO_2, soil temperature and volumetric soil water content were measured since August 2014 within the vadose zone at 0.15 m and 1.5 m depths below the surface by means of CO_2 molar fraction sensors with soil adapters and hydrophobic filters, thermistors and water content reflectometers, respectively (Table 1). Measurements were made every 30 s and stored as 5 min averages. Missing data corresponded to 1% over the hydrological year 2014/2015. Data processing was performed according to Sánchez-Cañete et al. (2013).

3. RESULTS

3.1. ANNUAL CUMULATIVE CO_2 RELEASE AND ITS RELATIONSHIP WITH WATER AVAILABILITY

The six hydrological years of study showed similar air temperature (T_{air}) and Bowen ratio (β) patterns. In fact, annual averages of T_{air} ranged from 17.9 to 18.7 °C and in case of β, annual averages were between 9.4-10.7, excepting for 2013/2014, which was the driest year with a higher annual average of 17 (Fig. 2). However, precipitation and, consequently, soil water content (SWC) differed among years. The hydrological year 2009/2010 was the rainiest year with a remarkable 535 mm of total precipitation, while 2013/2014 was the driest with

113 mm. During the rest of the study period, annual precipitation ranged from 219 to 296 mm. Generally, most of the precipitation occurs during November-May resulting in the highest values of SWC over the year (Fig. 2), and coinciding with the lowest values of T_{air} and β.
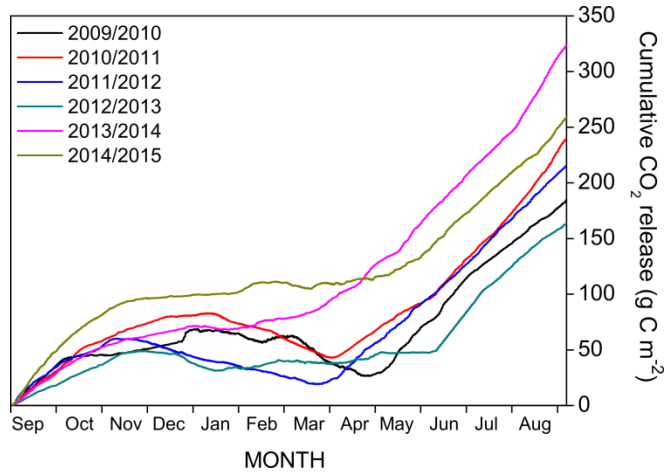
Figure 3. Cumulative CO_2 release of every hydrological year in Amoladeras.

Despite the large variability in annual precipitation over the study period, large CO_2 release was measured in Amoladeras (Fig. 3), even during the rainiest year 2009/2010. The annual cumulative CO_2 release in Amoladeras was on average 231 ± 48 g C m^{-2} year^{-1}. In this regard, the driest year (2013/2014), when annual precipitation was 42% lower than the mean precipitation over the study period, corresponded to the highest amount of CO_2 released to the atmosphere (324 g C m^{-2} year^{-1}; Fig. 4e). Similarly, the lowest annual cumulative CO_2 releases were registered in the rainiest years of the study period: 2012/2013 and 2009/2010 had releases of 163 and 185 g C m^{-2} year^{-1} and annual precipitation of 296 and 535 mm, respectively (Fig. 4d and 4a, respectively).
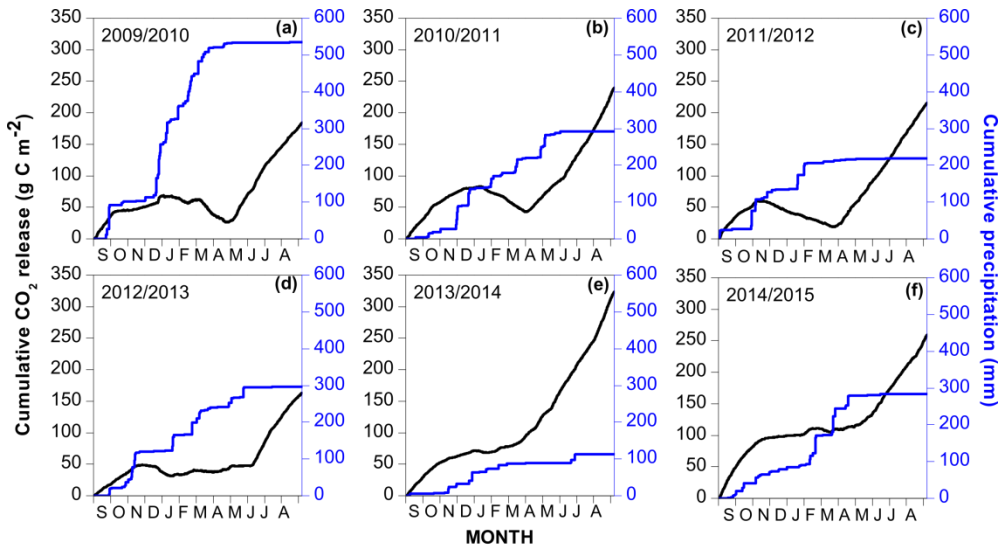
Figure 4. Cumulative CO_2 release (black line) and precipitation (blue line) for every hydrological year over the study period.

Differences among years depend on the length and strength of the net CO_2 uptake observed during the growing season, which was determined by the magnitude and timing of precipitation. For example, during 2009-2012, when rainfall events occurred in both autumn and winter months, although not always evenly distributed, Amoladeras acted as a net CO_2 sink during several months (Fig. 4a, 4b and 4c). In contrast, during the remaining years, net CO_2 uptake occurred during just one winter month (Fig. 4d, 4e, 4f). Concretely, in 2012/2013 and 2014/2015, rainfall was very low or absent in December and January but some precipitation events occurred during autumn and early spring (Fig. 4d and 4f). In 2013/2014, which was the driest year, very low-magnitude precipitation events were registered (Fig. 4e). Generally, large amounts of CO_2 were released from Amoladeras during late spring, summer and early autumn (i.e. from April-May to November-December), with the exception of 2012/2013, when the CO_2 balance remained almost unchanged from February to June (Fig. 4d).

3.2. SEASONAL AND DIURNAL NET CO_2 EXCHANGE VARIABILITY

As expected, we found distinct meteorological conditions over growing and dry seasons (Table 2). In general, air and soil temperature, vapor pressure deficit and net radiation (T_{air}, T_{soil}, VPD and R_n, respectively) were lower during the growing season, while precipitation (P) and SWC were considerably higher, compared to the dry season (Table 2). The meteorological variable with the greatest variability among years is precipitation, for both the growing and dry seasons (coefficient of variation, CV, of 44 and 82%, respectively; Table 2). The season length also varied from year to year, with 2012/2013 and 2013/2014 having the longest growing and dry season, respectively (Table 2). In addition, the growing season cumulative net CO_2 exchange was only negative (i.e. net CO_2 uptake) in 2011/2012, with releases of less than 80 g CO_2 m^{-2} for the other years (Table 2). In contrast, dry season cumulative net CO_2 exchange was always above 130 g CO_2 m^{-2} and showed lower inter-annual variability (CV=22%) than that observed over the growing season (CV=67%; Table 2).

Growing season	Length (days)	T_{air} (ºC)	T_{soil} (ºC)	SWC ($m^3 m^{-3}$)	VPD (hPa)	R_n ($W m^{-2}$)	P (mm)	ET (mm)	Net CO_2 release ($g C m^{-2}$)
2009/2010	236	16 ± 4	17 ± 6	0.30 ± 0.19	6 ± 4	48 ± 44	523	208 ± 62	21 ± 7
2010/2011	220	15 ± 4	16 ± 6	0.17 ± 0.07	6 ± 3	56 ± 52	290	188 ± 53	45 ± 5
2011/2012	172	14 ± 5	15 ± 7	0.16 ± 0.06	6 ± 3	34 ± 44	213	122 ± 5	-1 ± 6
2012/2013	240	15 ± 3	16 ± 5	0.14 ± 0.05	6 ± 2	57 ± 52	295	179 ± 51	28 ± 4
2013/2014	140	14 ± 4	14 ± 6	0.12 ± 0.03	6 ± 2	38 ± 43	107	67 ± 26	53 ± 3
2014/2015	226	15 ± 4	16 ± 5	0.13 ± 0.03	6 ± 3	49 ± 42	282	156 ± 5	78 ± 5
CV (%)	18	4	5	35	4	18	44	31	67

Dry season	Length (days)	T_{air} (ºC)	T_{soil} (ºC)	SWC ($m^3 m^{-3}$)	VPD (hPa)	R_n ($W m^{-2}$)	P (mm)	ET (mm)	Net CO_2 release ($g C m^{-2}$)
2009/2010	129	23 ± 4	33 ± 4	0.06 ± 0.02	11 ± 5	130 ± 25	12	40 ± 19	163 ± 6
2010/2011	145	23 ± 4	32 ± 6	0.06 ± 0.01	11 ± 4	111 ± 39	2	39 ± 19	195 ± 6
2011/2012	194	21 ± 5	27 ± 6	0.07 ± 0.02	9 ± 4	102 ± 94	6	54 ± 3	218 ± 8
2012/2013	125	23 ± 4	30 ± 6	0.06 ± 0.02	12 ± 6	113 ± 31	1	35 ± 25	135 ± 5
2013/2014	225	21 ± 4	26 ± 5	0.07 ± 0.01	10 ± 4	107 ± 37	6	48 ± 22	271 ± 8
2014/2015	139	24 ± 4	32 ± 5	0.06 ± 0.01	13 ± 6	121 ± 29	1	41 ± 2	182 ± 7
CV (%)	23	6	8	9	14	8	82	15	22

Table 2. Daily mean values of air and soil temperature (T_{air} and T_{soil}, respectively), soil water content, vapor pressure deficit (VPD) and net radiation (R_n), and sums of precipitation (P), evapotranspiration (ET) and net C emission during growing and dry seasons for each hydrological year (2009-2015). Coefficients of variation (CV; %) for each variable are also shown.

Although the general net CO_2 exchange behavior for every season is similar over the study period, some differences among hydrological years were found (Fig. 5).
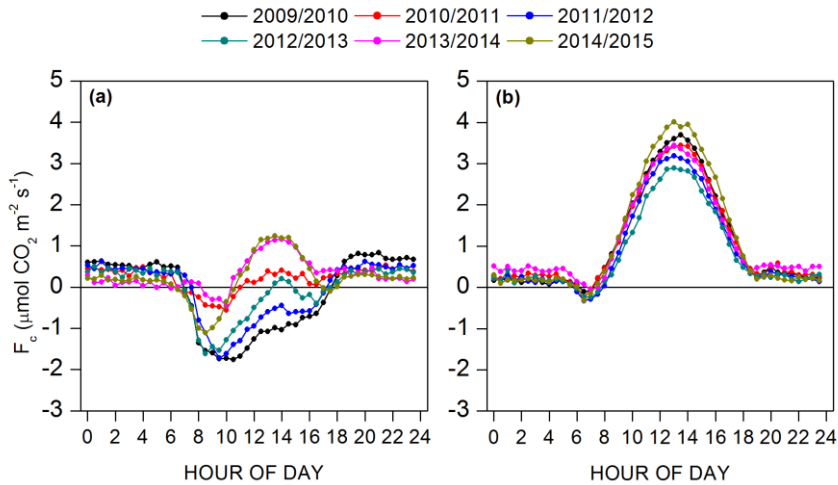
Figure 5. Diurnal patterns of net CO_2 fluxes over: **(a)** the growing season and **(b)** dry season, for every hydrological year over the study period in Amoladeras. Half-hourly CO_2 flux data correspond to non-gapfilled and maximum quality fluxes.

For instance, the maximum daytime net CO_2 uptake (ca. -2 µmol m^{-2} s^{-1}) and maximum nighttime net CO_2 emission (ca. 0.6 µmol m^{-2} s^{-1}) occurred during the growing season of 2009/2010, the year when water availability was the highest (Fig. 5a; Table 2). In addition, growing season F_c patterns of 2009/2010, 2011/2012 and 2012/2013 showed net CO_2 uptake rates during most of the daytime hours (Fig. 5a). However, in the remaining years (i.e. 2010/2011, 2013/2014 and 2014/2015), CO_2 release was measured after 10 am (Fig. 5a). In fact, a symmetric release pattern is noticeable for 2013/2014 and 2014/2015 curves. Related to the dry season diurnal patterns, the highest release peak of ca. 4 µmol m^{-2} s^{-1} occurred in 2014/2015, while the lowest was observed in 2012/2013 (less than 3 µmol m^{-2} s^{-1}; Fig. 5b). Nonetheless, the net CO_2

exchange over the drought period showed considerably less variability among years compared to the growing season patterns.

3.3. BIOLOGICAL AND NON-BIOLOGICAL PROCESSES COMPOSING THE NET CO$_2$ EXCHANGE

Regarding biotic processes composing the net CO$_2$ exchange, growing season data were analyzed with the aim to explore ecosystem photosynthesis and respiration. In the case of ecosystem respiration, we found no significant relationship between half-hourly nighttime F_c and T_{soil} for any hydrological year (data not shown).
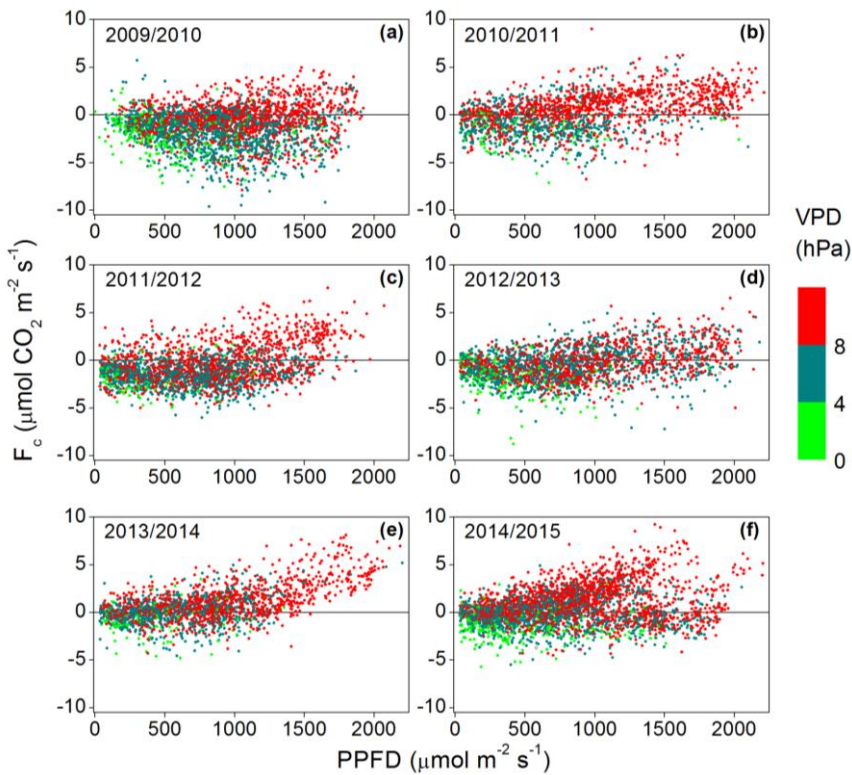
Figure 6. Light response curves of daytime half-hourly net CO$_2$ fluxes (F_c) at different levels of vapor pressure deficit (VPD), corresponding to the growing season of each hydrological year over the study period in Amoladeras. Half-hourly F_c data correspond to non-gapfilled and maximum quality fluxes.

Hence, we centered our analysis on photosynthesis via light curve fitting. Our results show that net CO_2 uptake was affected by VPD, since half-hourly daytime F_c were more related to the photosynthetic photon flux density (PPFD) when VPD was at or below 4 hPa (Fig. 6). In fact, when PPFD and VPD were maximal, net CO_2 release fluxes were observed (i.e. positive daytime half-hourly F_c; Fig. 6). Likewise, we found that net CO_2 release occurred when u_* was approximately above 0.45 m s^{-1}, while net CO_2 uptake corresponded to lower u_* values (Fig. 7).
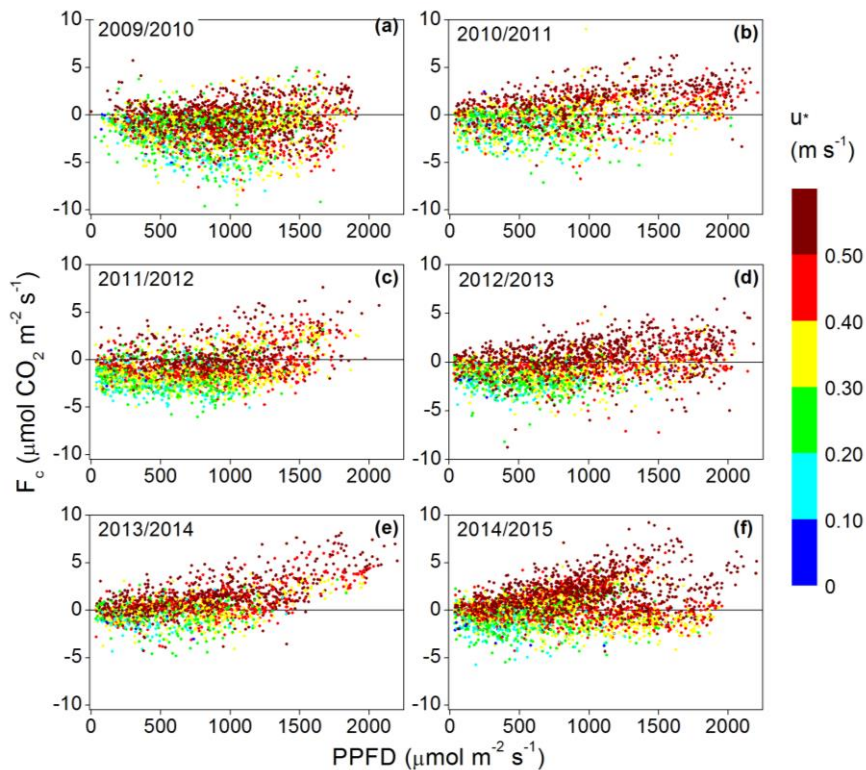
Figure 7. Light response curves of daytime half-hourly net CO_2 fluxes at different levels of friction velocity (u_*), corresponding to the growing season of each hydrological year over the study period in Amoladeras. Half-hourly F_c data correspond to non-gapfilled and maximum quality fluxes.

Therefore, only data corresponding to lower water stress and turbulence conditions (VPD$\leq$4 hPa and u_*<3 m s^{-1}) were used to fit the rectangular hyperbolic model (Eq. 1). Although the fitting procedure was not successful for the last hydrological year (2014/2015; Table 3), we obtained non-linear fit coefficients for the other years. Fitting parameters of maximum gross primary productivity (GPP$_{max}$) ranged from 4.05 to 9.28 µmol m^{-2} s^{-1}, and daytime ecosystem respiration (R_d) was often positive but not significant (p-value>0.05), since the parameter error exceeded the parameter values for all years (Table 3). Finally, the best fit with significant GPP$_{max}$ coefficient was obtained in 2011/2012 (Adj. R^2=0.27; Table 3).

Year	n	GPP$_{max}$		k		R_d		Adj. R^2
		Value	Error	Value	Error	Value	Error	
2009/2010	126	-9.28	7.55	1469.94	2162.88	-0.45	0.70	0.25
2010/2011	54	-4.28	5.17	813.93	2471.14	-0.49	1.17	0.11
2011/2012	82	-4.24*	1.97	511.62	638.24	-0.91	0.52	0.27
2012/2013	87	-4.05	2.58	557.47	916.57	-0.86	0.67	0.16
2013/2014	38	-7.60	6.59	1082.08	1082.08	0.09	0.71	0.37
2014/2015	-	-	-	-	-	-	-	-

Table 3. Michaelis-Menten light curve fit parameters (value and error) for every hydrological year over the study period: gross primary production at infinite light (GPP$_{max}$; µmol m^{-2} s^{-1}), level of photosynthetic photon flux density at which net CO_2 flux is half of GPP$_{max}$ (k; µmol m^{-2} s^{-1}) and daytime ecosystem respiration (R_d; µmol m^{-2} s^{-1}). Adjusted R-squared is also shown and asterisk denotes p-value<0.05. Daytime half-hourly net CO_2 fluxes used for curve fitting are those corresponding to vapor pressure deficit equal or lower than 4 hPa and friction velocity below 0.3 m s-1. Empty space denotes no fit convergence.

To look at non-biological processes, we delved into subterranean ventilation by means of the net CO_2 fluxes (F_c) and the relationship with the friction velocity (u_*) over both growing and dry season. We found a significant linear relationship (p-value<0.05) between u_* and daytime half-hourly F_c for VPD>4 hPa, over the growing seasons of all hydrological years (R^2=0.10; Table 4).

Year	n	Intercept	Slope	R^2
2009/2010	1688	0.53*	1.12*	0.05*
2010/2011	2710	-0.1*	3.26*	0.25*
2011/2012	926	1.08*	1.16*	0.02*
2012/2013	3021	-0.04	2.11*	0.15*
2013/2014	1457	0.03	3.08*	0.14*
2014/2015	2286	-0.37*	2.76*	0.13*
All years	12088	0.39*	2.22*	0.10*

Table 4. Fit parameters (intercept, slope, and R-squared) obtained via linear regression between daytime half-hourly net CO_2 fluxes ($\mu mol\ m^{-2}\ s^{-1}$) and friction velocity ($m\ s^{-1}$) when vapor pressure deficit is above 4 hPa over the growing season in Amoladeras. Half-hourly net CO_2 flux data correspond to non-gapfilled and maximum quality fluxes. Data corresponding to rainfall events are excluded. Asterisk denotes p-values <0.05.

The variance explained by u_* increased to 25% in 2010/2011, and reached its minimum in 2009/2010 and 2011/2012 ($R^2=0.05$ and $R^2=0.02$, respectively), and most of the fit parameters obtained for every year were significant (p-value<0.05). We also examined the influence of u_* on F_c fluxes over the dry season, but taking into account the influence of R_n (Fig. 8). Based on the fit parameters obtained, a significant linear relationship was found at the three levels of R_n used and for all hydrological years (p-value<0.05; Fig. 8). Moreover, the highest R_n level ($R_n>470\ W\ m^{-2}$) had the best linear fit for 2009/2010 and 2011/2012 data ($R^2=0.68$ and 0.59, respectively; Fig. 8a and 8c) and even when pooling dry season data together ($R^2=0.41$; data not shown). However, in the cases of 2012/2013 and 2013/2014, variance explained by u_* at the highest level of R_n ($R^2=0.42$ and 0.33, respectively; Fig. 8d and 8e) was equivalent to that obtained by using the whole range of daytime R_n values ($R_n>10\ W\ m^{-2}$), and even, in 2014/2015, the fit was better when using all daytime R_n values ($R^2=0.26$; Fig. 8f). Finally, 2010/2011 was unusual since data showed the best linear fit ($R^2=0.55$; Fig. 8b) at the intermediate R_n level ($240<R_n\leq470\ W\ m^{-2}$).
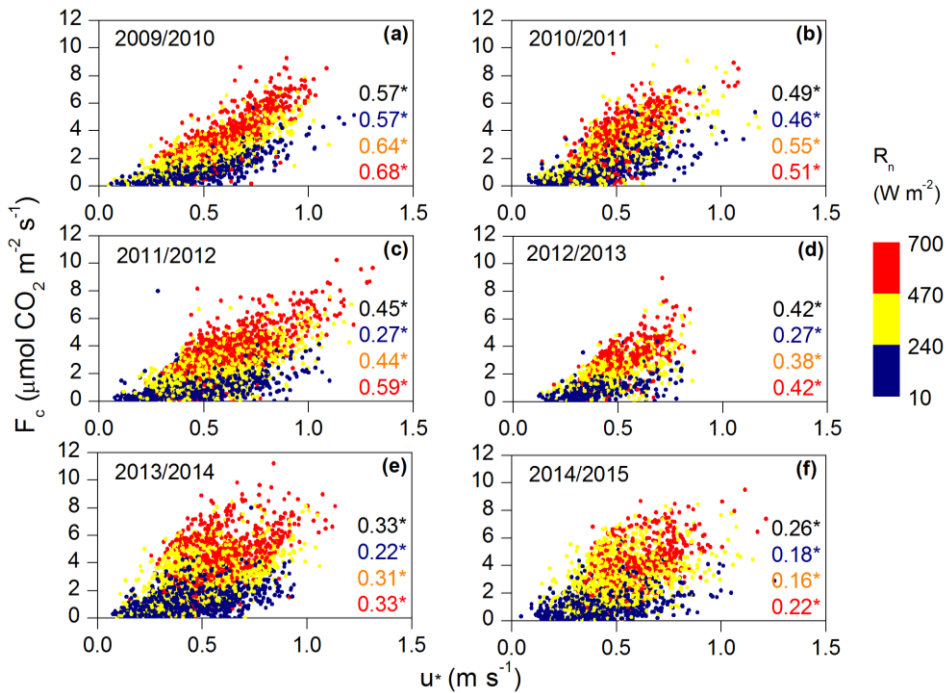
Figure 8. Relationship between daytime half-hourly net CO_2 fluxes (F_c) and friction velocity (u_*) together with the coefficient of determination (R^2) for every simple linear regression performed at low (dark blue), intermediate (yellow), high (red) and the whole daytime range (black) of net radiation (R_n) levels. Asterisk denotes p-values <0.05. Data used correspond to the dry season of each hydrological year in Amoladeras. Half-hourly F_c data correspond to non-gapfilled and maximum quality fluxes excluding rainfall events.

3.4. SUBSOIL CO_2 MOLAR FRACTIONS

Regarding CO_2 measurements within the vadose zone, we found that subsoil CO_2 molar fraction at 1.5 m was, on average, 180% higher than that measured at 0.15 m over the 2014/2015 hydrological year (Fig. 9).
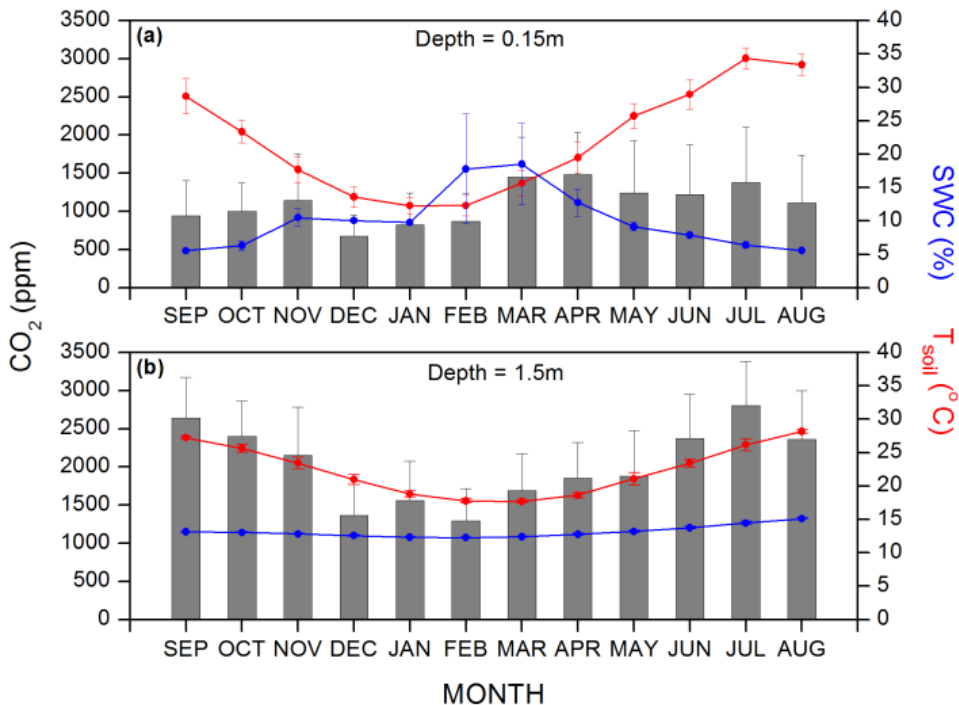
Figure 9. Monthly averages of subsurface CO_2 (grey bars), volumetric soil water content (SWC; blue lines) and soil temperature (T_{soil}; red lines) at **(a)** 0.15 m and **(b)** 1.5 m depths over the hydrological year of 2014/2015.

In addition, differing patterns were also observed between depths; while CO_2 peaked during March and April at 0.15 m (ca. 1500 ppm; Fig. 9a), maximum CO_2 molar fraction was observed from June to October at 1.5 m (ca. 2500; Fig. 9b). Apart from that, sustained medium-high CO_2 values were observed during summer months at the shallowest depth despite the lowest SWC registered, and there was more variability at 0.15 m than at 1.5 m (Fig. 9).

4. DISCUSSION

Our study site, Amoladeras, is located in the driest part of Europe and is part of the 33% of global land area covered by (semi-)arid ecosystems (Okin, 2001). In the present study, we have found very large CO_2 release over the whole study period (2009-2015), averaging 230 g CO_2 m^{-2} year^{-1}, which is far higher than those reported in the literature. Among the available CO_2 balance data measured in water-limited ecosystems with similar precipitation regimes, the maximum values of annual cumulative CO_2 emission measured by EC systems are frequently near or below 150 g CO_2 m^{-2} year^{-1} (Mielnick et al., 2005, Rey et al., 2012, Scott et al., 2015). The extreme CO_2 release observed in in Amoladeras, exceeding 300 g CO_2 m^{-2} year^{-1} in 2013/2014, are likely inconsistent with variations of organic carbon pools within this ecosystem (Schlesinger, 2016). In this regard, the soil organic C (SOC) pool in Amoladeras, where soil is 10 cm deep on average, equates to ~1.24 kg C m^{-2}, according to Amoladeras´ published soil data (Rey et al., 2011). However, only 20% (~250 g C m^{-2}, maximum) of this SOC would be accessible to microorganisms (Aranda & Oyonarte, 2005, Oyonarte et al., 2007) and hence susceptible to respiratory CO_2 emission. This value is very similar to the annual averaged CO_2 release measured in Amoladeras (230 g CO_2 m^{-2} year^{-1}), which leads us to think that other non-local C sources should be involved in the measured net CO_2 exchange. Otherwise, based on our measurements, this CO_2 release would result in total depletion of SOC pool in a few years.

In fact, the largest CO_2 releases occurred during the driest months which, in turn, support the idea that these fluxes cannot be related to concurrent *in situ* respiration, mainly because, as is widely-known, hydric stress inhibits any biological activity (Huxman et al., 2004). Furthermore, we did not find clear temperature-dependence of night-time net CO_2 fluxes, and the application of the

light-response model did not succeed for most of the years of study (Table 3). Rather, sustained subsoil CO_2 molar fractions are observed at 0.15 m depth over dry season despite the high temperatures and low water availability (Fig. 9a), and even, at 1.5 m, maximum CO_2 values coincided with summer months (Fig. 9b). Additionally, CO_2 molar fractions increased with depth, in accordance with what Amundson & Davidson (1990) observed in several ecosystems distributed globally. Accordingly, we hypothesize that two possible origins may be behind this extreme CO_2 release.

On one hand, the first hypothesis supposes a geological origin of the released CO_2, as a direct supply of geologic CO_2 gas from the underlying area near the experimental site. This would correspond, based on Kerrick (2001), to mantle-derived CO_2 from either subaerial dormant volcanos - since Amoladeras is situated near the Cabo de Gata volcanic complex where the last volcanic activity dates to 7.5 million of years ago (Braga-Alarcón et al., 2003) - or to subaerial non-volcanic CO_2 degassing, which has been associated with geothermal systems, seismicity and fault zones, among others. In this regard, the Carboneras Fault Zone crosses near the field site (see Appendix A), which could entail seismicity and CO_2 degassing (Kerrick, 2001), as proposed by Rey et al. (2012b). This could even act as a conduit facilitating the escape of deep CO_2 (Kerrick, 2001), occasionally via advective transport (i.e. subterranean ventilation; Covington, 2016). However, recognizing that spatial heterogeneity of CO_2 content in the vadose could not be completely assessed with two sensors, the subsoil CO_2 concentrations at 0.15 m and 1.5 m equate to 0.11 and 0.20%, respectively, which are similar to those measured by Rey et al. (2012b) but much lower values than those measured in typical high-temperature magmatic gases and low-temperature hydrothermal gases (0.5-12%; Fischer & Chiodini, 2015). Similarly, CO_2 contents are usually higher in karstic ecosystems, as

shown by Sánchez-Cañete et al., (2016) in a Mediterranean shrubland where a similar experimental design was installed.
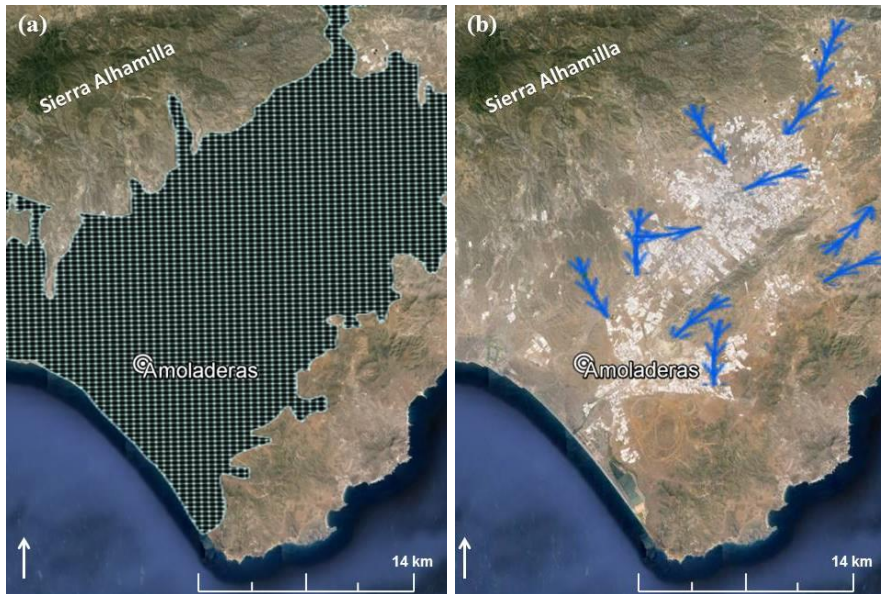
Figure 10. Hydrogeological characteristics of Amoladeras and surrounding areas: **(a)** Detritic aquifer system (black-dotted surface) and **(b)** subterranean water flux paths (blue arrows). Source: Mapa de información general de aguas subterráneas de Andalucía (REDIAM, Junta de Andalucía).

On the other hand, we hypothesize that subterranean air and water movement could be responsible for CO_2 recharge below the site. The topographic and geological characteristics of Amoladeras are consistent with this theory, since our experimental site is situated within an alluvial basin filled with high permeability sediment (Kerrick, 2001) and is surrounded by terrain at higher altitudes. Additionally, there is an aquifer system (Fig. 10a) where groundwater moves down gradient towards the southwest and Amoladeras (Fig. 10b; Junta de Andalucía, 2013).
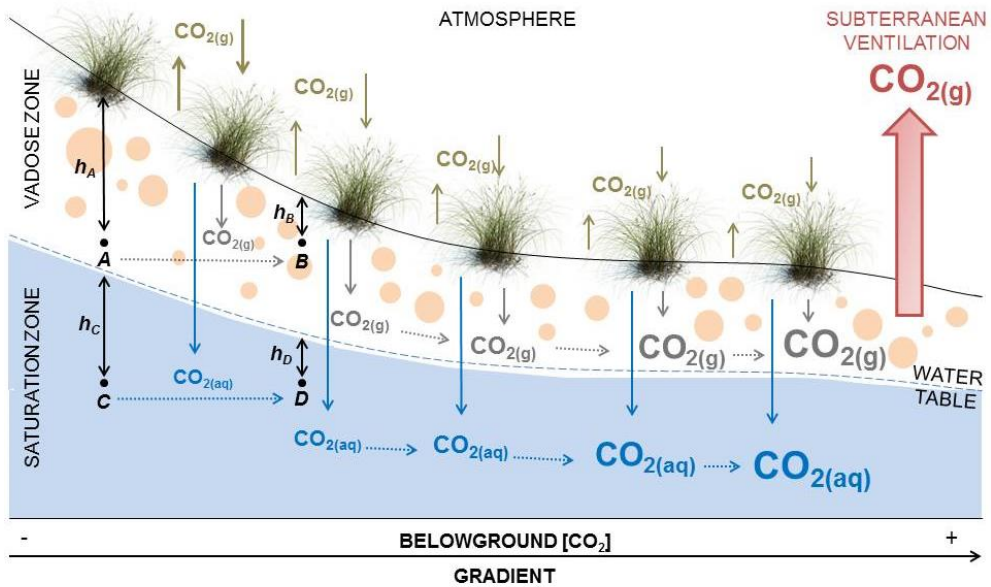
Figure 11. Diagram describing the lateral and vertical movement of aqueous and gaseous CO_2 above and below the surface. At point C, the hydraulic head is higher than at point D. Similarly, at point A, the head of CO_2-rich air is higher than at point B. Within the vadose and saturation zones, respectively, these heads force air and water flow to the right, towards lower altitudes.

In this context, we suggest that the CO_2 in both aqueous and gaseous phases is translocated from nearby areas such as Sierra Alhamilla (to the NW) – where belowground CO_2 production can be related to geothermal (Cerón et al., 2000; Rey et al. 2012b) and/or to biological activity given the higher water-availability and milder temperatures, compared to Amoladeras – through the vadose and saturated zones. Within the saturated zone, this transport occurs due to the gradient in the hydraulic head; similarly, a gradient exists in the vadose zone because, like water, CO_2-rich air is denser than atmospheric air (Sánchez-Cañete et al., 2013b). Hence, both gradients establish a downhill pressure gradient force (Fig. 11). Therefore, as suggested by Li et al., (2015), there might be an accumulation of CO_2 under arid basins, but this CO_2 can occasionally escape to

the atmosphere via subterranean ventilation, strongly affecting the C balance as proposed by Bourges et al., (2012).

In this regard, based on our results, we suggest that the main process behind this large CO_2 release is subterranean ventilation, which should be conceived as a non-diffusive mass transport process that can be detectable by EC systems under specific conditions. Firstly, the air located in the vadose zone must be significantly CO_2-rich; secondly, soil pores must have low water content to allow gas flow; and thirdly, high turbulence conditions are indispensable to penetrate the soil and transfer the CO_2-rich air from the vadose zone to the atmosphere. We found all these conditions in Amoladeras, especially during the dry season. This leads us to conclude that ventilation played a large role in the sizeable CO_2 release at the site, as also suggested by other studies developed in nearby ecosystems (Kowalski et al., 2008, Rey et al., 2012, Sanchez-Cañete et al., 2011, Serrano-Ortiz et al., 2009). Accordingly, we avoided the widely used terms of Net Ecosystem Carbon Balance (NECB) or Net Ecosystem Exchange (NEE) to refer to the net CO_2 exchange we measured because the released CO_2 is probably not exclusively local and because part of the vadose zone is actually beyond the ecosystem conceptual boundaries (Chapin et al., 2006). We suggest that Amoladeras may be considered as a surface through which the CO_2 accumulated within the vadose zone can be transported to the atmosphere.

Consequently, although some of our results over the growing season indicate photosynthetic activity in Amoladeras (Fig. 5a), the application of the ecophysiological models commonly used to quantify the light and temperature dependencies of net CO_2 fluxes (F_c) did not work well in our case (Table 3), as observed also by Kowalski et al., (2008). In fact, over the growing period of most years, the cumulative CO_2 balance was positive (Table 2) and CO_2 releases

were registered at high turbulence and VPD conditions (Fig. 6, 7). In contrast, during the dry season, ventilative fluxes were much more evident especially during daytime when symmetric CO_2 release patterns were measured for all hydrological years (Fig. 5b), similar to a nearby karstic Mediterranean shrubland (Serrano-Ortiz et al., 2009). In addition, the proportion of F_c variance explained by u_* was greater over the dry season (Fig. 8), and even though regression results were generally better at higher R_n levels this is probably due to the strength of solar heating, which is an important mechanism that triggers turbulence (Stull, 1988). Thus, similar to what Rey et al. (2012) proposed, we suggest that the higher R_n values registered in summer (Table 2) may result in higher convective energy of eddies that could penetrate the water-free soil pores of the deep vadose zone, where CO_2 molar fractions are higher (Fig. 9), and displace the stored CO_2-rich air to the atmosphere. Conversely, at nighttime, atmospheric stability, water deposition (i.e., dew) and vapor adsorption near the soil surface may inhibit ventilation, as suggested by several studies (Cuezva et al., 2011, Kowalski et al., 2008, Roland et al., 2013, Sanchez-Cañete et al., 2011) since over the dry season relative humidity peaks and u_* reaches its minimum at nighttime hours (data not shown) in Amoladeras. In fact, in a nearby experimental site (23 km far), dewfall represented from 9% to 23% of annual rainfall over 2007-2010 (Uclés et al., 2014).

5. CONCLUSIONS

Overall, our study highlights the relevance of subterranean ventilation as an advective transport process that may affect drylands' C balance, especially under dry and high-turbulence conditions. Additionally, based on our results, we suggest that the large amount of ventilated CO_2 cannot be derived from concurrent, *in situ* respiration. Therefore, we hypothesize, based on published

literature, that potential origins of the released CO_2 can be either direct geological degassing or subterranean translocation of CO_2 in both gaseous and aqueous phases, or both.

However, future research is needed in order to understand how CO_2 transport and production processes interact and modulate the C balance of semiarid and arid regions. Some future steps could be to determine CO_2 content and isotopic signal of belowground air and water in Amoladeras but also through an altitudinal gradient in order to detect the CO_2 translocation. Additionally, it would be very helpful to accurately locate fractures and fissures within the study area.

Finally, in addition to effects on photosynthesis and respiration of heatwaves and dry spells (Reichstein et al., 2013), the present study demonstrates that such climate extremes can provoke great CO_2 release via subterranean ventilation. This transport process should become more relevant with global warming and associated aridification (Gao & Giorgi, 2008), and furthermore represents a positive feedback to climate change.
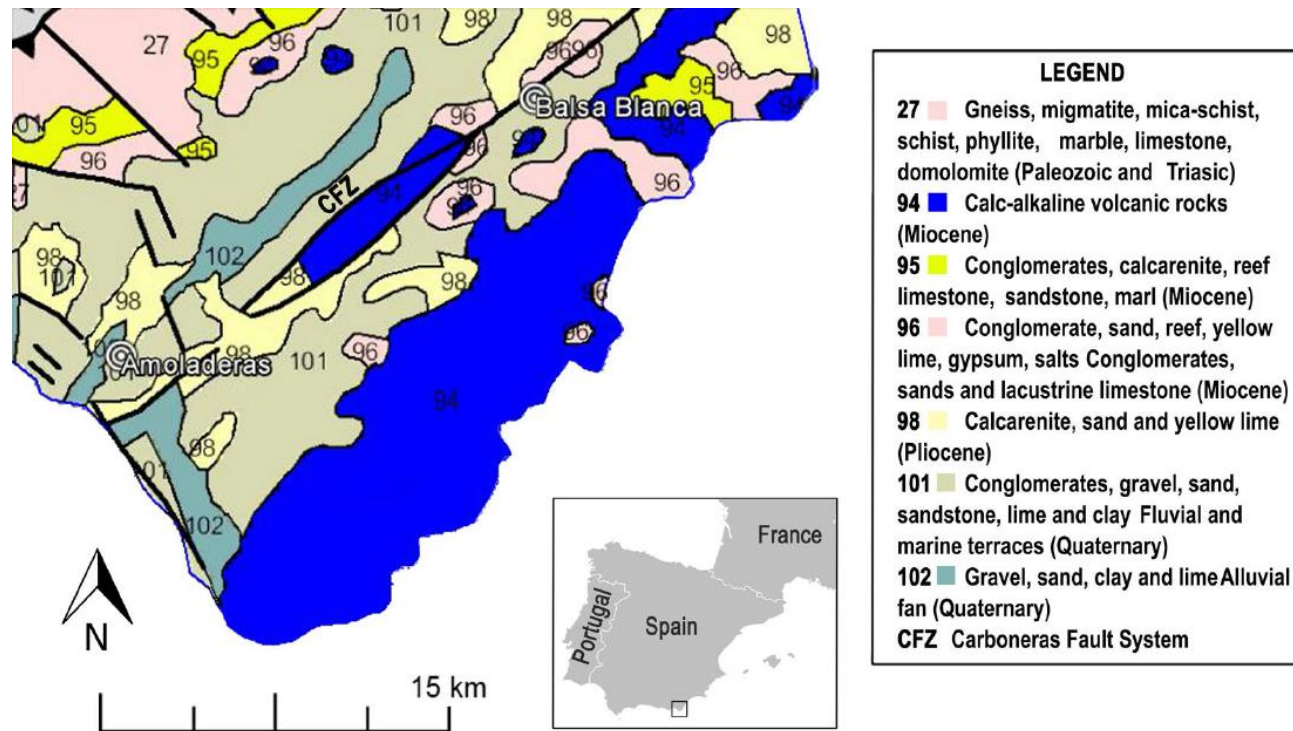
SUPPLEMENTARY MATERIAL: **APPENDIX A. Geologic map of the study area.** Geologic characterization of the area is shown in the geologic map, along with the locations of Amoladeras (the present study field site), Balsa Blanca (a nearby, previously studied experimental site that is mentioned in the publication), and Carboneras Fault Zone (CFZ). Source: Rodríguez-Fernández LR, et al. (2015) Mapa geológico de la Península Ibérica, Baleares y Canarias a escala 1/1.000.000. Instituto Geológico y Minero de España (IGME).

141

GENERAL CONCLUSIONS

1. Over whole study period (six hydrological years, 2009-2015), the average annual C balance was -23 ± 20 g C m^{-2} at Balsa Blanca and 231 ± 48 g C m^{-2} at Amoladeras, the two ecosystems of study. Hence, Balsa Blanca, the less degraded site (or site of reference), acted as a soft C sink while a great amount of C was released to the atmosphere at Amoladeras, the more degraded site.

2. Biological processes dominated the net C exchange measured at Balsa Blanca, whereas non-biological processes, especially subterranean ventilation, played an outstanding role in the net C exchange observed at Amoladeras.

3. Drought modulated the relative relevance of the component processes since biological ones were constrained due to the hydric stress and subterranean ventilation was enhanced owing to the greater water-free space within soil pores and cracks.

4. Land degradation influences the C balance of semiarid ecosystems by directly decreasing the C sequestration capacity especially during the growing seasons: the annual averaged net C uptake measured at the site of reference (Balsa Blanca) was 162% higher than at the more degraded site (Amoladeras), where the growing season lasted ~40 days less, evapotranspiration fluxes and EVI values were 3-24% and 3-37% higher, respectively, during the growing season.

5. Land degradation can also potentially enhance interconnectivity between vadose zone and atmosphere and thus, promote the escape of subsoil CO_2-rich air from vadose zone to the atmosphere through subterranean ventilation, especially during drought periods.

6. This study probed that similar and nearby ecosystems can show striking differences in their C budgets, despites showing a more similar behavior when observing evapotranspiration rates and satellite spectral indices, such as the Enhanced Vegetation Index.

7. Rain pulses, which correspond to isolated and unevenly distributed precipitation events during the dry season, usually provoke a net C emission from ecosystems to the atmosphere. While only large rain pulses (> 20 mm) cause net C uptake, the majority of rain pulses are

small-sized (< 20 mm) and trigger net C emission, which represented ~40% of the C emitted during the dry seasons.

8. The manipulative experiment used to decompose the ecosystem response after a rain pulse into their biological processes showed the significant and dominant role of soil respiration in the overall ecosystem C flux by contributing up to 80% during the days of maximum ecosystem C emission. In contrast, plant aboveground respiration and net primary production represented up to 17% and 40% of the ecosystem response during the days with the lowest ecosystem C emission, respectively.

9. Subterranean ventilation, a non-biological and poor-known process, can play a relevant role in the net C exchange measured at semiarid ecosystems, especially under dry and high-turbulence conditions, by causing anomalous and large net CO_2 release that represented from 43% to 64% of the annual amount of exchanged C.

10. Principal drivers of the subterranean ventilation are friction velocity, net radiation, soil moisture and vadose zone CO_2 molar fraction. In this regard, the great amount of subsoil CO_2 found in the degraded site (Amoladeras) that is ventilated to the atmosphere must be related to other sources apart from in situ biological respiration.

11. The characterization of vadose zone morphology and belowground air and water in both experimental sites and in the surroundings will be crucial to understand how subterranean fluid movement (gas and water) can interact and modulate the C balance of semiarid and arid regions.

12. Future research should entail the continuity of long-term monitoring stations, such as eddy covariance towers and subsoil CO_2 profiles, especially in drylands, in order to get an unbiased and representative estimation of terrestrial ecosystems behavior under future climate change scenarios.

REFERENCES

Ahlström, A. et al., 2015. The dominant role of semi-arid ecosystems in the trend and variability of the land CO2 sink. Science, 348(6237): 895-899.

Aires, L.M.I., Pio, C.A. and Pereira, J.S., 2008. Carbon dioxide exchange above a Mediterranean C3/C4 grassland during two climatologically contrasting years. Global Change Biology, 14(3): 539-555.

Alados, C. et al., 2004. Variations in landscape patterns and vegetation cover between 1957 and 1994 in a semiarid Mediterranean ecosystem. Landscape ecology, 19(5): 543-559.

Alados, C.L., Puigdefábregas, J. and Martínez-Fernández, J., 2011. Ecological and socio-economical thresholds of land and plant-community degradation in semi-arid Mediterranean areas of southeastern Spain. Journal of Arid Environments, 75(12): 1368-1376.

Allen-Diaz, B. et al., 1995. Rangelands in a changing climate: impacts, adaptations, and mitigation. Climate change: 131-158.

Amundson, R.G. and Davidson, E.A., 1990. Carbon dioxide and nitrogenous gases in the soil atmosphere. Journal of Geochemical Exploration, 38(1): 13-41.

Aranda, V. and Oyonarte, C., 2005. Effect of vegetation with different evolution degree on soil organic matter in a semi-arid environment (Cabo de Gata-Níjar Natural Park, SE Spain). Journal of Arid Environments, 62(4): 631-647.

Aubinet, M. et al., 1999. Estimates of the Annual Net Carbon and Water Exchange of Forests: The EUROFLUX Methodology. In: A.H. Fitter and D.G. Raffaelli (Editors), Advances in Ecological Research. Academic Press, pp. 113-175.

Austin, A.T. and Vivanco, L., 2006. Plant litter decomposition in a semi-arid ecosystem controlled by photodegradation. Nature, 442(7102): 555-558.

Baena-Pérez, J., Voermans, F., Ruiz Reig, P., 1977. Mapa Geológico de España 1:50000, Hoja 1045, Instituto Geológico y Minero de España (IGME).

Bajocco, S., De Angelis, A. and Salvati, L., 2012. A satellite-based green index as a proxy for vegetation cover quality in a Mediterranean region. Ecological Indicators, 23: 578-587.

Balaguer, L. et al., 2002. Ecophysiological significance of chlorophyll loss and reduced photochemical efficiency under extreme aridity in Stipa tenacissima L. Plant and Soil, 240(2): 343-352.

Baldocchi, D., 2008. TURNER REVIEW No. 15. 'Breathing' of the terrestrial biosphere: Lessons learned from a global network of carbon dioxide flux measurement systems. Australian Journal of Botany, 56(1): 1-26.

Baldocchi, D. et al., 2001. FLUXNET: A New Tool to Study the Temporal and Spatial Variability of Ecosystem-Scale Carbon Dioxide, Water Vapor, and Energy Flux Densities. Bulletin of the American Meteorological Society, 82(11): 2415-2434.

Baldocchi, D.D., Hincks, B.B. and Meyers, T.P., 1988. Measuring biosphere-atmosphere exchanges of biologically related gases with micrometeorological methods. Ecology, 69(5): 1331-1340.

Barron-Gafford, G.A., Scott, R.L., Jenerette, G.D., and Huxman, T.E., 2011. The relative controls of temperature, soil moisture, and plant functional group on soil CO_2 efflux at diel, seasonal, and annual scales, Journal of Geophysical Research: Biogeosciences, 116(G1), G01023.

Beier, C. et al., 2012. Precipitation manipulation experiments - challenges and recommendations for the future. Ecology Letters.

Berner, L.T., Law, B.E. and Hudiburg, T.W., 2017. Water availability limits tree productivity, carbon stocks, and carbon residence time in mature forests across the western US. Biogeosciences, 14(2): 365-378.

Birch, H.F., 1959. The effect of soil drying on humus decomposition and nitrogen availability. Plant and Soil, 10(1): 9-31.

Brandt, L.A., Bonnet, C. and King, J.Y., 2009. Photochemically induced carbon dioxide production as a mechanism for carbon loss from plant litter in arid ecosystems. Journal of Geophysical Research: Biogeosciences, 114(2).

Board, M.E.A., 2005. Ecosystems and human well-being: desertification synthesis.

Bohnert, H.J. and Jensen, R.G., 1996. Strategies for engineering water-stress tolerance in plants. Trends in Biotechnology, 14(3): 89-97.

Bourges, F., Genthon, P., Genty, D., Mangin, A. and D'Hulst, D., 2012. Comment on "Carbon uptake by karsts in the Houzhai Basin, southwest China" by Junhua Yan et al. Journal of Geophysical Research: Biogeosciences, 117(G3).

Bowling, D.R. and Massman, W.J., 2011. Persistent wind-induced enhancement of diffusive CO_2 transport in a mountain forest snowpack. Journal of Geophysical Research: Biogeosciences, 116(4).

Bown, H.E., Fuentes, J.-P., Perez-Quezada, J.F. and Franck, N., 2014. Soil respiration across a disturbance gradient in sclerophyllous ecosystems in Central Chile. Ciencia e Investigación Agraria, 41(1): 89-106.

Braga-Alarcón, J. C., Baena, J. and Calaforra, J., 2003. The Almeria-Nijar Basin. In: Villalobos M (ed.) Geology of the arid zone of Almeria (SE Spain). Regional Ministry of Environment and State Water Company for the Southern Basin SA (ACUSUR).

Brandt, L.A., Bonnet, C. and King, J.Y., 2009. Photochemically induced carbon dioxide production as a mechanism for carbon loss from plant litter in arid ecosystems. Journal of Geophysical Research: Biogeosciences, 114(2).

Cable, J.M. et al., 2012. Shrub encroachment alters sensitivity of soil respiration to temperature and moisture. Journal of Geophysical Research: Biogeosciences, 117(1).

Cammeraat, L.H., 1996. The MEDALUS core field programme: an overview of sites and methodology, in: Brandt, C.J., Thornes, J.B. (Eds.), Mediterranean Desertification and Land Use. John Wiley & Sons Ltd, Chichester, pp. 87-110.

Carbone, M.S. et al., 2011. Seasonal and episodic moisture controls on plant and microbial contributions to soil respiration. Oecologia, 167(1): 265-278.

Carrasco, A., 1988. Hidrogeología del Campo de Níjar y acuíferos «marginales» (Almería). TIAC'88, II: 1-36.

Cerón, J.C., Martín-Vallejo, M. and García-Rossell, L., 2000. CO_2-rich thermomineral groundwater in the Betic Cordilleras, southeastern Spain: Genesis and tectonic implications. Hydrogeology Journal, 8(2): 209-217.

Chapin, F.S. et al., 2006. Reconciling Carbon-cycle Concepts, Terminology, and Methods. Ecosystems, 9(7): 1041-1050.

Charley, J. L. and West, N. E., 1975. Plant-Induced soil chemical patterns in some shrub-dominated semi-desert ecosystems of Utah, Journal Of Ecology 63, 945–963.

Cleverly, J. et al., 2013. Dynamics of component carbon fluxes in a semi-arid Acacia woodland, central Australia. Journal of Geophysical Research: Biogeosciences, 118(3): 1168-1185.

Comas, X., Slater, L. and Reeve, A., 2007. In situ monitoring of free-phase gas accumulation and release in peatlands using ground penetrating radar (GPR). Geophysical Research Letters, 34(6): L06402.

Comas, X., Slater, L. and Reeve, A.S., 2011. Atmospheric pressure drives changes in the vertical distribution of biogenic free-phase gas in a northern peatland. Journal of Geophysical Research: Biogeosciences, 116(G4): G04014.

Cook, B.I., Smerdon, J.E., Seager, R. and Coats, S., 2014. Global warming and 21st century drying. Climate Dynamics, 43(9): 2607-2627.

Covington, M.D., 2016. 8. The importance of advection for CO_2 dynamics in the karst critical zone: An approach from dimensional analysis. Geological Society of America Special Papers, 516: 113-127.

Cross, A. and Schlesinger, W., 1999. Plant regulation of soil nutrient distribution in the northern Chihuahuan Desert. Plant Ecology, 145(1): 11-25.

Cuezva, S. et al., 2011. Short-term $CO_2(g)$ exchange between a shallow karstic cavity and the external atmosphere during summer: Role of the surface soil layer. Atmospheric Environment, 45(7): 1418-1427.

del Barrio, G., Puigdefabregas, J., Sanjuan, M.E., Stellmes, M. and Ruiz, A., 2010. Assessment and monitoring of land condition in the Iberian Peninsula, 1989–2000. Remote Sensing of Environment, 114(8): 1817-1832.

Dlugokencky, E., Tans, P., 2014. Trends in Atmospheric Carbon Dioxide. National Oceanic & Atmospheric Administration, Earth System Research Laboratory (NOAA/ESRL), available at: http://www.esrl.noaa.gov/gmd/ccgg/trends.

Dregne, H.E., 2002. Land degradation in the drylands. Arid Land Research and Management, 16(2): 99-132.

EddyPro® (Version 5) (Computer software]. 2014. Lincoln, NE. LI-COR, Inc; Infrastructure for Measurements of the European Carbon Cycle consortium.

Ehleringer, J. R., Schwinning, S. and Gebauer, R. 1999. Water-use in arid land ecosystems, in Plant physiological ecology, edited by M. C. Press et al., pp. 347-365, Blackwell, Edinburgh.

Emmerich, W.E., 2003. Carbon dioxide fluxes in a semiarid environment with high carbonate soils. Agricultural and Forest Meteorology, 116(1-2): 91-102.

Etheridge, D.M. et al., 1996. Natural and anthropogenic changes in atmospheric CO_2 over the last 1000 years from air in Antarctic ice and firn. Journal of Geophysical Research: Atmospheres, 101(D2): 4115-4128.

Fan, J., Jones, S.B., Qi, L.B., Wang, Q.J. and Huang, M.B., 2012. Effects of precipitation pulses on water and carbon dioxide fluxes in two semiarid ecosystems: Measurement and modeling. Environmental Earth Sciences, 67(8): 2315-2324.

Feng, Q. et al., 2006. Effect of climatic changes and human activity on soil carbon in desertified regions of China. Tellus B, 58(2): 117-128.

Feng, S. and Fu, Q., 2013. Expansion of global drylands under a warming climate. Atmos. Chem. Phys., 13(19): 10081-10094.

Fensholt, R. et al., 2013. Assessing land degradation/recovery in the African Sahel from long-term earth observation based primary productivity and precipitation relationships. Remote Sensing, 5(2): 664-686.

Finkelstein, P.L. and Sims, P.F., 2001. Sampling error in eddy correlation flux measurements. Journal of Geophysical Research: Atmospheres, 106(D4): 3503-3509.

Fischer, T. B. and Chiodini, G., 2015. Volcanic, Magmatic and Hydrothermal Gases. In: Sigurdsson H et al. (eds.), The Encyclopedia of Volcanoes. Elsevier.

Frisia, S. et al., 2011. Carbon mass-balance modelling and carbon isotope exchange processes in dynamic caves. Geochimica et Cosmochimica Acta, 75(2): 380-400.

Foken, T. and Wichura, B., 1996. Tools for quality assessment of surface-based flux measurements. Agricultural and Forest Meteorology, 78(1): 83-105.

Foyer, C.H. and Noctor, G., 2000. Tansley Review No. 112. Oxygen processing in photosynthesis: regulation and signalling. New Phytologist, 146(3): 359-388.

Fujiyoshi, R. et al., 2009. Tracing the sources of gaseous components (^{222}Rn, CO_2 and its carbon isotopes) in soil air under a cool-deciduous stand in Sapporo, Japan. Environmental Geochemistry and Health, 32(1): 73-82.

Gao, X., Huete, A.R., Ni, W. and Miura, T., 2000. Optical–Biophysical Relationships of Vegetation Spectra without Background Contamination. Remote Sensing of Environment, 74(3): 609-620.

Gao, X. and Giorgi, F., 2008. Increased aridity in the Mediterranean region under greenhouse gas forcing estimated from high resolution simulations with a regional climate model. Global and Planetary Change, 62(3-4): 195-209.

Haase, P., Pugnaire, F.I., Clark, S.C. and Incoll, L.D., 1999. Environmental control of canopy dynamics and photosynthetic rate in the evergreen tussock grass Stipa tenacissima. Plant Ecology, 145(2): 327-339.

Hamerlynck, E.P., Scott, R.L., Sánchez-Cañete, E.P. and Barron-Gafford, G.A., 2013. Nocturnal soil CO_2 uptake and its relationship to subsurface soil and ecosystem carbon fluxes in a Chihuahuan Desert shrubland. Journal of Geophysical Research G: Biogeosciences, 118(4): 1593-1603.

Hirsch, A.I., Trumbore, S.E. and Goulden, M.L., 2004. The surface CO_2 gradient and pore-space storage flux in a high-porosity litter layer. Tellus, Series B: Chemical and Physical Meteorology, 56(4): 312-321.

Holling, C.S., 1973. Resilience and Stability of Ecological Systems. Annual Review of Ecology and Systematics, 4: 1-23.

Hou, X., Wang, Z., Michael, S.P., Ji, L. and Yun, X., 2014. The response of grassland productivity, soil carbon content and soil respiration rates to different grazing regimes in a desert steppe in northern China. The Rangeland Journal, 36(6): 573-582.

Hupp, J., 2012. The importance of water vapor measurements and corrections. LI-COR Biosciences Inc. Application Note, 129.

Huxman, T.E. et al., 2004a. Response of net ecosystem gas exchange to a simulated precipitation pulse in a semi-arid grassland: The role of native versus non-native grasses and soil texture. Oecologia, 141(2): 295-305.

Huxman, T.E. et al., 2004b. Precipitation pulses and carbon fluxes in semiarid and arid ecosystems. Oecologia, 141(2): 254-268.

Inglima, I. et al., 2009. Precipitation pulses enhance respiration of Mediterranean ecosystems: The balance between organic and inorganic components of increased soil CO_2 efflux. Global Change Biology, 15(5): 1289-1301.

IPCC (Intergovernmental Panel on Climate Change), 2012. Summary for policymakers, in Managing the Risks of Extreme Events and Disasters to Advance Climate Change Adaptation edited by Field, C.B. et al. A Special Report of Working Groups I and II of the Intergovernmental Panel on Climate Change. Cambridge University Press, Cambridge, UK, and New York, NY, USA, pp. 1–19.

IPCC (Intergovernmental Panel on Climate Change), 2007: Climate Change 2007: The Physical Science Basis. Contribution of Working Group I to the Fourth Assessment Report of the Intergovernmental Panel on Climate Change (Solomon, S., D. Qin, M. Manning, Z. Chen, M. Marquis, K.B. Averyt, M.Tignor and H.L. Miller (eds.)]. Cambridge University Press, Cambridge, United Kingdom and New York, NY, USA.

IPCC (Intergovernmental Panel on Climate Change), 2001: Climate Change 2001: Working Group I: The Scientific Basis, Summary for Policymakers, Cambridge University Press, Cambridge.

Janssens, I.A. et al., 2001. Productivity overshadows temperature in determining soil and ecosystem respiration across European forests. Global Change Biology, 7(3): 269-278.

Jarvis, P. et al., 2007. Drying and wetting of Mediterranean soils stimulates decomposition and carbon dioxide emission: The "Birch effect". Tree Physiology, 27(7): 929-940.

Jenerette, G. D., Scott, R. L., and Huxman, T. E. 2008. Whole ecosystem metabolic pulses following precipitation events, Functional Ecology, 22(5), 924-930.

Jobbágy, E.G. and Jackson, R.B., 2000. The vertical distribution of soil organic carbon and its relation to climate and vegetation. Ecological applications, 10(2): 423-436.

Jongen, M., Pereira, J.S., Aires, L.M.I. and Pio, C.A., 2011. The effects of drought and timing of precipitation on the inter-annual variation in ecosystem-atmosphere exchange in a Mediterranean grassland. Agricultural and Forest Meteorology, 151(5): 595-606.

Joos, F. and Spahni, R., 2008. Rates of change in natural and anthropogenic radiative forcing over the past 20,000 years. Proceedings of the National Academy of Sciences of the United States of America, 105(5): 1425-1430.

Junta de Andalucía, Consejería de Medio Ambiente y Ordenación del Territorio, 2013. Mapa de información general de aguas subterráneas de Andalucía. Red de Información Ambiental de Andalucía (REDIAM).

Kerrick, D.M., 2001. Present and past nonanthropogenic CO_2 degassing from the solid earth. Reviews of Geophysics, 39(4): 565-585.

Kottek, M., Grieser, J., Beck, C., Rudolf, B., and Rubel, F.: World map of the Köppen-Geiger climate classification updated, Meteorologische Zeitschrift, 15, 259-263, 2006.

Kowalski, A.S., Anthoni, P.M., Vong, R.J., Delany, A.C. and Maclean, G.D., 1997. Deployment and Evaluation of a System for Ground-Based Measurement of Cloud Liquid Water Turbulent Fluxes. Journal of Atmospheric and Oceanic Technology, 14(3): 468-479.

Kowalski, A.S. et al., 2008. Can flux tower research neglect geochemical CO_2 exchange? Agricultural and Forest Meteorology, 148(6-7): 1045-1054.

Kutzbach, L. et al., 2007. CO_2 flux determination by closed-chamber methods can be seriously biased by inappropriate application of linear regression. Biogeosciences, 4(6): 1005-1025.

Lal, R., 2001. Potential of Desertification Control to Sequester Carbon and Mitigate the Greenhouse Effect. Climatic Change, 51(1): 35-72.

Lasslop, G. et al., 2010. Separation of net ecosystem exchange into assimilation and respiration using a light response curve approach: critical issues and global evaluation. Global Change Biology, 16(1): 187-208.

Lauenroth, W. K., and Bradford, J. B., 2012. Ecohydrology of dry regions of the United States: Water balance consequences of small precipitation events, Ecohydrology, 5(1), 46-53.

Lázaro, R., Rodrigo, F.S., Gutiérrez, L., Domingo, F. and Puigdefábregas, J., 2001. Analysis of a 30-year rainfall record (1967–1997) in semi–arid SE Spain for implications on vegetation. Journal of Arid Environments, 48(3): 373-395.

Leon, E. et al., 2014. Hot spots, hot moments, and spatio-temporal controls on soil CO_2 efflux in a water-limited ecosystem. Soil Biology and Biochemistry, 77: 12-21.

Le Houérou, H.N., 1990. Global Change: population, land-use and vegetation in the Mediterranean basin by the mild-21st century, in Greenhouse effect, sea level and drought edited by R. Paepe et al., pp 301-367, Kluwer Academic Publishers, Dordrecht.

Le Quéré, C. et al., 2009. Trends in the sources and sinks of carbon dioxide. Nature Geoscience, 2(12): 831-836.

Le Quéré, C. et al., 2015. Global Carbon Budget 2015. Earth Syst. Sci. Data, 7(2): 349-396.

Li, F., Zhao, W. and Liu, H., 2013. The Response of Aboveground Net Primary Productivity of Desert Vegetation to Rainfall Pulse in the Temperate Desert Region of Northwest China. PLoS ONE, 8(9).

Li, Y., Wang, Y.G., Houghton, R.A. and Tang, L.S., 2015. Hidden carbon sink beneath desert. Geophysical Research Letters, 42(14): 5880-5887.

LI-COR, Inc. 2014.EddyPro® 5 Help and User's Guide. LI-COR, Inc. Lincoln,NE.

Livingston, G. P. and Hutchinson, G. L., 1995. Enclosure-based measurement of trace gas exchange: applications and sources of error, in: Matson, P. A. and Harriss, R. C. (Eds.), Biogenic Trace Gases: Measuring Emissions from Soil and Water. Blackwell Science Ltd, Oxford, pp. 15–51.

Lloyd, J. and Taylor, J., 1994. On the temperature dependence of soil respiration. Functional ecology: 315-323.

López-Ballesteros, A. et al., 2017. Subterranean ventilation of allochthonous CO_2 governs net CO_2 exchange in a semiarid Mediterranean grassland. Agricultural and Forest Meteorology, 234–235: 115-126.

López-Ballesteros, A. et al., 2016. Enhancement of the net CO_2 release of a semiarid grassland in SE Spain by rain pulses. Journal of Geophysical Research: Biogeosciences, 121(1): 2015JG003091.

Ma, S., Baldocchi, D.D., Hatala, J.A., Detto, M. and Curiel Yuste, J., 2012. Are rain-induced ecosystem respiration pulses enhanced by legacies of antecedent photodegradation in semi-arid environments? Agricultural and Forest Meteorology, 154-155: X203-213.

Ma, S., Baldocchi, D., Wolf, S. and Verfaillie, J., 2016. Slow ecosystem responses conditionally regulate annual carbon balance over 15 years in Californian oak-grass savanna. Agricultural and Forest Meteorology, 228–229: 252-264.

Maestre, F.T. et al., 2009. Shrub encroachment can reverse desertification in semi-arid Mediterranean grasslands. Ecology Letters, 12(9): 930-941.

Maestre, F. T., Ramírez, D. A., and Cortina, J., 2007. Ecología del esparto (Stipa tenacissima L.) y los espartales de la Península Ibérica, Ecosistemas 16(2), 111-130.

Maier, M. et al., 2012. Turbulence effect on gas transport in three contrasting forest soils. Soil Science Society of America Journal, 76(5): 1518-1528.

Maier, M., Schack-Kirchner, H., Hildebrand, E.E. and Holst, J., 2010. Pore-space CO_2 dynamics in a deep, well-aerated soil. European Journal of Soil Science, 61(6): 877-887.

Mainguet, M. and Da Silva, G., 1998. Desertification and drylands development: what can be done? Land Degradation & Development, 9(5): 375-382.

Marañón-Jiménez, S. et al., 2011. Post-fire soil respiration in relation to burnt wood management in a Mediterranean mountain ecosystem. Forest Ecology and Management, 261(8): 1436-1447.

Mauder, M., Foken, T., 2004. Documentation and instruction manual of the eddy covariance software package TK3. Abt Mikrometeorologie, 46.

Mauder, M. and Foken, T., 2006. Impact of post-field data processing on eddy covariance flux estimates and energy balance closure. Meteorologische Zeitschrift, 15(6): 597-609.

Mayor, Á.G., Bautista, S. and Bellot, J., 2011. Scale-dependent variation in runoff and sediment yield in a semiarid Mediterranean catchment. Journal of Hydrology, 397(1–2): 128-135.

Mbow, C., Brandt, M., Ouedraogo, I., de Leeuw, J. and Marshall, M., 2015. What four decades of earth observation tell us about land degradation in the Sahel? Remote Sensing, 7(4): 4048-4067.60.

McMillen, R., 1988. An eddy correlation technique with extended applicability to non-simple terrain. Boundary-Layer Meteorology, 43(3): 231-245.

Metcalfe, D.B., 2014. Climate science: A sink down under. Nature.

Michaelis, L., Menten, M.L.: Die Kinetik der Invertinwirkung. Biochem. Z. 49, 333–369. 1913.

Mielnick, P., Dugas, W.A., Mitchell, K. and Havstad, K., 2005. Long-term measurements of CO_2 flux and evapotranspiration in a Chihuahuan desert grassland. Journal of Arid Environments, 60(3): 423-436.

Migliavacca, M. et al., 2011. Semiempirical modeling of abiotic and biotic factors controlling ecosystem respiration across eddy covariance sites. Global Change Biology, 17(1): 390-409.

Moldrup, P. et al., 2000. Predicting the Gas Diffusion Coefficient in Repacked Soil Water-Induced Linear Reduction Model. Soil Science Society of America Journal, 64(5): 1588-1594.

Moncrieff, J.B. et al., 1997. A system to measure surface fluxes of momentum, sensible heat, water vapour and carbon dioxide. Journal of Hydrology, 188–189(0): 589-611.

Moncrieff, J., Clement, R., Finnigan, J. and Meyers, T., 2005. Averaging, Detrending, and Filtering of Eddy Covariance Time Series. In: X. Lee, W. Massman and B. Law (Editors), Handbook of Micrometeorology. Atmospheric and Oceanographic Sciences Library. Springer Netherlands, pp. 7-31.

Moreno-Mateos, D. et al., 2017. Anthropogenic ecosystem disturbance and the recovery debt. Nature Communications, 8: 14163.

Noy-Meir, I., 1973. Desert Ecosystems: Environment and Producers. Annual Review of Ecology and Systematics, 4(1): 25-51.

Okin, G. S., 2001. Wind-Driven Desertification: Process Modeling, Remote Monitoring, and Forecasting, PhD Thesis, California Institute of Technology Pasadena, California, Pasadena, California.

Omuto, C., 2011. A new approach for using time-series remote-sensing images to detect changes in vegetation cover and composition in drylands: A case study of eastern Kenya. International journal of remote sensing, 32(21): 6025-6045.

Omuto, C., Vargas, R., Alim, M. and Paron, P., 2010. Mixed-effects modelling of time series NDVI-rainfall relationship for detecting human-induced loss of vegetation cover in drylands. Journal of Arid Environments, 74(11): 1552-1563.

Oñate-Rubalcaba, J.J., 1993. Caracterización de los cambios climáticos en la península ibérica y Canarias desde principios de siglo. Thesis Report. Autónoma de Madrid.

Oyonarte, C., Mingorance, M.D., Durante, P., Piñero, G. and Barahona, E., 2007. Indicators of change in the organic matter in arid soils. Science of the Total Environment, 378(1-2): 133-137.

Oyonarte, C., Rey, A., Raimundo, J., Miralles, I. and Escribano, P., 2012. The use of soil respiration as an ecological indicator in arid ecosystems of the SE of Spain: Spatial variability and controlling factors. Ecological Indicators, 14(1): 40-49.

Padilla, F.M., Miranda, J.D., Armas, C. and Pugnaire, F.I., 2015. Effects of changes in rainfall amount and pattern on root dynamics in an arid shrubland. Journal of Arid Environments, 114: 49-53.

Parton, W. et al., 2012. Impact of precipitation dynamics on net ecosystem productivity. Global Change Biology, 18(3): 915-927.

Pérez-Priego, O., Testi, L., Orgaz, F. and Villalobos, F.J., 2010. A large closed canopy chamber for measuring CO_2 and water vapour exchange of whole trees. Environmental and Experimental Botany, 68(2): 131-138.

Pérez-Priego, O., Serrano-Ortiz, P., Sánchez-Cañete, E.P., Domingo, F. and Kowalski, A.S., 2013. Isolating the effect of subterranean ventilation on CO_2 emissions from drylands to the atmosphere. Agricultural and Forest Meteorology, 180: 194-202.

Pérez-Priego, O. et al., 2015. Analysing uncertainties in the calculation of fluxes using whole-plant chambers: random and systematic errors. Plant and Soil, 393(1-2): 229-244.

Poulter, B. et al., 2014. Contribution of semi-arid ecosystems to interannual variability of the global carbon cycle. Nature, 509(7502): 600-603.

Prince, S., Becker-Reshef, I. and Rishmawi, K., 2009. Detection and mapping of long-term land degradation using local net production scaling: Application to Zimbabwe. Remote Sensing of Environment, 113(5): 1046-1057.

Pugnaire, F.I. and Haase, P., 1996. Comparative physiology and growth of two perennial tussock grass species in a semi-arid environment. Annals of Botany, 77(1): 81-86.

Pugnaire, F.I., Haase, P., Incoll, L.D. and Clark, S.C., 1996. Response of the tussock grass Stipa tenacissima to watering in a semi-arid environment. Functional Ecology, 10(2): 265-274.

Puigdefábregas, J. and Mendizabal, T., 1998. Perspectives on desertification: western Mediterranean. Journal of Arid Environments, 39(2): 209-224.

Ramírez, D. A., 2006. Estudio de la transpiración del esparto (Stipa tenacissima L.) en una cuenca del semiárido alicantino: un análisis pluriescalar, PhD thesis, Dept. Ecology, University of Alicante, Alicante, Spain.

Redeker, K.R., Baird, A.J. and Teh, Y.A., 2015. Quantifying wind and pressure effects on trace gas fluxes across the soil–atmosphere interface. Biogeosciences, 12(24): 7423-7434.

Reichstein, M. et al., 2013. Climate extremes and the carbon cycle. Nature, 500(7462): 287-295.

Reichstein, M. et al., 2005. On the separation of net ecosystem exchange into assimilation and ecosystem respiration: review and improved algorithm. Global Change Biology, 11(9): 1424-1439.

Reicosky, D., Wagner, S. and Devine, O., 1990. Methods of calculating carbon dioxide exchange rates for maize and soybean using a portable field chamber. Photosynthetica, 24(1): 22-38.

Rey, A. et al., 2011. Impact of land degradation on soil respiration in a steppe (Stipa tenacissima L.) semi-arid ecosystem in the SE of Spain. Soil Biology and Biochemistry, 43(2): 393-403.

Rey, A. et al., 2012. Wind as a main driver of the net ecosystem carbon balance of a semiarid Mediterranean steppe in the South East of Spain. Global Change Biology, 18(2): 539-554.

Rey, A. et al., 2013. Partitioning the net ecosystem carbon balance of a semiarid steppe into biological and geological components. Biogeochemistry: 1-19.

Rey, A., Oyonarte, C., Morán-López, T., Raimundo, J. and Pegoraro, E., 2017. Changes in soil moisture predict soil carbon losses upon rewetting in a perennial semiarid steppe in SE Spain. Geoderma, 287: 135-146.

Rejos, F. J., 2000. La Atocha (Stipa tenacissima Loefl. ex L.) en el centro peninsular: aspectos vegetativos y reproductivos, PhD thesis, University of Alcalá, Madrid, Spain.

Rodríguez-Fernández, L. R., López-Olmedo, F., Oliveira, J. T., Medialdea, T., Terrinha, P., Matas, J., Martín-Serrano, A., Martín-Parra, L. M., Rubio, F., Marín, C., Montes, M. and Nozal, F., 2015. Mapa geológico de la Península Ibérica, Baleares y Canarias a escala 1/1.000.000. InstitutoGeológico y Minero de España (IGME).

Roland, M. et al., 2013. Atmospheric turbulence triggers pronounced diel pattern in karst carbonate geochemistry. Biogeosciences, 10(7): 5009-5017.

Ross, I. et al., 2012. How do variations in the temporal distribution of rainfall events affect ecosystem fluxes in seasonally water-limited Northern Hemisphere shrublands and forests? Biogeosciences, 9(3): 1007-1024.

Rutledge, S., Campbell, D.I., Baldocchi, D. and Schipper, L.A., 2010. Photodegradation leads to increased carbon dioxide losses from terrestrial organic matter. Global Change Biology, 16(11): 3065-3074.

Rutter, E.H., Faulkner, D.R. and Burgess, R., 2012. Structure and geological history of the Carboneras Fault Zone, SE Spain: Part of a stretching transform fault system. Journal of Structural Geology, 45: 68-86.

Rychnovská, M., 1964. A contribution to the ecology of the genus Stipa II. Water relations of plants and habitat on the hill Krížová hora Near the Town of Moravský. Preslia (Praha) 37, 42-52.

Safriel, U. and Adeel, Z., 2005. Dryland Systems.‖ In Ecosystems and Human Well-being: Current State and Trends. Vol. 1, edited by R. Hassan, R. Scholes, & N. Ash, 623–662. Washington, DC: Island Press.

Sala, O.E. and Lauenroth, W.K., 1985. Root profiles and the ecological effect of light rainshowers in arid and semiarid regions. American Midland Naturalist, 114(2): 406-408.

Sanchez-Cañete, E.P., Serrano-Ortiz, P., Kowalski, A.S., Oyonarte, C. and Domingo, F., 2011. Subterranean CO_2 ventilation and its role in the net ecosystem carbon balance of a karstic shrubland. Geophysical Research Letters, 38(9).

Sánchez-Cañete, E.P., Kowalski, A.S., Serrano-Ortiz, P., Pérez-Priego, O. and Domingo, F., 2013a. Deep CO_2 soil inhalation/exhalation induced by synoptic pressure changes and atmospheric tides in a carbonated semiarid steppe. Biogeosciences, 10(10): 6591-6600.

Sánchez-Cañete, E.P., Serrano-Ortiz, P., Domingo, F. and Kowalski, A.S., 2013b. Cave ventilation is influenced by variations in the CO_2-dependent virtual temperature. International Journal of Speleology, 42(1): 1-8.

Sánchez-Cañete, E.P. and Kowalski, A.S., 2014. Comment on "Using the gradient method to determine soil gas flux: A review" by M. Maier and H. Schack-Kirchner. Agricultural and Forest Meteorology, 197(0): 254-255.

Sánchez-Cañete, E.P. et al., 2016. Winds induce CO_2 exchange with the atmosphere and vadose zone transport in a karstic ecosystem. Journal of Geophysical Research: Biogeosciences.

Schlesinger, W.H., 1990. Evidence from chronosequence studies for a low carbon-storage potential of soils. Nature, 348(6298): 232-234.

Schlesinger, W., 1997. Biogeochemistry: An Analysis of Global Change (San Diego, CA: Academic).

Schlesinger, W.H., 2016. An Evaluation of Abiotic Carbon Sinks in Deserts. Global Change Biology.

Schulz, K. et al., 2016. Grazing deteriorates the soil carbon stocks of Caatinga forest ecosystems in Brazil. Forest Ecology and Management, 367: 62-70.

Schwinning, S. and Sala, O., 2004. Hierarchy of responses to resource pulses in arid and semi-arid ecosystems. Oecologia, 141(2): 211-220.

Scott, R.L., Hamerlynck, E.P., Jenerette, G.D., Moran, M.S. and Barron-Gafford, G.A., 2010. Carbon dioxide exchange in a semidesert grassland through drought-induced vegetation change. Journal of Geophysical Research: Biogeosciences, 115(3).

Scott, R.L., Serrano-Ortiz, P., Domingo, F., Hamerlynck, E.P. and Kowalski, A.S., 2012. Commonalities of carbon dioxide exchange in semiarid regions with monsoon and Mediterranean climates. Journal of Arid Environments, 84: 71-79.

Scott, R.L., Biederman, J.A., Hamerlynck, E.P. and Barron-Gafford, G.A., 2015. The carbon balance pivot point of southwestern U.S. semiarid ecosystems: Insights from the 21st century drought. Journal of Geophysical Research: Biogeosciences, 120(12): 2612-2624.

Seok, B. et al., 2009. An automated system for continuous measurements of trace gas fluxes through snow: An evaluation of the gas diffusion method at a subalpine forest site, Niwot Ridge, Colorado. Biogeochemistry, 95(1): 95-113.

Serrano-Ortiz, P. et al., 2009. Interannual CO_2 exchange of a sparse Mediterranean shrubland on a carbonaceous substrate. Journal of Geophysical Research G: Biogeosciences, 114(4).

Serrano-Ortiz, P. et al., 2010. Hidden, abiotic CO_2 flows and gaseous reservoirs in the terrestrial carbon cycle: Review and perspectives. Agricultural and Forest Meteorology, 150(3): 321-329.

Serrano-Ortiz, P. et al., 2011. Corrigendum to "Hidden, abiotic CO_2 flows and gaseous reservoirs in the terrestrial carbon cycle: Review and perspectives" (Agric. Forest Meteorol. 150 (2010) 321–329]. Agricultural and Forest Meteorology, 151(4): 529.

Serrano-Ortiz, P., Sánchez-Cañete, E.P. and Oyonarte, C., 2012. The carbon cycle in drylands, Recarbonization of the Biosphere. Springer, pp. 347-368.

Serrano-Ortiz, P. et al., 2014. Ecological functioning in grass–shrub Mediterranean ecosystems measured by eddy covariance. Oecologia, 175(3): 1005-1017.

Shoshany, M. and Karnibad, L., 2015. Remote Sensing of Shrubland Drying in the South-East Mediterranean, 1995–2010: Water-Use-Efficiency-Based Mapping of Biomass Change. Remote Sensing, 7(3): 2283-2301.

Solomon, S., Plattner, G.K., Knutti, R. and Friedlingstein, P., 2009. Irreversible climate change due to carbon dioxide emissions. Proceedings of the National Academy of Sciences of the United States of America, 106(6): 1704-1709.

Sponseller, R.A., 2007. Precipitation pulses and soil CO_2 flux in a Sonoran Desert ecosystem. Global Change Biology, 13(2): 426-436.

Stull, R. B., 1988. An Introduction to Boundary Layer Meteorology, Kluwer Academic Publishers, Dordrecht.

Subke, J.-A., Reichstein, M. and Tenhunen, J.D., 2003. Explaining temporal variation in soil CO_2 efflux in a mature spruce forest in Southern Germany. Soil Biology and Biochemistry, 35(11): 1467-1483.

Takle, E.S. et al., 2004. Influence of high-frequency ambient pressure pumping on carbon dioxide efflux from soil. Agricultural and Forest Meteorology, 124(3-4): 193-206.

Tang, J. and Baldocchi, D.D., 2005. Spatial–temporal variation in soil respiration in an oak–grass savanna ecosystem in California and its partitioning into autotrophic and heterotrophic components. Biogeochemistry, 73(1): 183-207.

Thomey, M.L. et al., 2011. Effect of precipitation variability on net primary production and soil respiration in a Chihuahuan Desert grassland. Global Change Biology, 17(4): 1505-1515.

Thompson, M. et al., 2009. Mapping grazing-induced degradation in a semi-arid environment: a rapid and cost effective approach for assessment and monitoring. Environmental management, 43(4): 585.

Uclés, O., Villagarcía, L., Moro, M.J., Canton, Y. and Domingo, F., 2014. Role of dewfall in the water balance of a semiarid coastal steppe ecosystem. Hydrological Processes, 28(4): 2271-2280.

Unger, S., Máguas, C., Pereira, J. S., David, T. S., and Werner, C,. 2010. The influence of precipitation pulses on soil respiration – Assessing the "Birch effect" by stable carbon isotopes, Soil Biology and Biochemistry, 42(10), 1800-1810.

Unger, S., Máguas, C., Pereira, J. S., David, T. S., and Werner, C., 2012. Interpreting post-drought rewetting effects on soil and ecosystem carbon dynamics in a Mediterranean oak savannah, Agricultural and Forest Meteorology, 154-155, X9-18.

United Nations Convention to Combat Desertification (UNCCD), 1994. General Assembly.

Valladares, F. and Pugnaire, F.I., 1999. Tradeoffs Between Irradiance Capture and Avoidance in Semi-arid Environments Assessed with a Crown Architecture Model. Annals of Botany, 83(4): 459-469.

Vickers, D. and Mahrt, L., 1997. Quality Control and Flux Sampling Problems for Tower and Aircraft Data. Journal of Atmospheric and Oceanic Technology, 14(3): 512-526.

Wagner, S.W., Reicosky, D.C. and Alessi, R.S., 1997. Regression models for calculating gas fluxes measured with a closed chamber. Agronomy Journal, 89(2): 279-284.

Wang, W., Guo, J. and Oikawa, T., 2007. Contribution of root to soil respiration and carbon balance in disturbed and undisturbed grassland communities, northeast China. Journal of Biosciences, 32(2): 375-384.

Wang, Y., Yan, X. and Wang, Z., 2016. A preliminary study to investigate the biogeophysical impact of desertification on climate based on different latitudinal bands. International Journal of Climatology, 36(2): 945-955.

Watanabe, M.D.B. and Ortega, E., 2011. Ecosystem services and biogeochemical cycles on a global scale: valuation of water, carbon and nitrogen processes. Environmental Science & Policy, 14(6): 594-604.

Webb, E.K., Pearman, G.I. and Leuning, R., 1980. Correction of flux measurements for density effects due to heat and water vapour transfer. Quarterly Journal of the Royal Meteorological Society, 106(447): 85-100.

Weijermars, R., 1991. Geology and tectonics of the Betic Zone, SE Spain. Earth-Science Reviews, 31(3–4): 153-236.

Williams, C.A., Hanan, N., Scholes, R.J. and Kutsch, W., 2009. Complexity in water and carbon dioxide fluxes following rain pulses in an African savanna. Oecologia, 161(3): 469-480.

Wingler, A., Lea, P.J., Quick, W.P. and Leegood, R.C., 2000. Photorespiration: metabolic pathways and their role in stress protection, 355, 1517-1529 pp.

Wohlfahrt, G., Fenstermaker, L.F. and Arnone Iii Iii, J.A., 2008. Large annual net ecosystem CO_2 uptake of a Mojave Desert ecosystem. Global Change Biology, 14(7): 1475-1487.

World Reference Base for Soil Resources (WRB, 2006) World Soil Resources Reports 103. FAO, Rome, Italy.

Xu, L., Baldocchi, D.D. and Tang, J., 2004. How soil moisture, rain pulses, and growth alter the response of ecosystem respiration to temperature. Global Biogeochemical Cycles, 18(4): GB4002.

Yan, L., Chen, S., Huang, J. and Lin, G., 2011. Water regulated effects of photosynthetic substrate supply on soil respiration in a semiarid steppe. Global Change Biology, 17(5): 1990-2001.

Zhang, L. et al., 2014. Net ecosystem productivity of temperate grasslands in northern China: An upscaling study. Agricultural and Forest Meteorology, 184(0): 71-81.

Zika, M. and Erb, K.-H., 2009. The global loss of net primary production resulting from human-induced soil degradation in drylands. Ecological Economics, 69(2): 310-318.

LIST OF ACRONYMS

3-D	Three dimensional
ANPP	Aboveground Net Primary Production
AR	Autotrophic RespirationC
CC	Climate Change
CV	Coefficient of Variation
EC	Eddy Covariance
EVI	Enhanced Vegetation Index
GHG	Green House Gas
GHGs	Green House Gases
GPP	Gross Primary Production
HR	Heterotrophic Respiration
IRGA	Infrared Gas Analyzer
IQR	Interquartil Range
LAI	Leaf Area Index
MODIS	Moderate Resolution Imaging Spectroradiometer
NECB	Net Ecosystem Carbon Balance
NEE	Net Ecosystem CO_2 Exchange
NEP	Net Ecosystem Productivity
NIR	Near Infrared
NPP	Net Primary Productivity
PAR	Photosynthetic Active Radiation
PPFD	Photosynthetic Photon Flux Density
SIC	Soil Inorganic Carbon
SOC	Soil Organic Carbon
SWC	Soil Water Content
UNFCCC	United Nations Framework Convention on Climate Change
UV	Ultraviolet
VPD	Vapor Pressure Deficit
VWC	Volumetric Water Content
WS	Wind Speed

LIST OF SYMBOLS AND ABBREVIATIONS

C	Carbon
CO_2	Carbon dioxide
u	Horizontal wind speed
w	Vertical wind speed
v	Cross-stream wind speed
T_s	Sonic temperature
ρ_a	Moist air density
ρ_c	Carbon dioxide density
ρ_d	Dry air density
ρ_v	Water vapor density
σ	Standard deviation
F_c	Carbon dioxide flux
F_v	Water vapor flux
LE	Latent heat flux
H	Sensible heat flux
ET	Evapotranspiration
λ	Specific evaporation heat
M_{H2O}	Molecular weight of water
c_p	Moist air heat capacity at constant pressure
μ	Ratio between dry air and water vapor molar masses
Q	Specific humidity
X_c	CO_2 Molar fraction
X_v	Water vapor molar fraction
T_{air}	Air temperature
e	Partial pressure of water vapor
P	Pressure
V	Volume
R	Ideal gas constant
T_{soil}	Soil temperature
z	Soil depth
D_s	Effective diffusion coefficient of the CO_2 in the soil
D_a	Diffusivity coefficient of CO_2 in air
ξ	Gas tortuosity factor
Φ	Soil porosity

θ	Volumetric soil water content
R_n	Net radiation
G	Soil heat flux
u_*	Friction velocity
dP	Differential pressure
dCO_2	Differential CO_2 molar fraction
P	Precipitation
β	Bowen ratio
k	Level of PPFD corresponding to half of the GPP_{max}
R_d	Daytime ecosystem respiration
$CO_{2,\,0.05m}$	Subsoil CO_2 measured at 0.05 m depth
$CO_{2,\,1.50m}$	Subsoil CO_2 measured at 1.50 m depth
NEE_{plot}	Net Ecosystem CO_2 Exchange measured at plot scale
NEE_{EC}	Net Ecosystem CO_2 Exchange
R_{soil}	Soil respiration
$R_{aboveground}$	Aboveground respiration
R_{eco}	Ecosystem respiration
$R_{soil\_vaisala}$	Soil respiration calculated using vaisala sensors
$T_{0.05m}$	Subsoil temperature measured at 0.05 m depth
$T_{1.50m}$	Subsoil temperature measured at 1.50 m depth
$VWC_{0.05m}$	Subsoil VWC measured at 0.05 m depth
$VWC_{1.50m}$	Subsoil VWC measured at 1.50 m depth
VWC_{soil}	Volumetric soil Water Content
WS_{max}	Maximum wind speed

ABSTRACT

Climate change represents the most important global challenge of the 21st century and global warming is one of the backbones of the climate change paradigm, which is greatly caused by the increase of atmospheric carbon dioxide (CO_2). Fossil fuel combustion, industrial activities and land use change have provoked the rise of atmospheric CO_2 molar fraction since the pre-Industrial Era to the present, from ~280 ppm to 406 ppm. However, the CO_2 growth rate within the atmosphere is half than expected owing to the mitigation role of biosphere, where terrestrial and aquatic ecosystems globally act as carbon sinks. In this regard, terrestrial ecosystems absorb a higher amount of atmospheric CO_2 compared to the ocean and also present a higher inter-annual variability that greatly drives the atmospheric CO_2 patterns. Therefore, it is necessary to deeply understand the global carbon (C) cycle in order to improve terrestrial C models that will allow us to identify the feedback mechanisms between terrestrial biosphere and global change and also to design proper mitigation and adaptation policies.

Nevertheless, besides their great global extension and their demonstrated influence in global C budget, drylands are underrepresented in global long-term monitoring infrastructures designated to directly measure biosphere-atmosphere CO_2 exchange. Additionally, the functioning of these water-limited ecosystems differs from the better-known temperate ecosystems, where main limiting factors are light and temperature instead of water. Thus, the principal aim of this thesis has been to investigate the relevant processes involved in the C balance of drylands and especially, of semiarid ecosystems, which correspond to the drylands' subtype with the largest global extension. Concretely, this thesis is spatially framed in two experimental sites, Amoladeras and Balsa Blanca, located in the Cabo de Gata-Níjar Natural Park (Almeria), in southeast Spain, the most arid region of Europe where ecosystems are subjected to high aridity conditions and degradation processes. For that, we have used the eddy

covariance technique, a standardized methodology used worldwide, and other additional methodologies, such as flux chambers and soil CO_2 probes, that also allow the measurement of CO_2 exchange between terrestrial ecosystems and the atmosphere.

The results of this thesis can be considered as a step towards more accurate quantification and understanding of the C cycle in semiarid ecosystems. The chapters included in this thesis investigate key issues that are especially relevant in drylands' C cycle, such as their vulnerability against degradation processes (Chapter 1), their dependency to water inputs or rain pulses (Chapter 2) and the potentially important role of subterranean ventilation (Chapter 3), a poor-known non-biological process responsible of sizeable CO_2 release from vadose zone to the atmosphere. Over the whole study period (six hydrological years, 2009-2015), the average annual C balance was -23 ± 20 g C m^{-2} at Balsa Blanca and 231 ± 48 g C m^{-2} at Amoladeras. Hence, Balsa Blanca, the less degraded site (or site of reference), acted as a soft C sink while a great amount of C was released to the atmosphere at Amoladeras, the more degraded site. Additionally, ecosystem functioning also differed between sites. Biological processes dominated the net C exchange measured at Balsa Blanca, whereas non-biological processes, especially subterranean ventilation, played an outstanding role in the net C exchange observed at Amoladeras. Moreover, drought modulated the relative relevance of the component processes since biological ones were constrained due to the hydric stress and subterranean ventilation was enhanced owing to the greater water-free space within soil pores and cracks.

Overall, this thesis has resulted in a more accurate knowledge of drylands' C cycle but also has led to new research questions. One of them is the potential role of vadose zone morphology and belowground air and water movement in the C balance of semiarid and arid regions. Additionally, the behavior of

terrestrial biosphere under future climatic scenarios is still uncertain, since we need to know how climate extremes, such as dry spells or heat waves, affect the ecosystems functioning at both the short- and the long-term. Hence, the continuity of monitoring stations, such as eddy covariance towers and subsoil CO_2 profiles, evenly distributed in the whole globe are an indispensable requisite to answer these questions.

RESUMEN

El cambio climático constituye el reto global más importante del siglo 21. En este contexto, el calentamiento global es uno de los ejes principales del paradigma del cambio climático, el cual está causado mayoritariamente por el aumento de dióxido de carbono (CO_2) en la atmósfera terrestre. La combustión de combustibles fósiles, las actividades industriales y los cambios de uso de suelo han provocado el aumento de la fracción molar de CO_2 atmosférico desde la era pre-industrial hasta el presente, de en torno a 280 ppm a 406 ppm. Sin embargo, la tasa de incremento de CO_2 en la atmósfera es la mitad a la esperada debido al papel mitigador de la biosfera, donde tanto ecosistemas terrestres y acuáticos actúan como sumideros de CO_2. En este sentido, los ecosistemas terrestres absorben una mayor cantidad de CO_2 en comparación a los océanos y además, presentan una mayor variabilidad interanual que notablemente determina los patrones del CO_2 atmosférico. Por lo tanto, es necesario comprender en profundidad el ciclo del carbono (C) global con el objetivo de mejorar los modelos de C terrestres que nos permitirán, por un lado, identificar mecanismos de retroalimentación entre la biosfera y el cambio global y por el otro, diseñar políticas de mitigación y adaptación adecuadas.

Sin embargo, a pesar de su gran extensión y de que su influencia en el balance global de C ha sido demostrada, las regiones áridas están infrarrepresentadas en las redes globales de monitorización continua destinadas el intercambio de CO_2 entre biosfera y atmósfera directamente. Además, el funcionamiento de estos ecosistemas difiere del funcionamiento de los ecosistemas templados, los cuales han sido más estudiados y donde los factores limitantes principales son la luz y la temperatura, en lugar del agua. De este modo, el principal objetivo de esta tesis ha sido investigar los procesos más relevantes que están involucrados en el balance de C de regiones áridas, y especialmente de ecosistemas semiáridos, los cuales ocupan la mayor fracción a escala global. Concretamente, esta tesis está enmarcada espacialmente en dos

sitios experimentales, Amoladeras y Balsa Blanca, situados en el Parque Natural de Cabo de Gata-Níjar (Almería), en el sudeste de España, que coincide con la región más árida de Europa donde los ecosistemas naturales están sujetos a condiciones de gran aridez y son susceptibles a la degradación. Para ello, hemos usado la técnica *eddy covariance,* una metodología estandarizada que es usada mundialmente, junto con otras metodologías adicionales, como las cámaras de flujo o los sensores de CO_2 de suelo que igualmente permiten la medida del intercambio de CO_2 entre los ecosistemas terrestres y la atmósfera.

Los resultados de esta tesis se pueden considerar como un paso hacia adelante con respecto a la cuantificación precisa y el conocimiento de los procesos del ciclo del C de ecosistemas semiáridos. Los capítulos incluidos en esta tesis investigan asuntos clave que son especialmente relevantes en el ciclo de C de ecosistemas semiáridos, como su vulnerabilidad frente a los procesos de degradación (Capítulo 1), su dependencia a los pulsos de precipitación (Capítulo 2) y al papel potencialmente importante de la ventilación subterránea (Capítulo 3), un proceso no biológico y poco conocido responsable de grandes emisiones de CO_2, desde la zona vadosa hacia la atmósfera. Durante el período de estudio (seis años hidrológicos, 2009-2015), el balance de C anual fue -23 ± 20 g C m^{-2} en Balsa Blanca y 231 ± 48 g C m^{-2} en Amoladeras. Por tanto, Balsa Blanca, es sitio menos degradado (o sitio de referencia), se comportó como un sumidero de C de pequeña magnitud mientras que una gran cantidad de C fue emitida a la atmósfera en Amoladeras, el sitio más degradado. Además, el funcionamiento de ambos ecosistemas de estudio fue distinto. Los procesos biológicos dominaron el intercambio de C neto medido en Balsa Blanca, mientras que los procesos no biológicos, especialmente la ventilación subterránea que jugó un papel crucial en el intercambio de C neto medido en Amoladeras. Asimismo, la sequía moduló la importancia relativa de estos procesos, ya que el estrés hídrico, por una parte, restringió la actividad biológica y, por la otra promovió la

presencia de la ventilación subterránea debido al aumento del espacio libre de agua de poros y grietas en el suelo y la zona vadosa.

En general, esta tesis ha resultado en un conocimiento más preciso del ciclo de C en zonas áridas, pero también ha conducido a nuevas preguntas. Una de ellas es el papel potencial que puede jugar la morfología de la zona vadosa y del movimiento subterráneo de agua y aire en el balance de C de ecosistemas áridos y semiáridos. Además, el comportamiento de la biosfera terrestre en escenarios futuros de cambio climático es aún incierto, ya que necesitamos conocer cómo eventos climáticos extremos, como sequías y olas de calor, afectan actualmente y afectarán al funcionamiento de los ecosistemas tanto a corto como a largo plazo. Por tanto, la continuidad de las estaciones de monitorización continua, tales como las torres *eddy covariance* y los perfiles de CO_2 en el suelo, distribuidas uniformemente por todo el planeta son un requisito indispensable para responder a estas preguntas.